UNIVERSITÀ DEGLI STUDI DI TRIESTE

XXX CICLO DEL DOTTORATO DI RICERCA IN AMBIENTE E VITA

INTERANNUAL VARIABILITY OF THE PLANKTONIC FOOD WEB IN THE GULF OF TRIESTE: AN INVERSE MODELLING APPROACH

Settore scientifico-disciplinare: **BIO/07**

DOTTORANDO
GIANLUCA COIDESSA

COORDINATORE
PROF. GIORGIO ALBERTI

SUPERVISORE DI TESI
DOTT. COSIMO SOLIDORO

ANNO ACCADEMICO 2016/2017

ABSTRACT

During the last 20 years ecology has evolved towards a vision of the ecosystem as a system of interactions where the centre of interest is represented by interactions between them, quantified by flows of matter and energy. The quantitative mapping of food web flows based on empirical data is crucial and it is a difficult task in ecology: it is hard to comprehend the nature of complex food webs through direct observation, because the number of flows of matter and energy involved can be overwhelming. Furthermore, it is generally difficult to measure or quantify the exchange of mass or energy between the compartments of a system. The planktonic food web of the Gulf of Trieste was studied using linear inverse modelling. We computed both the LIM – MN and the LIM – MCMC following literature criterions, in order to get the best solution for our planktonic food web case. We implemented a new compartment, the growth compartment, in order to have a more realistic view of the food web, trying to take into account the possibility of compartment growing. We compared the solutions of the two methods with the *a priori* scientific knowledge of the Gulf of Trieste to determine which could be defined the best way of solving the food web fluxes. The LIM – MN selects the best solution minimizing the sum of squared flows, while the LIM – MCMC selects the solution by an exhaustive sampling of the solution space. Both solutions respect the inequalities and all the ecological requests and therefore both of them are valid. The LIM- MN usually underestimates all the fluxes, while the LIM – MCMC gives a good representation of the flows ranges, rarely overestimating not very well bounded fluxes. Growth fluxes behave well, especially the LIM – MCMC ones, and give a good response as they are in agreement with the scientific knowledge of the Gulf of Trieste. Implementing this type of compartment could be a good compromise in using steady state conditions. It is our opinion that LIM – MCMC solution is the best way to depict all the planktonic food web fluxes of the Gulf of Trieste. Values of fluxes represent better what is the *a priori* ecological knowledge found in the literature. In particular, the solution explains the important role of bacterial compartments that are fundamental for the Gulf of Trieste marine life, as they channeled most of the carbon inside the food web. The so-called microbial loop is very strong, and poses the microzooplankton as the main actor in channelling carbon from lower ecotrophic level to higher ones, including fishes. Moreover, thanks to the values found in this study, the Gulf of Trieste planktonic ecosystem could be compared with more productive ecosystems on a world scale.

UNIVERSITÀ DEGLI STUDI DI TRIESTE

XXX CICLO DEL DOTTORATO DI RICERCA IN AMBIENTE E VITA

INTERANNUAL VARIABILITY OF THE PLANKTONIC FOOD WEB IN THE GULF OF TRIESTE: AN INVERSE MODELLING APPROACH

Settore scientifico-disciplinare: **BIO/07**

DOTTORANDO
GIANLUCA COIDESSA

COORDINATORE
PROF. GIORGIO ALBERTI

SUPERVISORE DI TESI
DOTT. COSIMO SOLIDORO

ANNO ACCADEMICO 2016/2017

To my Wife

SUMMARY

1. INTRODUCTION

The aim of the Scientists has always been to understand how nature and nature forces work. They try to depict and predict functioning and behavior of the ecosystems. In the last decades the interest has shifted from a properly scientific knowledge point of view to a more holistic one, in order to understand how humans are affecting the Earth system. The focus is on "Global changes" (Nicholas and Robinson, 1992) and human induced ones. Nowadays scientists try to define and quantify "planetary boundaries" that allow sustainable growth and development of humanity (Rockstrom et al., 2009; Steffen et al., 2015). Planetary boundaries are defined for Biogeochemical cycles and fluxes too (Rockstrom et al., 2009; Steffen et al., 2015). Biogeochemical cycles have a huge impact on the whole Earth system as they are related to all the system components: biosphere (living matter), atmosphere (air), geosphere (earth) and hydrosphere (water). Carbon cycle is one of the major biogeochemical cycles describing the flow of essential elements from the environment to living organisms and back to the environment again. In particular carbon most important fluxes are inside the Ocean. One of the pivotal actors of the ocean carbon cycle is plankton, and especially phytoplankton. Phytoplankton is recognized to be capable of impacting climate change because of its capacity to transport carbon and other elements from the surface ocean and in contact with the atmosphere, to the deep ocean and sediments (Falkowsky et al., 1998; Sigman and Boyle, 2000; Sarmiento and Gruber, 2006; Willliams and Follows, 2011). Phytoplankton, performing photosynthesis (primary production), converts inorganic nutrients into organic compounds. Most of the primary productivity is recycled locally through complex pathways of biological and chemical transformations, while only a smaller fraction is delivered into the deep ocean (biological carbon pump). Among the part channelled in the deeper layers the smallest one is buried into marine sediments, whereas the most is remineralized in the water column. Therefore, understanding how the plankton community behaves is important to better estimate carbon biogeochemical fluxes, especially in shallow coastal ecosystems. Coastal ecosystems are the most complex environmental framework in marine ecology as - due to shallow water - all biogeochemical processes are faster and strongly linked. Moreover, coastal ecosystems are the most endangered and affected by human activities. In the past, in order to understand the impacts of human activities on marine systems, scientists focused on the biomasses state of organisms: the idea was to study ecosystems through their biomasses state. During the last 20 years ecology has evolved towards a vision of the ecosystem as a system of interactions (Fasham 1984) where the centre of interest is no longer the state of the biomasses of the different groups of organisms, but the interactions between them, quantified by flows of matter and energy (Ulanowics and Wolff, 1990; Niquil et al., 1999; Bondavalli et al., 2006; Kones et al., 2009).

The challenge, however, still remains comprehending the nature of a system's interactions, given their complexity (Kones et al., 2009). The quantitative mapping of food web flows based on empirical data is a crucial yet difficult task in ecology (Oevelen et al., 2010). Furthermore, it is difficult to comprehend the nature of complex food webs through direct observation, because the number of flows of matter and energy involved can be overwhelming (Pimm 1982; Szymer and Ulanowics 1987). A food web structure shows how primary production is channeled via complex interactions between the biotic and abiotic compartments in a food web and eventually lost through dissipation or export. It is generally difficult to measure or quantify the exchange of mass or energy between the compartments of a system (Kones et al., 2009). In most ecological applications there are more unknown food web flows to be estimated than formulated equations, with an average ratio of 4:1 (Vézina and Pahlow, 2003). Therefore, food web flows cannot be uniquely determined from the available data. One way to deal with this under determinacy has been the use of linear inverse method (LIM) (Kones et al., 2009). This LIM finds the food web configuration that agrees with the available quantitative data (e.g. Vézina and Platt, 1988; Niquil et al., 1998; Donali et al., 1999; Vézina and Savenkoff, 1999; Leguerrier et al., 2003), the designed food web and the solution chosen.

1.1 INVERSE MODELLING

Inverse modelling problems are common in geophysical sciences for the study of earth and ocean characteristics that couldn't be measured directly (Parker 1977, Wunsch 1978). Only in the 80's they have been used and translated into the field of ecology and quantitative biology. In particular, they have been used for the study of food webs, which are high dynamic expressions of ecology interactions in an ecosystem. Food webs can be defined as the formal expression of the exchanges of energy or matter among living and non-living compartments in an ecosystem (Van Ovelen, 2006).

The work of Vezina and Platt (1988) could be defined as the milestone of inverse modelling applied to marine ecosystems, focusing in particular on the planktonic food web. The planktonic food web is the base/lower level of all marine ecosystems. Vezina and Platt were the first that used a combination of equalities and inequalities merging field data with the *a priori* knowledge from literature and experiments. They underline the great importance of field data estimated *in situ*, considering them as a priority compared to theoretical ones. The set of equations comprised the mass balance of each compartments plus a set of measured *in situ* flows. All other information was arranged in a set of inequalities. Missing flow values were selected minimising the quadratic norm (e.g. the sum of squared flows).

Based on the definition of Niquil et al. (2011), Vezina and Platt method could be named the "LIM – MN" method, because of a linear inverse approach with a minimum norm (quadratic norm). This

method is highly flexible because it depends on the user's choices to determine the best solutions. The definition of a criterion of choice together with the weighting scheme of flows are directly chosen by the user. Furthermore, the LIM depicts a polytope - space of solutions - defining the ranges of possible values of the flows, giving the user a more comprehensive view of the food web and an important way of interpretation.

The LIM – MN has a strong mathematical construct, but it has a great uncertainty in the interpretation of results because the solution choice is based on a minimization. The minimization could not be the best option when the user is depicting the interactions inside an ecosystem. Thus, new techniques built on the previous algorithm were defined. The aim of this new method was to depict the complete set of solutions for each flow.

It can be called LIM – MCMC technique (Niquil et al 2011) as the algorithm includes a Monte Carlo Markov Chain algorithm to randomly sample the solutions. The high number of dimensions (one for each flow) of the polytope and its complex geometry (defined by the interactions of flows) led to computational problems. Van den Meerche et al (2009) suggested a new method that decreases the computational capacity needed.

They proposed a LIM – MCMC with a mirror technique that uses the "borders" of the polytope as reflecting axes if the points chosen by the random sampling fall outside the polytope. This method defines samples of flows that fall inside the polytope and permits to save time in the choice of solutions. The important factor of the LIM – MCMC is to choose an appropriate number of iteration and of jump length (the space between each point of the solution). If these operations are performed in a good way, the method will give a representative sample of the PDF (Probability Density Function) for each flow.

Van Ovelen (2010) has shown how the mean of each set of solutions – i.e. the mean of each probability density function, being a linear operation - could be used to generate a mass balanced solution that fits all the constraints. PDF could be not normal, sometimes truncated by the inequality constraints and sometimes uniform if the model and data are not sufficient to constrain the value of a flow (Niquil et al 2010).

It is important to note how the evolution of methodologies goes from a direct optimization to a range of solutions that better depict the solutions space for each flow.

1.2 AIM OF THE WORK

The planktonic food web of the Gulf of Trieste was studied using linear inverse modelling. We computed both the LIM – MN and the LIM – MCMC following literature criterion, in order to get the best solution for our planktonic food web case. We implemented a new compartment - the growth compartment - to have a more realistic view of the food web, trying to go beyond the limits of the steady state modelling that does not take into account what is the behaviour of compartments from a biomasses point of view, as a snapshot of data is usually used. We then compared the two methods solutions with the *a priori* scientific knowledge of the Gulf of Trieste to determine which could be defined the best way of solving the food web fluxes. With the Gulf of Trieste case study, we would like to contribute to literature advances in the LIM methodology. Our aim is to understand which LIM approach would be the best in studying complex planktonic food webs.

2. METHODS

2.1 MODEL CONSTRUCTION

Before speaking thoroughly about the mathematical techniques that are beyond the inverse modelling procedures, it is important to explain how the system of equalities and inequalities is constructed. It is important to understand that in this work we deal with undetermined problems, and we focus only on these specific types of problems, leaving out all the other general cases: we'll report functions and methodologies that deal with this type of problems only.

First of all, the user has to define the *a priori* model that can better represent the food web of the ecosystem he wants to study. The *a priori* model is divided into two major components, the living and the non-living compartments. Usually, and in our case studies, non-living compartments have no mass balance. Living compartments are divided into minor components, depending on how deeply the user wants to investigate the ecosystems and on data available principally.

Once the model is defined, a mass balance equation is written for each compartment. The terms of the equations define which are the relations between all the compartments that exchange fluxes with the compartment depicted. Flows measured *in situ* have to be included in the system of equation too, as well as all the inequalities constraints that define the ranges of each flow - the limits of the polytope. These mathematical constructions have to be put in a matrix form to better handle the inverse model problem.

The representation of the food web in a matricial form is depicted as follow:

$$\begin{cases} Ax \cong b \\ Ex = f \\ Gx \geq h \end{cases}$$

$A\,x = b$ represents the set of equalities depicted by the mass balance equations. In particular, x is the vector of the unknowns that has to be determined, A is the matrix of 0 and 1 that defines the equalities, b is the numerical vector that contains the ratios of each mass balance. $E\,x = f$ is the set of equalities that defines which flows have to be met exactly, e.g. *in situ* measurement of known flows. $G\,x \geq h$ represents the set of inequalities explaining the upper and lower limit of each flow, derived from literature data. A graphic help of the model construction is given by the following image, modified from Niquil et al. (2011)

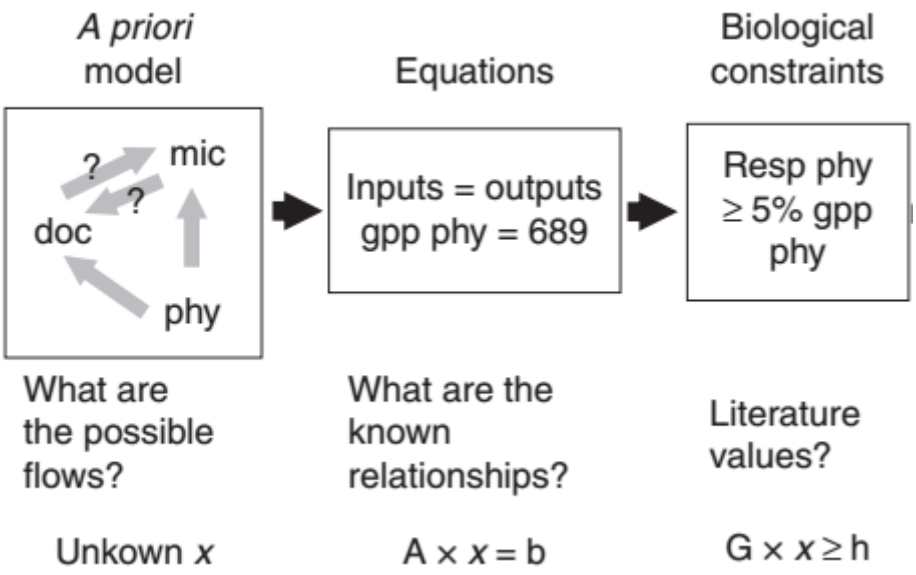

Figure 1: LIM approach modified from Niquil et al. (2011)

R Encoding

Soetart et al. (2009) published an R package that permits the user to build an inverse modelling model in a declarative way that can help not to make mistakes in writing model matrices. The LIM package is designed for reading, implementing and solving and inverse model. The first step is to declare all the LIM elements:

- *Compartments* – Components between which flows are defined.
- *Externals* – Compartments that represent the external world.
- *Parameters* – Parameters that have constant values.
- *Flows* – Flows between two compartments written in the form Source → Sink.
- *Variables* – A linear expression involving flows, parameters and variables too.
- *Equalities* – Relationships between unknowns or measured values that are assumed to be perfectly known (e.g. *in situ* measurement).
- *Inequalities* – Relationships between unknowns or values that defines unknown ranges.

All these declarations have to be settled in a *.lim* R document.

Then, we test the *.lim* document with the function *Read* that looks for errors and tests if all the parts are well declared. If not, errors warnings are declared.

To set up the LIM problems we will use the function *Setup* that automatically builds the matrices we need and implements the LIM problem in a matrix way, as a function of the unknowns. At this point

in the work environment the user will have all the parts needed to proceed with the solution (Matrices *A*, *E*, and *G*, vectors *x*, *b*, *f* and *h*).

More detailed explanations are written in the manual and vignettes of LIM packages.

2.2 LIM – MN

The solution of the process relies on the principle of parsimony (Vezina and Platt, 1988). Through this way of solving the LIM, the user will generate a set of values for the unknowns that satisfies the minimisation of the quadratic norm $||A\ x - b||^2$ and the constraints of inequalities and mass balance.

The first step is to find the solution of the continuity equation

$$A^{-1}\ b = x$$

As in inverse problems there are fewer equations (*m*) than unknowns (*n*), A^{-1} does not exist as it is not quadratic. A solution to inverse problem can be found reparametrizing the continuity equation in terms of *k* unknowns, where *k* is the number of the solvable unknowns, solved explicitly. To achieve this, the *n* - dimensional space of solutions/unknowns has to be reduced to a *k* - dimensional space.

The continuity equation can be solved explicitly for *k* unknowns by factoring *A* in *k* – dimensional subspaces of its observations and parameter spaces. A solution of the continuity equation can be reconstructed knowing the relationships between those unknowns and the original parameters. The SVD (Singular Value Decomposition) of *A* is the mathematic method that permits the user to achieve the solution. We rewrite *A* as:

$$A\ =\ U\ L\ V^T$$

Where *U* is a *m x K* matrix containing *k* linear independent linear combinations of the rows of *A* (observation space), *V* is an *n x k* matrix of linear combinations of the column of *A* (parameter space) and *L* is a diagonal *k x k* matrix of scaling factors. At this level the continuity equations will be written as:

$$ULV^T\ x\ =\ b$$

Which can be solved explicitly for *x*:

$$x =\ VL^{-1}U^T\ b$$

Defining $c\ =\ L^{-1}U^T\ b$, where *c* is a *k x 1* vector of unknowns that can be solved explicitly, the continuity equation can be written as:

$$x = Vc$$

that defines the relationship between *k* solvable unknowns and *n*. Adding *n – k* column vectors to that are usually independent and independent of the original *k* columns, we can make *V* a square matrix. This new *V* would be an equivalent representation of the parameter space of *A*, leading to a new solution that also satisfies the continuity equation, appending arbitrary values to *c* increasing its length to *n*. Therefore, the new solution to the continuity equation can be written as

$$x_n = Vc + V' d$$

Where *V'* is a matrix of additional vectors with dimensions *n x n - k* and *d* a *n - k x 1* vector of arbitrary constant. We can also rewrite the last equation as:

$$x_n = x + V'd$$

It is important to understand that infinite solutions could be generated changing the components of *d*.

Now we can implement the information that comes from the constraints. They are defined by the inequalities of constraints.

$$G\,x \geq h$$

We have to update the inequalities related to the new form of the solutions:

$$G(x + V'd) \geq h$$

$$GV'd \geq h - Gr$$

Through diverse mathematical techniques (refer to Vezina and Platt 1988), after implementing the *V'* matrix, which contains the *n - k* independent linear combinations that span the null space of *A*, we will obtain a new form of inequalities constraints, that is

$$G'd \geq h'$$

Where *G' = GV'* and *h' = h – Gr*. The vector *d* can be now substituted in the

$$x_n = Vc + V' d$$

to recover the constrained solution.

The least squares solution method, e.g. minimising the residual of $||Ax - b||$, is the best way to solve the inverse modelling because it is a compromise between the error left by the solution and the increasing complexity of the solution *x*. The method implemented in the *limSolve* package from Soetart et al. derives from the Haskell and Hanson "algorithm for linear least squares problems with

equality and non-negativity constraints" (1981). The least squares method used is the one that minimises the sum of $||Ax - b||^2$, i.e. $\sum \varepsilon^2$. The residual of the solutions ($e = A\,x - b$) could be useful in the choice of a solution or in comparing different solutions.

R Encoding

Once we got the matrices that we need to solve the inverse problem, we can implement the function that will give us the first solution.

The function is the *lsei()* function from the R package *limSolve* (Functions that find the minimum/maximum of a linear or quadratic function: min or max *(f(x))*, where $f(x) = ||Ax-b||^2$ or *f(x) = sum(a_i*x_i)* subject to equality constraints $Ex = f$ and/or inequality constraints $Gx>=h$. Sample an underdetermined or overdetermined system $Ex = f$ subject to $Gx >= h$, and if applicable $Ax~=b$ solve a linear system $Ax=B$ for the unknown x. It includes banded and tridiagonal linear systems. The package calls Fortran functions from 'LINPACK'), Soetart et al. 2009.

lsei (*A* = NULL, *B* = NULL, *E* = NULL, *F* = NULL, *G* = NULL, *H* = NULL, *Wx* = NULL, *Wa* = NULL, type = 1, tol = sqrt(Machine$double.eps), tolrank = NULL, fulloutput = FALSE, verbose = TRUE)

INPUT:

- *A*: numeric matrix containing the coefficients of the quadratic function to be minimised, $||Ax - B||^2$; if the columns of *A* have a names attribute, they will be used to label the output.
- *B*: numeric vector containing the right-hand side of the quadratic function to be minimised.
- *E*: numeric matrix containing the coefficients of the equality constraints, $Ex = F$; if the columns of *E* have a names attribute, and the columns of *A* do not, they will be used to label the output.
- *F*: numeric vector containing the right-hand side of the equality constraints.
- *G*: numeric matrix containing the coefficients of the inequality constraints, $Gx >= H$; if the columns of *G* have a names attribute, and the columns of *A* and *E* do not, they will be used to label the output.
- *H*: numeric vector containing the right-hand side of the inequality constraints.
- *Wx*: numeric vector with weighting coefficients of unknowns (length = number of unknowns).
- *Wa*: numeric vector with weighting coefficients of the quadratic function (*Ax-B*) to be minimised (length = number of number of rows of *A*).
- Type: integer code determining algorithm to use 1 = *lsei*, 2 = *solve.QP* from R-package quadprog.
- Tol: tolerance (for singular value decomposition, equality and inequality constraints).

- Tolrank: only used if type = 1; if not NULL then tolrank should be a two - valued vector containing the rank determination tolerance for the equality constraint equations (1st value) and for the reduced least squares equations (2nd value).
- Fulloutput: if TRUE, also returns the covariance matrix of the solution and the rank of the equality constraints - only used if type = 1.
- Verbose: logical to print error messages.

OUTPUT:

- *X*: vector containing the solution of the least squares problem.
- residualNorm: scalar, the sum of absolute values of residuals of equalities and violated inequalities.
- solutionNorm: scalar, the value of the minimised quadratic function at the solution, i.e. the value of $||Ax - b||^2$.
- IsError: logical, TRUE if an error occurred.
- type the string: "*lsei*", such that how the solution was obtained can be traced.
- Covar: covariance matrix of the solution; only returned if fulloutput = TRUE.
- RankEq: rank of the equality constraint matrix.; only returned if fulloutput = TRUE.
- RankApp: rank of the reduced least squares problem (approximate equations); only returned if fulloutput = TRUE.

2.3 LIM – MCMC

This type of algorithm randomly samples the feasible region of the undermined linear problem in a uniform way, where the feasible region of linear problem is the part of the parameter space that contains all the solutions of the reduced problem (the problem is reduced due to the equalities and inequalities constraints).

When we write the problem as $Ax = b + \varepsilon$, with ε as an error in the data vector b, the generated sample in the feasible region are not uniformly distributed as x is subjected to inequalities constraints ($G\,x \geq h$). Thus, Van den Merschee et al. (2009) proposed a truncated distribution for x:

$$p(\mathrm{x}) \propto e^{-\frac{1}{2}(Ax-b)^T W^2 (Ax-b)} \; if \; x \in L; \; p(x) = 0 \; if \; x \notin L$$

Where W is the weight matrix $W = diag(s^{-1})$ (s = standard deviation).

The method consists of two steps. The first step consists in eliminating the equality constraints $E\,x = f$ to get independent samples; the second step consists in performing the sampling through a Metropolis algorithm with a Mirror algorithm.

In order to eliminate the linear dependencies between x_i (they are coupled by the equations $E\,x = f$), they have to be transformed in a vector q, which elements q_i are linear independent. All solutions can be rewritten as:

$$x = x_0 + Zq$$

where Z is a matrix obtained through the QR-decomposition or SVD of E ($Z^T Z = I$, $E\,Z = 0$). As there are no equalities constraints, the inverse problem can be rewritten in the form:

$$\begin{cases} A' q - b' = \varepsilon \\ G' q - h' \geq 0 \end{cases}$$

Where $A' = A\,Z$, $b' = Ap - b$, $G'\,G\,Z$ and $h' = G\,x_0 - h$. Using the function *xsample()*, a particular solution *x0* could be used, the one that comes out from the Lsei method (previous chapter) to take advantage into the calculations.

It is important to notice that the trivial solution of the inverse problem is 0 ($q = 0$), as p meets the inequality constraints: so, the x_0, from which the new points will be sampled, is now 0.

At this point we have to see the distribution of q to get the targeted distribution of the sample set x. The PDF (probability density function) of q is a product of the PDF of x and the jacobian determinant if a vector $x(q)$ is a function of q:

$$p(q) = p(x)\left|\left|\frac{\partial x}{\partial q}\right|\right|$$

as Z is orthonormal, the norm is equal to 1, the jacobian is 1 and therefore $p(x) = p(q)$. So, if q is sampled uniformly, x is sampled uniformly, too.

As x is transformed into q, it is possible to go on sampling q properly.

The function *xsample()* is based on two algorithms to sample the feasible region: the metropolis algorithm (Roberts 1996) and the Mirror algorithm (Van de Meerche et al., 2009). The Mirror algorithm is an algorithm in which new samples are taken from a normal jump distribution with q_1 as average and a fixed standard deviation called *jump* length. With a high number of constraints, a lot of new points that should be defined by the Metropolis algorithm will be outside of the feasible region slowing down the performance of the algorithm and have to be rejected.

It is important to point out that, in a Euclidean space, every inequality defines a boundary of the feasible space of the solution. Each boundary is a hyperplane in the solution space, inside of it there is the feasible region in which the inequalities are met, outside of it there is the non-feasible region. The hyperplanes are defined from the set of equations here:

$$G'_{(,i)}q - h'_{(i)} = 0 \; \forall i$$

If q_1 is a point for which the inequalities are fulfilled, we will use it as the starting point for the sampling distribution. A new point q_2 can be sampled: first, a point $q_{2\text{-}0}$ is sampled from a normal distribution in the space not taking into account the inequality constraints. So

$$q_{2-0} = q_1 + \eta$$

with η drawn from a normal distribution with mean 0 and fixed standard deviation. $I\eta$ is called the jump length of the Markov Chain Montecarlo and is very important as it has an important role in the efficiency of the algorithm: it defines the distance covered by the algorithm in one iteration. If $q_{2\text{-}0}$ is in the feasible region, it is accepted as the new sample point q_2 and evaluated in the Metropolis algorithm.

If not, i.e. some inequalities are violated, the $q_{2\text{-}0}$ is mirrored consecutively in the hyperplanes that represent the inequalities violated: the line that connects the point q_1 and q_2 crosses the hyperplanes. For each hyperplane we can calculate a scalar value α as:

$$(G')_{(,i)}(q_1 + \alpha_{(i)}\eta) + h'_{(i)} = 0$$

With $\eta = q_{2\text{-}0} - q_1$. The hyperplane with the smallest non-negative $\alpha(i)$, which is called $\alpha(s)$, is the hyperplane that is crossed first by the line that connect the point q_1 and q_2. $Q_{2\text{-}0}$ is mirrored around this hyperplane.

If the constraints are still violated, a new set of $\alpha_{(i)}$ is calculated from the line between the new point and the intersection of the previous line and the first hyperplane. Again, the algorithm chooses the smallest non-negative α, and along the line that held the lower α is reflected the point $q_{2\text{-}1}$. This procedure is repeated until the inequalities are met. The new point q_2 is in the feasible subspace of the solution space and it is selected. A graphic support is represented by the following figure from Van den Meerche et al. (2009)

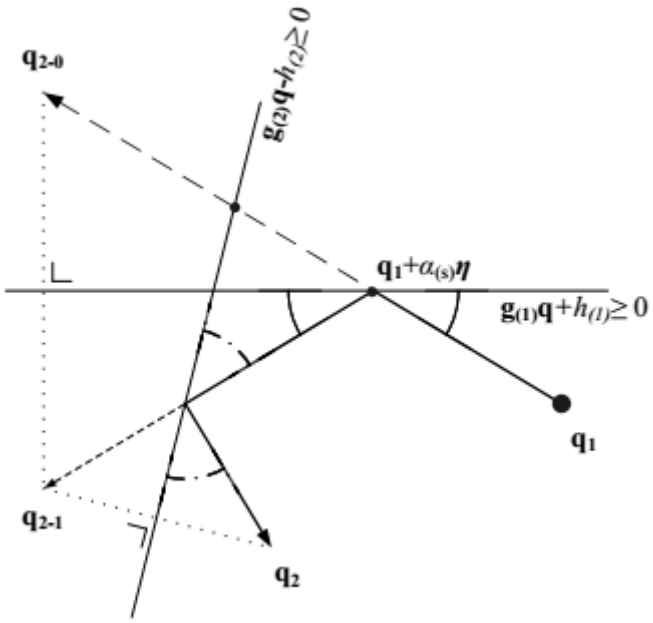

Figure 2: Functioning scheme of the mirror algorithm from Van den Meerche et al. (2009)

Going back to the metropolis algorithm, it evaluates the point q_2 in case it is immediately sampled in the feasible region of the space solution.

The Metropolis algorithm produces samples whose distribution respects an established target distribution. In the function *xsample()* is designed randomly from a *jump* distribution with a probability density function (PDF $j(.|q_1)$ that depends on the previous point q_1 accepted. The new sample q_2 is accepted or rejected on the base of the following statement:

$$\text{if } r \leq \frac{p(q_2)}{p(q_1)} \quad (\text{with } 0 < r \leq 1)$$

the algorithm accepts q_2 else keeps q_1 and re-iterate the sample procedure. The important and only prerequisite for the sample distribution is that the *jump* distribution from which q_2 is drawn has to be symmetrical: the probability to jump from q_1 to q_2 ($j(q_2|q_1)$ has to be the same probability to jump to q_2 to q_1 ($j\ q_1|q_1$). The jump distribution is written as:

$$if\ G'\ q \geq p(q) \propto e^{-\frac{1}{2}\sigma^{-2}(A\prime q-b\prime)^T W^2 (A\prime q-b\prime)}$$

$$else\ p(q) = 0$$

where $\sigma = 1$ and $W = diag\ (s^{-1})$. If it is not set, σ is estimated from fitting the unconstrained model $Ax - b \sim N(0,\sigma)$.

R encoding

Random sampling of inverse linear problems with linear equality and inequality constraints. *Xsample* function uses Random algorithm mixed with a Mirroring technique for sampling.

xsample (*A* = NULL, *B* = NULL, *E* = NULL, *F* =NULL, *G* = NULL, *H* = NULL, *sdB* = NULL, *W* = 1, iter = 3000, outputlength = iter, burninlength = NULL, type = "mirror", jmp = NULL, tol = sqrt(Machine$double.eps), *x0* = NULL, fulloutput = FALSE, test = TRUE)

INPUT:

- *A*: numeric matrix containing the coefficients of the (approximate) equality constraints, *Ax 'B*.
- *B:* numeric vector containing the right-hand side of the (approximate) equality constraints.
- *E*: numeric matrix containing the coefficients of the (exact) equality constraints, *Ex = F*.
- *F*: numeric vector containing the right-hand side of the (exact) equality constraints.
- *G*: numeric matrix containing the coefficients of the inequality constraints, *Gx >= H*.
- *H*: numeric vector containing the right-hand side of the inequality constraints.
- *sdB*: vector with standard deviation on *B*. Defaults to NULL.
- *W*: weighting for *Ax 'B*. Only used if *sdB*=NULL and the problem is overdetermined. In that case, the error of *B* around the model *Ax* is estimated based on the residuals of *Ax 'B*. This error is made proportional to 1/*W*. If *sdB* is not NULL, *W = diag(sdB−1)*.
- Iter: integer determining the number of iterations.
- Outputlength: number of iterations kept in the output; at most equal to iter.
- Burninlength: a number of extra iterations, performed at first, to "warm up" the algorithm.
- Type: type of algorithm: one of: "mirror", (mirroring algorithm), "rda" (random directions algorithm) or "cda" (coordinates directions algorithm).
- Jmp: jump length of the transformed variables *q: x = x0+Zq* (only if type=="mirror"); if jmp is NULL, a reasonable value is determined by *xsample*, depending on the size of the NULL space.
- Tol: tolerance for equality and inequality constraints; numbers whose absolute value is smaller than tol are set to zero.
- *x0*: initial (particular) solution.
- Fulloutput: if TRUE, also outputs the transformed variables *q*.
- Test: if TRUE, *xsample* will test for hidden equalities (see details). This may be necessary for large problems, but slows down execution a bit.

OUTPUT:

- *X*: matrix whose rows contain the sampled values of *x*.
- Acceptedratio: ratio of acceptance (i.e. the ratio of the accepted runs / total iterations).
- *Q*: only returned if fulloutput is TRUE: the transformed samples *Q*.
- *P*: only returned if fulloutput is TRUE: probability vector for all samples (e.g. one value for each row of *X*).
- Jmp: the jump length used for the random walk. Can be used to check the automated jump length.

3. MATERIALS

3.1 STUDY SITE

The study site is placed in the Gulf of Trieste, the east-northernmost edge of the Adriatic Sea (Umani et al 2012). The Gulf of Trieste is a shallow basin (23 m maximum depth, Umani et al., 2007), with a 600 km^2 surface and a 9.5 km^3 volume (Cossarini and Solidoro, 2008). It is highly influenced by the river runoff, especially the one of the Soca-Isonzo river, with the highest river discharge in spring and autumn, opposite to winter and summer that are the drought periods. The seasonal alternation of stratification and mixing and the occurrence of wind events (Querin et al., 2006) deeply influence and characterize the Gulf of Trieste systems. The hydrological station C1 (Latitude 45°42'2.99"N Longitude 13°42'36.00"E) is located in the middle east part of the gulf of Trieste, in a shallow coastal zone (17 m), at the outer board of the Protected Sea Area of Miramare. It is part of the Adriatic Long Term Ecological Research (LTER). Long term research provides a consistent picture of the trophodynamics interactions that define the Gulf of Trieste and permits to recognize some patterns that are recorded every year. In particular, spring and autumn are characterized by surface blooms of large diatoms, while in summer the presence of small phytoplankton - that is relevant in the oligotrophic and stratification condition - is observed (Malej et al., 1995; Umani, 1996; Terzic et al., 1998). At the end of spring, at the begin of summer and during autumn, mixed filter feeders and herbivorous (copepod species) are present (Umani et al., 1992; Cataletto et al., 1995; Mozetic et al., 1998). Ciliates, tintinnids and metazoans (Microzooplankton) are present during the whole year and dominate in summer (Mozetic et al., 1998; Cataletto et al., 1995; Umani and Beran, 2003).
A crucial role in the flow of energy from dissolved organic matter to higher trophic levels is played by heterotrophic bacteria, through the protozoans grazing processes (Umani and Beran, 2003).

3.2 THE *A PRIORI* MODEL

We have decided to maintain the structure of the dataset, identifying three compartments of autotrophs, i.e. autotrophic picoplankton (Cyanobacteria – CB), autotrophic nanoplankton (AN), microphytoplankton (MP), and four compartments of heterotrophs: heterotrophic picoplankton (heterotrophic bacteria – HB), heterotrophic nanoplankton (HNF), microzooplankton (MIZ) and mesozooplankton (MEZ): There are also four external compartments: a CO2-Respiration compartment (CO2), a DOC compartment, a Detritus compartment (DET) and a growth compartment (GR). The Growth compartment is implemented in order to allow the model to consider compartments biomass growth, as we have secondary production data. Every compartment has an outflow to CO2

compartment (respiration), to DOC compartment (exudation and sloppy feeding), to DET compartments (death, faecal pellets, sloppy feeding) and to growth compartment (net primary production or secondary production). Heterotrophic bacteria feed on DOC, while they are predated by HNF and MIZ in the same way as autotrophic bacteria. MIZ and MEZ predate on autotrophic nanoplankton and microphytoplankton. MIZ also predates on HNF while it is predated by MEZ only. The ingestion of detritus is allowed for all heterotrophic compartment (HNF, MIZ and MEZ), except for heterotrophic bacteria. Heterotrophic bacteria ingestion is defined as DOC uptake flux.

Hereby we report the compartments and fluxes as they are implemented and explained in the model.

Autotrophs compartments:

- CB = Cyanobacteria (Autotrophic Picoplankton).
- AN = Nanoplankton (Autotrophic Nanoplankton).
- MP = Microphytoplankton.

Heterotrophs compartments:

- HB = Hetererotrophic Bacteria (Hetererotrophic-Pikoplankton).
- HNF = Heterotrophic_Nanoplankton.
- MIZ = Microzooplankton.
- MEZ = Mesozooplankton.

External compartments:

- CO2 = Respiration + GPP.
- DOC = Dissolved organic carbon.
- DET = Detritus.
- GROWTH = C to growth.

Flows are written in the form source → sink, respecting model and literature standards.

CB Flows (Cyanobacteria):

- CO2_CB: Flow (CO2, CB); GPP.
- CB_DOC: Flow (CB, DOC); Exudation.
- CB_CO2: Flow (CB, CO2); Respiration.
- CB_DET: Flow (CB, DET); To detritus.
- CB_HNF: Flow (CB, HNF); Predation by HNF.
- CB_MIZ: Flow (CB, MIZ); Predation by MIZ.
- CB_GR: Flow (CB, GROWTH); Net primary production.

AN flows (Nanoplankton):

- CO2_AN: Flow (CO2, AN); GPP.

- AN_DOC: Flow (AN, DOC); Exudation.
- AN_CO2: Flow (AN, CO2); Respiration.
- AN_DET: Flow (AN, DET); To POC.
- AN_MIZ: Flow (AN, MIZ); Predation by MIZ.
- AN_MEZ: Flow (AN, MEZ); Predation by MEZ.
- AN_GR: Flow (AN, GROWTH); Net primary production.

MP Flows (Microphytoplankton):

- CO2_MP: Flow (CO2, MP); GPP.
- MP_DOC: Flow (MP, DOC); Exudation.
- MP_CO2: Flow (MP, CO2); Respiration.
- MP_DET: Flow (MP, DET); To detritus.
- MP_MIZ: Flow (MP, MIZ); Predation by MIZ.
- MP_MEZ: Flow (MP, MEZ); Predation by MEZ.
- MP_GR: Flow (MP, GROWTH); NET primary production.

HB Flows (Heterotrophic picoplankton):

- HB_CO2: Flow (HB, CO2); Respiration.
- HB_DOC: Flow (HB, DOC); Exudation.
- HB_DET: Flow (HB, DET); To detritus.
- HB_HNF: Flow (HB, HNF); Predation by HNF.
- HB_MIZ: Flow (HB, MIZ); Predation by MIZ.
- HB_GR: Flow (HB, GROWTH); Secondary production

HNF Flows (Heterotrophic nanoplankton):

- HNF_CO2: Flow (HNF, CO2); Respiration.
- HNF_DOC: Flow (HNF, DOC); Exudation.
- HNF_DET: Flow (HNF, DET); To detritus.
- HNF_MIZ: Flow (HNF, MIZ); Predation by MIZ.
- HNF_GR: Flow (HNF, GROWTH); Secondary production.

MIZ Flows (Microzooplankton):

- MIZ_CO2: Flow (MIZ, CO2); Respiration.
- MIZ_DOC: Flow (MIZ, DOC); Exudation and sloppy feeding.
- MIZ_DET: Flow (MIZ, DET); To detritus.
- MIZ_MEZ: Flow (MIZ, MEZ); Predation by MEZ.
- MIZ_GR: Flow (MIZ, GROWTH); Secondary production.

MEZ Flows (Mesozooplankton):

- MEZ_CO2: Flow (MEZ, CO2); Respiration.
- MEZ_DOC: Flow (MEZ, DOC); Exudation and sloppy feedings.
- MEZ_DET: Flow (MEZ, DET); To detritus (sloppy feeding, fecal pellets).
- MEZ_GR: Flow (MEZ, GROWTH); Secondary production.

DET Flows (Detritus):

- DET_HNF: Flow (DET, HNF); Ingestion by HNF.
- DET_MIZ: Flow (DET, MIZ); Ingestion by MIZ.
- DET_MEZ: Flow (DET, MEZ); Ingestion by MEZ.

DOC Flow:

DOC_HB: Flow (DOC, HB); DOC uptake.

Mass equation for each compartment:

- CO2_CB - CB_DOC - CB_CO2 - CB_DET - CB_HNF - CB_MIZ - CB_GR = 0
- CO2_AN - AN_DOC - AN_CO2 - AN_DET - AN_MIZ - AN_MEZ - AN_GR = 0
- CO2_MP - MP_DOC - MP_CO2 - MP_DET - MP_MIZ - MP_MEZ - MP_GR = 0
- DOC_HB - HB_CO2 - HB_DOC - HB_DET - HB_HNF - HB_MIZ - HB_GR = 0
- CB_HNF + HB_HNF + DET_HNF - HNF_CO2 - HNF_DOC - HNF_DET - HNF_MIZ - HNF_GR = 0
- CB_MIZ + AN_MIZ + MP_MIZ + HNF_MIZ + DET_MIZ - MIZ_CO2 - MIZ_DOC - MIZ_DET - MIZ_MEZ - MIZ_GR = 0
- MP_MEZ + MIZ_MEZ + DET_MEZ - MEZ_CO2 - MEZ_DOC - MEZ_DET - MEZ_GR = 0

3.3 DATA

All the data used in this work (Table 1) are taken from the paper "*Carbon fluxes in the pelagic ecosystem of the Gulf of Trieste (Northern Adriatic Sea)"*, by Serena Fonda Umani, Francesca Malfatti and Paola Del Negro, published in 2012 in *Estuarine, Coastal and Shelf Sciences*. Data are divided into different days of sampling, reported by season, and they include all field measurements and laboratory experiment data. We screened the dataset to select those case studies in which all the different plankton compartments biomass is measured: in particular we focus on the 2001 samplings, as the whole year is portrayed (winter, spring, summer and autumn). We use both biomass data, expressed in carbon content, and fluxes data as ingestions rates and secondary production (Table1) as input data for inverse modelling. We tried to use also net primary production and respiration rates, but they frequently didn't match the constraining requests of the inverse model.

DATA	SYMBOL	UNIT	12/02/2001	07/05/2001	07/08/2001	15/11/2001
Temperature	T	C	10.27	15.71	25.33	14.59
Chlorophyll content	chl	$\mu g\ l^{-1}$	3.39	0.36	4.63	0.74
Photosynthetically active radiation	PAR	$\mu E\ m^{-2}\ s^{-1}$	1048.81	340.43	1756.24	1006.98
Autotrophic Picoplankton biomass	CB_biomass	$\mu g\ C\ l^{-1}$	8.24	16	40.1	5.85
Autotrophic Nanoplankton biomass	AN_biomass	$\mu g\ C\ l^{-1}$	6.61	6.82	6.57	6.24
Microphytoplankton biomass	MP_biomass	$\mu g\ C\ l^{-1}$	151	3.35	14.8	5.27
Heterotrophic Picoplankton biomass	HB_biomass	$\mu g\ C\ l^{-1}$	25	24.7	27	20.3
Heterotrophic Nanoplankton biomass	HNF_biomass	$\mu g\ C\ l^{-1}$	1.33	1.7	1.3	0.84
Microzooplankton biomass	MIZ_biomass	$\mu g\ C\ l^{-1}$	4.4	2.88	5.86	5.41
Mesozooplankton biomass	MEZ_biomass	$\mu g\ C\ l^{-1}$	13.52	11.41	12.51	3.03
Microzoo ingestion on microphytoplankton	MP_MIZ	$\mu g\ C\ l^{-1}\ d^{-1}$	77.16	0.49	8.58	/
Microzoo ingestion on AN	AN_MIZ	$\mu g\ C\ l^{-1}\ d^{-1}$	6.46	2.43	9.61	3.38
Microzoo ingestion on HNF	HNF_MIZ	$\mu g\ C\ l^{-1}\ d^{-1}$	0.77	/	/	/
Microzoo ingestion on HP	HB_MIZ	$\mu g\ C\ l^{-1}\ d^{-1}$	9.83	32.16	53.44	11.34
Microzoo ingestion on AP	CB_MIZ	$\mu g\ C\ l^{-1}\ d^{-1}$	3.02	7.21	28.23	/
Mesozoo ingestion on AN	AN_MEZ	$\mu g\ C\ l^{-1}\ d^{-1}$	3.56	6.11	/	/
Mesozoo ingestion on microphytopl	MP_MEZ	$\mu g\ C\ l^{-1}\ d^{-1}$	47.08	1.9	/	/
Mesozoo ingestion on microzoo	MIZ_MEZ	$\mu g\ C\ l^{-1}\ d^{-1}$	0.22	1.76	/	/
HNF ingestion on Heterotrophic Picoplankton	HB_HNF	$\mu g\ C\ l^{-1}\ d^{-1}$	2.54	/	36.75	9.94
HNF ingestion on Autotrophic Picoplankton	CB_HNF	$\mu g\ C\ l^{-1}\ d^{-1}$	0.38	/	37-75	1.46
BCP (3H) leucine	HB_GR	$\mu g\ C\ l^{-1}\ d^{-1}$	4.8	16.32	53.21	3.58
HNF production	HNF_GR	$\mu g\ C\ l^{-1}\ d^{-1}$	0.24	/	0.35	/
Microzoo production	MIZ_GR	$\mu g\ C\ l^{-1}\ d^{-1}$	/	0.81	4.94	/

Table 1: Data from Umani et al., 2012

3.4 GROSS PRIMARY PRODUCTION (GPP)

We chose gross primary production equalities from Jassby and Platt (1976), later modified by Lazzari et al. (2012). We modified the equation as we linearized it obtaining the final form we needed:

$$GPP = fpt * fpe * fpp * pc * r0p$$

where *fpt* indicates a function of temperature, *fpe* a function of light availability, *fpp* a function of nutrient availability, *pc* is the parameter about biomasses data of the compartment studied and *r0p* is the growth parameter of the compartment studied.

FPT expresses the GPP relation with temperature (in the form: $q10^{((T-10)/10)}$, where *q10* is the characteristic coefficient of each compartment and *T* is the temperature value). *FPE* represents the GPP dependence from light availability and is in the form:

$$fpe = (1- exp(- ((alpha*Epar*pl)/(r0p*pc))))$$

where *Epar* is the photosynthetically active radiation multiplied for the per day light availability in seconds (winter: 10.5 daylight hours, spring: 15 daylight hours, summer: 14 daylight hours and autumn: 9 daylight hours), *pl* is the chl concentrations in µg chl m^{-3}, *alpha* is the maximum light utilization coefficient in mg C $(mg\ chl)^{-1}$ ($1.035\ 10^{-5}$ for MP, $1.52\ 10^{-5}$ for CB and $0.46\ 10^{-5}$ for AN), *r0p* is the growth parameter of the compartment studied (2 for AN, 3.5 for CB and 2 for MP), *pc* is the parameter about biomasses data of the compartment studied. All parameters explanation and values are drawn from the Biogeochemical Flux Model (BFM) manual version 5.1, by Vichi et al. (2015).

FPP is the nutrient limitation, but we considered no limitation at all, setting the *fpp* value equal to 1.

3.5 *W* PARAMETER

W parameter represents the mass cell weight to insert in all the inequalities. We chose to use the following *W* values:

- W_CB = 0.200 pg C $cell^{-1}$, from Umani et al. 2012.
- W_HB = 0.020 pg C $cell^{-1}$, from Umani et al. 2012.
- W_HNF = 5.63 pg C $cell^{-1}$, from Vezina et al. 2000.
- W_MIZ = 582.96 pg C $cell^{-1}$, from Vezina et al. 2000.
- W_MEZ = 3800000 pg C $cell^{-1}$, from Richardson et al., 2006.

3.6 INEQUALITIES

In table 2 inequalities used for the LIM methodology are reported. Inequalities are taken from Niquil et al. (2011) and represents the last upgrade of inequalities for inverse modelling found in literature.

Compartment	*Process*	*Bound*	*Description*	*Inequality*	*Reference*
Phytoplankton	Respiration	Both	Respiration of phytoplankton ranges between 5% and 30% of gross primary production.	Res–0.05 GPP ≥ 0 Res–0.30 GPP ≤ 0	Vézina and Platt (1988)
	Excretion	Both	Excretion of phytoplankton ranges between 10% and 55% of net primary production(NPP)	0.10 NPP – CphTOdoc ≤ 0 0.55 NPP – CphTOdoc ≥ 0	Modified from Vézina and Pace (1994)
Bacteria	Respiration	Lower	Respiration by bacteria is at least 20% of total ingestion	0.2 (Total ingestion) – Res ≤ 0	Vézina et al. (2000)
		Upper	Respiration by bacteria does not exceed maximum specific respiration (function of cell mass (W) and temperature (T) x biomass (B))	Max spe res = $3.6W^{-0.25}\ e^{0.0693(T-20)}$ (B × Max spe res)– Res ≤ 0	Vézina and Pace (1994) according to Moloney and Field (1989)
	Net production efficiency	Both	The sum of respiration and excretion by bacteria ranges between 50% and 75% of DOC uptake.	0.50 CdocTObac – (Res + CbacTOdoc) ≤ 0 0.75 CdocTObac – (Res + CbacTOdoc) ≥ 0	Vézina et al. (2000)
Protozoa	Respiration	Lower	Respiration by prototoza is at least 20% of total ingestion	0.2 (Total ingestion) – Res ≤ 0	Vézina and Pace (1994)
		Upper	Respiration by protozoa does not exceed maximum specific respiration (function of cell mass (W) and temperature (T) x biomass (B))	Max spe res = $14W^{-0.25}\ e^{0.0693(T-20)}$ (B × Max spe res)– Res ≤ 0	Vézina and Pace (1994) according to Moloney and Field (1989)
	Excretion	Both	DOC excretion by protozoa is at least 10% of total ingestion and does not exceed respiration.	0.10 (Total Ingestion) – CproTOdoc ≤ 0 Res – CproTOdoc ≥ 0	Vézina and pace (1994)
	Gross production efficiency	Both	Sum of respiration, excretion, and ejection by protozoa ranges between 50% and 75% of total ingestion.	0.50 (TotIng) – (Res + CproTOdoc + CproTOdet) ≤ 0 0.75 (TotIng) – (Res + CproTOdoc + CproTOdet) ≥ 0	Vézina et al. (2000)
	Ingestion	Upper	Total ingestion of protozoa does not exceed maximum specific ingestion (function of cell mass (W) and temperature (T) x biomass (B))	Max spe ing = $63W^{-0.25}\ e^{0.0693(T-20)}$ (B × Max spe ing) – TotIng ≤ 0	Vézina and Pace (1994) according to Moloney and Field (1989)
	Assimilation efficiency	Both	Assimilation efficiency of protozoa ranges between 50% and 90% of total ingestion	– 0.50 TotIng – CproTOder ≤ 0 – 0.10 TotIng – CproTOder ≥ 0	Vézina and Platt (1988)
Mesozooplankton	Respiration	Lower	Respiration by mesozooplankton is at least 20% of total ingestion	0.2 (Total ingestion) – Res ≤ 0	Vézina and Pace (1994)
		Upper	Respiration by mesozooplankton does not exceed maximum specific respiration (function of body mass(W) and temperature (T) × biomass (B))	Max spe res = $14W^{-0.25}\ e^{0.0693(T-20)}$ (B × Max spe res) – Res ≤ 0	Vézina and Pace (1994)according to Moloney and Field (1989)
	Excretion	Both	DOC excretion by protozoa is at least 10% of total ingestion and does not exceed respiration.	0.10 (Total Ingestion) – CproTOdoc ≤ 0 Res – CmesTOdoc ≥ 0	Vézina and Pace (1994)
	Gross production efficiency	Both	Sum of respiration, excretion, and ejection by mesozooplankton ranges between 50% and 75% of total ingestion.	0.50 (TotIng) – (Res + CproTOdoc + CmesTOdet) ≤ 0 0.75 (TotIng) – (Res + CmesTOdoc + CmesTOdet) ≥ 0	Vézina et al. (2000)
	Ingestion	Upper	Total ingestion of mesozooplankton does not exceed maximum specific ingestion (function of body mass (W) and temperature (T) × biomass (B))	Max spe ing = $63W^{-0.25}\ e^{0.0693(T-20)}$ (B × Max spe ing)– TotIng≤ 0	Vézina and Pace (1994)according to Moloney and Field (1989)
	Assimilation efficiency	Both	Assimilation efficiency of mesozooplankton ranges between 50% and 80% of total ingestion	– 0.50 TotIng – CmesTOdet ≤ 0 – 0.20 TotIng – CmesTOdet ≥ 0	Vézina and Platt (1988)

Table 2: Inequalities table modified from Niquil et al. 2011.

4. RESULTS

4.1 LIM - MN

In this section the solutions of the LIM – MN technique will be reported and described.

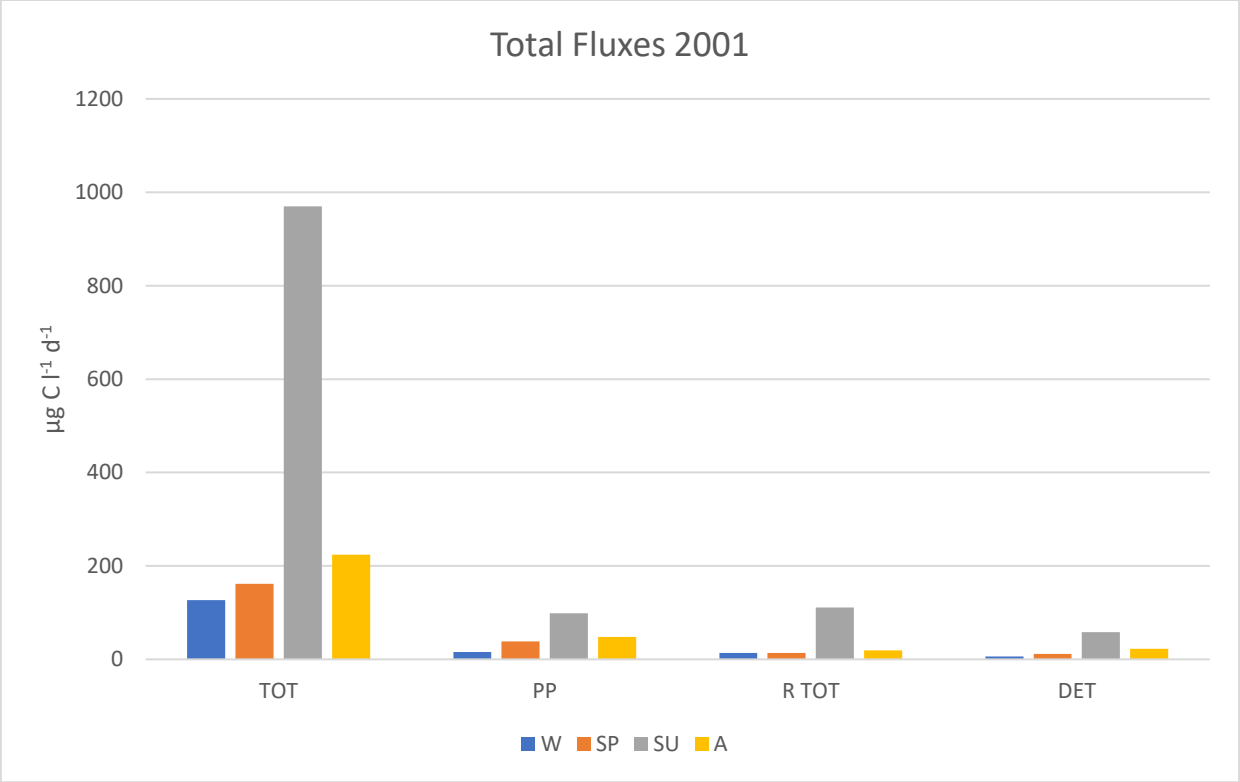

Figure 3: Total Carbon fluxes 2001 in µg C l^{-1} d^{-1}.

There is a great difference in the sum of certain total carbon fluxes during the year (Figure 3). The highest level of total carbon exchanged (which is equal to the sum of the whole fluxes in the selected season) is in summer with a total of 969.6 µg C l^{-1} d^{-1}, while the minimum is in winter with 127.1 µg C l^{-1} d^{-1}. Spring value is near to winter value with 161.9 µg C l^{-1} d^{-1}, followed by the autumn value of 224.3 µg C l^{-1} d^{-1}. Similar trends are designed for the total gross primary production and the total respiration of the entire food web. The total gross primary production is maximum in summer with a value of 98.4 µg C l^{-1} d^{-1}, sinking to a lower level in autumn and spring with a value of 47.1 µg C l^{-1} d^{-1} and 38.2 µg C l^{-1} d^{-1} respectively, and reaching the minimum of 15.8 µg C l^{-1} d^{-1} in winter. Total respiration goes from 110.8 µg C l^{-1} d^{-1} in summer to 13.41 µg C l^{-1} d^{-1} in spring, nearly coupled with the winter value of 13.8 µg C l^{-1} d^{-1}, while the value is about 19 µg C l^{-1} d^{-1} in autumn.

	FLUXES	LSEI_W	LSEI_SP	LSEI_SU	LSEI_A
1	CO2_CB	3.98	14.03	77.17	16.43
2	CB_DOC	0.38	1.72	7.33	2.56
3	CB_CO2	0.20	0.70	3.86	0.82
4	CB_DET	0.00	2.07	0.00	5.79
5	CB_HNF	0.38	0.25	37.75	1.46
6	CB_MIZ	3.02	7.21	28.23	0.00
7	CB_GR	0.00	2.07	0.00	5.79
8	CO2_AN	11.72	14.29	11.24	17.00
9	AN_DOC	1.11	1.36	1.07	2.67
10	AN_CO2	0.59	0.71	0.56	0.85
11	AN_DET	0.00	1.03	0.00	4.97
12	AN_MIZ	6.46	2.43	9.61	3.38
13	AN_MEZ	3.56	6.11	0.00	0.16
14	AN_GR	0.00	2.65	0.00	4.97
15	CO2_MP	0.14	9.95	10.04	14.49
16	MP_DOC	0.05	1.08	0.95	2.89
17	MP_CO2	0.04	0.50	0.50	0.72
18	MP_DET	0.02	3.00	0.00	4.79
19	MP_MIZ	0.00	0.49	8.58	0.00
20	MP_MEZ	0.00	1.90	0.00	1.29
21	MP_GR	0.02	3.00	0.00	4.79
22	HB_CO2	7.08	6.53	59.11	10.25
23	HB_DOC	10.09	9.79	84.29	14.61
24	HB_DET	0.00	0.00	0.00	0.00
25	HB_HNF	2.54	0.00	36.75	9.94
26	HB_MIZ	9.83	0.00	53.44	11.34
27	HB_GR	4.80	16.32	53.21	3.58
28	HNF_CO2	0.66	0.05	17.09	2.74
29	HNF_DOC	0.62	0.03	17.09	2.74
30	HNF_DET	0.63	0.05	21.69	2.77
31	HNF_MIZ	0.77	0.00	8.84	0.00
32	HNF_GR	0.24	0.12	0.35	3.16
33	MIZ_CO2	4.38	2.38	24.16	3.02
34	MIZ_DOC	5.74	2.38	24.16	3.02
35	MIZ_DET	4.72	2.80	30.06	3.31
36	MIZ_MEZ	0.22	1.76	25.39	1.52
37	MIZ_GR	5.02	0.81	4.94	3.86
38	MEZ_CO2	0.90	2.54	5.52	0.66
39	MEZ_DOC	0.90	2.38	5.52	0.66
40	MEZ_DET	0.96	2.40	6.79	0.80
41	MEZ_GR	1.01	2.45	7.57	0.85
42	DET_HNF	0.00	0.00	0.00	0.00
43	DET_MIZ	0.00	0.00	0.00	0.00
44	DET_MEZ	0.00	0.00	0.00	0.00
45	DOC_HB	34.34	32.64	286.80	49.72

Table 3: Carbon Fluxes 2001 in µg C l^{-1} d^{-1}.

Total fluxes to the detritus are characterized by a high value in summer, with 58.5 µg C l^{-1} d^{-1}, followed by 22.4 µg C l^{-1} d^{-1} in autumn, 11.3 µg C l^{-1} d^{-1} in spring and the minimum in winter with 6.3 µg C l^{-1} d^{-1}.

0 fluxes are always present in all the seasons: they vary from a number of seven in spring and autumn to ten in winter and twelve in summer. There are some fluxes that are always settled to 0 µg C l^{-1} d^{-1} as the particulate ingestion fluxes of heterotrophic nanoplankton, microzooplankton and mesozooplankton and the flux from heterotrophic bacteria to detritus. Most of the other 0 fluxes are mostly concentrated in winter and summer. Some of them are fluxes directed to the detritus as those ones of cyanobacteria and autotrophic nanoplankton, both in winter and in summer, coupled in both cases to the flux and to the growth compartment. MP to detritus and to GR in summer are null, too. The remaining fluxes settled to 0 µg C l^{-1} d^{-1} are predation fluxes: the ingestion of MIZ and MEZ on MP in winter, the predation of HNF and MIZ on HB and MIZ ingestion of HNF in spring. The predation of MEZ on AN and MP are null in summer. In autumn only MIZ predation on CB, MP and HNF are 0 µg C l^{-1} d^{-1}.

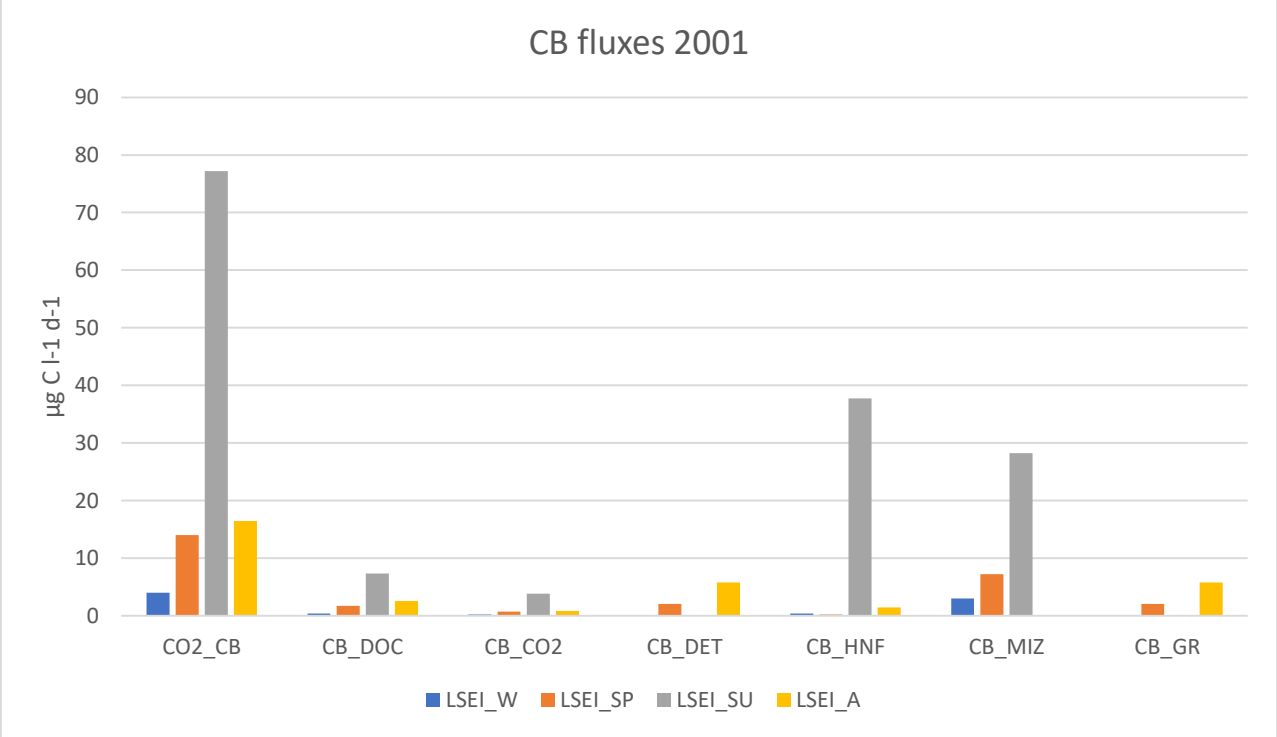

Figure 4: CB Carbon Fluxes 2001 in µg C l^{-1} d^{-1}.

Considering cyanobacteria (Figure 4), the highest flux detected is gross primary production in summer with a value of 77.1 µg C l^{-1} d^{-1}, while the minimum is in winter with 3.9 µg C l^{-1} d^{-1}. In spring and autumn gross primary production has similar values with 14 µg C l^{-1} d^{-1} in spring and 16.4 µg C l^{-1} d^{-1} in autumn. The highest predatory pressure is carried out by HNF and MIZ in summer with 37.75 µg C l^{-1} d^{-1} and 28.23 µg C l^{-1} d^{-1} respectively. MIZ predation is also relatively high in spring with 7.2 µg C l^{-1} d^{-1}. Fluxes to growth compartment are present in spring and summer with 2 µg C l^{-1} d^{-1} and 5.7 µg C l^{-1} d^{-1} respectively. Excretion of DOC is higher in summer with 7.3 µg C l^{-1} d^{-1} with a minimum of 0.3 µg C l^{-1} d^{-1} in winter. Detritus fluxes are detected in spring and autumn with 2 µg C l^{-1} d^{-1} and 5.7 µg C l^{-1} d^{-1} respectively.

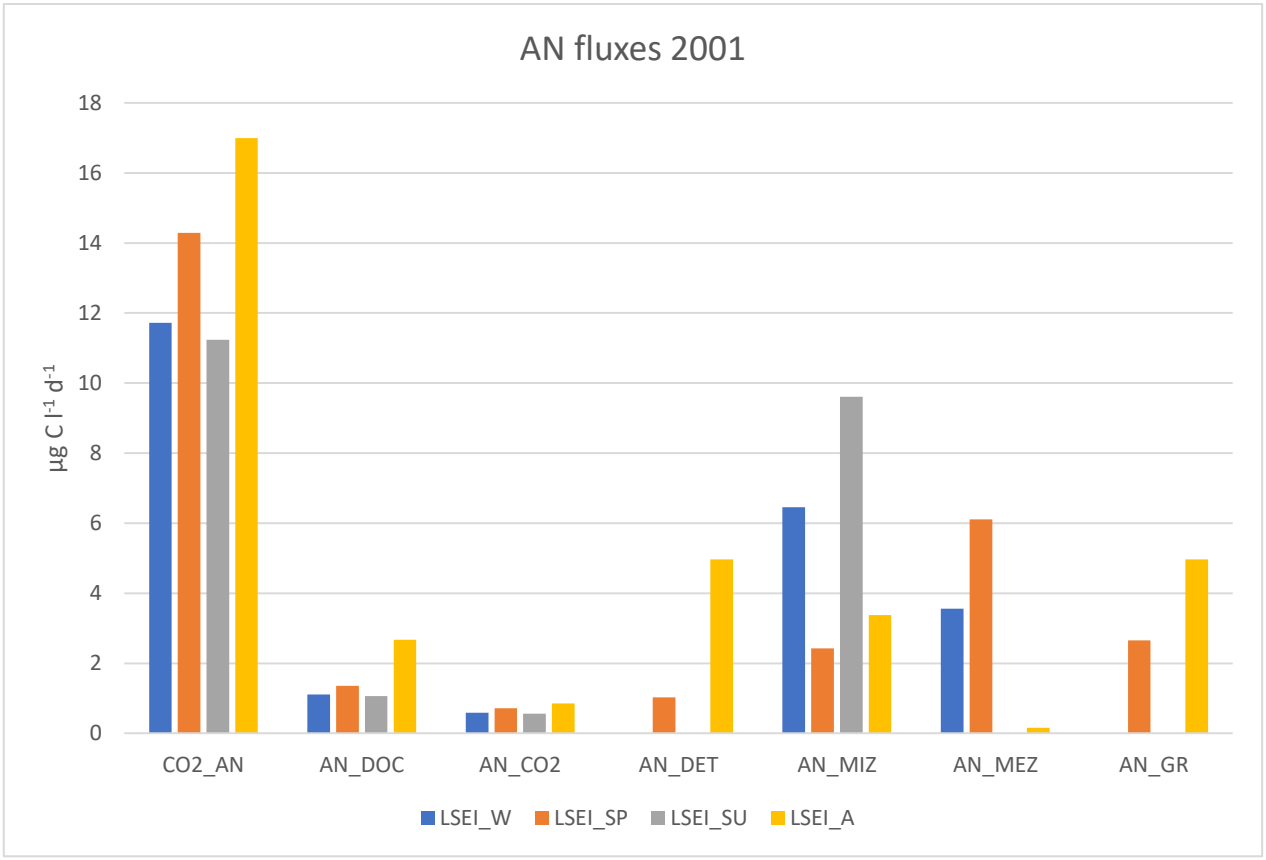

Figure 5: AN Carbon Fluxes 2001 in µg C l^{-1} d^{-1}.

Autotrophic nanoplankton is characterised by comparable levels of primary production during the year (Figure 5): the maximum value is autumn with 16.99 µg C l^{-1} d^{-1} and the minimum one is in summer with 11.23 µg C l^{-1} d^{-1}, passing through 11.7 µg C l^{-1} d^{-1} and 14.29 µg C l^{-1} d^{-1} in winter and

spring respectively. Doc exudation is nearly constant during the year (from 1.06 µg C l^{-1} d^{-1} to 1.3 µg C l^{-1} d^{-1}), with a peak of 2.6 µg C l^{-1} d^{-1}in autumn. Respiration fluxes are low during the year, going from a minimum of 0.56 µg C l^{-1} d^{-1} in summer to a maximum of 0.8 µg C l^{-1} d^{-1} in autumn. MIZ predatory pressure have a maximum in summer with 9.61 µg C l^{-1} d^{-1} and a minimum in spring with 2.43 µg C l^{-1} d^{-1}, while during winter and autumn they are about 6.46 and 3.38 µg C l^{-1} d^{-1} respectively. The predation behaviour of MEZ is opposite to the one of MIZ, with a maximum of 6.11 µg C l^{-1} d^{-1} in spring, a minimum of 0.15 µg C l^{-1} d^{-1} in autumn and 3.56 µg C l^{-1} d^{-1} in winter. Detritus fluxes vary from 4.9 µg C l^{-1} d^{-1} in autumn to 1.03 µg C l^{-1} d^{-1} in spring. Autumn growth flux is higher (4.9 µg C l^{-1} d^{-1}) than spring growth flux (2.65 µg C l^{-1} d^{-1}).

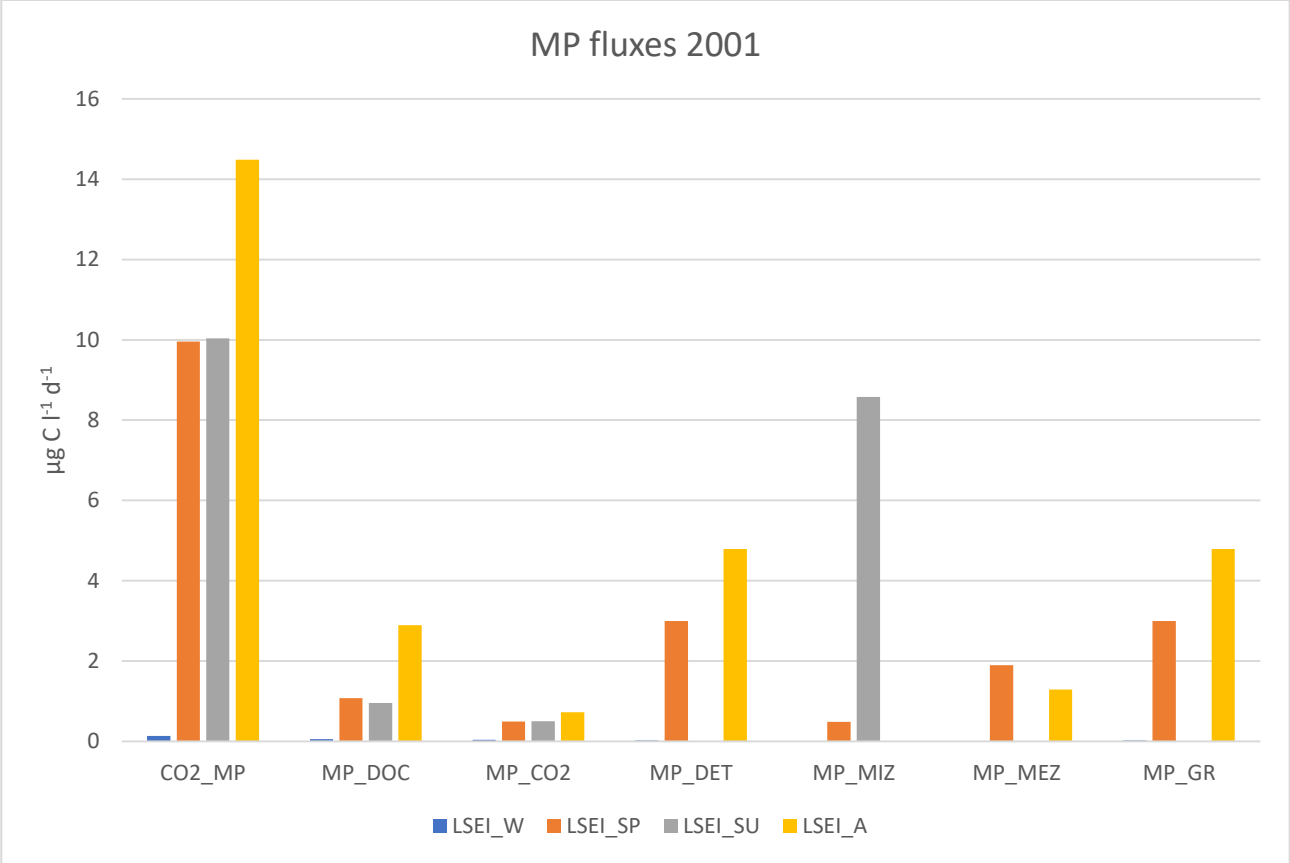

Figure 6: MP Carbon Fluxes 2001 in µg C l^{-1} d^{-1}.

Microphytoplankton gross primary production (Figure 6) grows during the year from 0.13 µg C l^{-1} d^{-1} in winter to 9.95 µg C l^{-1} d^{-1} in spring, 10.03 µg C l^{-1} d^{-1} in summer and 14.48 µg C l^{-1} d^{-1} in autumn. Respiration flux keeps a similar trend, with a minimum of 0.04 µg C l^{-1} d^{-1} in winter, 0.49 µg C l^{-1} d^{-}

^{1} in spring, 0.50 µg C l^{-1} d^{-1} in summer and a maximum of 0.72 µg C l^{-1} d^{-1} in autumn. Excretion of DOC varies from 0.05 µg C l^{-1} d^{-1} in winter to 2.88 µg C l^{-1} d^{-1} in autumn, with 1.07 µg C l^{-1} d^{-1} and 0.95 in spring and summer respectively. Predation by MIZ has a peak in summer with 8.58 µg C l^{-1} d^{-1}, while the MIZ maximum is in spring with 1.9 µg C l^{-1} d^{-1}. Growth flux varies from 4.79 µg C l^{-1} d^{-1} in autumn to 0.02 µg C l^{-1} d^{-1} in spring. Similar values are observed for the detritus fluxes, with 4.79 µg C l^{-1} d^{-1} in autumn and 0.02 µg C l^{-1} d^{-1} in winter.

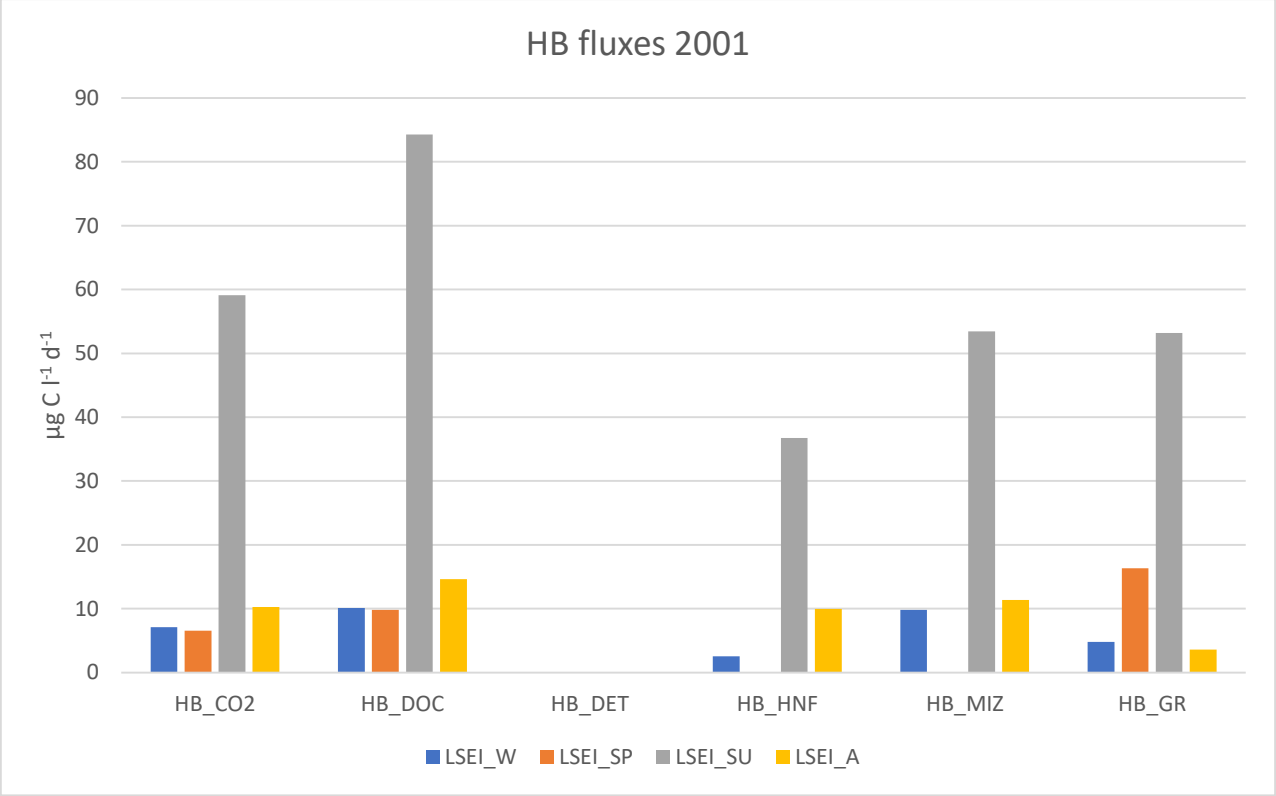

Figure 7: HB Carbon Fluxes 2001 in µg C l^{-1} d^{-1}.

Coming to speak of heterotrophic compartment, heterotrophic bacteria (Figure 7) are the compartment which is better described by field data as secondary production fluxes and predation fluxes have been directly detected by in situ measurements. Summer is the season in which carbon fluxes through the heterotrophic bacteria compartment are important in term of carbon. Maximum values are registered in this season as 286.8 µg C l^{-1} d^{-1} of DOC uptake, 84.28 µg C l^{-1} d^{-1} of DOC excretion, 59.11 µg C l^{-1} d^{-1} of respiration flux and 53.21 µg C l^{-1} d^{-1} of growth flux. In this period predation pressure gets to its maximum value, varying from 36.75 µg C l^{-1} d^{-1} by HNF to 53.44 by

MIZ. In the other seasons, fluxes are lower than summer fluxes. Doc uptake has similar values in winter and spring with 34.34 µg C l^{-1} d^{-1} and 32.64 µg C l^{-1} d^{-1} respectively. While it is a little higher in autumn with 49.72 µg C l^{-1} d^{-1}. Respiration fluxes go from 6.52 µg C l^{-1} d^{-1} in spring to 7.07 µg C l^{-1} d^{-1} in winter, with a higher value in autumn (10.24 µg C l^{-1} d^{-1}). Doc excretion has similar values in winter (10.09 µg C l^{-1} d^{-1}) and spring (9.79 µg C l^{-1} d^{-1}), and is higher in autumn (14.61 µg C l^{-1} d^{-1}). Growth fluxes are higher in spring with 16.32 µg C l^{-1} d^{-1}, lower in winter with 4.8 µg C l^{-1} d^{-1} and autumn 3.58 µg C l^{-1} d^{-1}. HNF predation in autumn (9.94 µg C l^{-1} d^{-1}) is three times higher than in winter (2.54 µg C l^{-1} d^{-1}), while MIZ predation flux is nearly the same in autumn (11.34 µg C l^{-1} d^{-1}) and in winter (9.83 µg C l^{-1} d^{-1}).

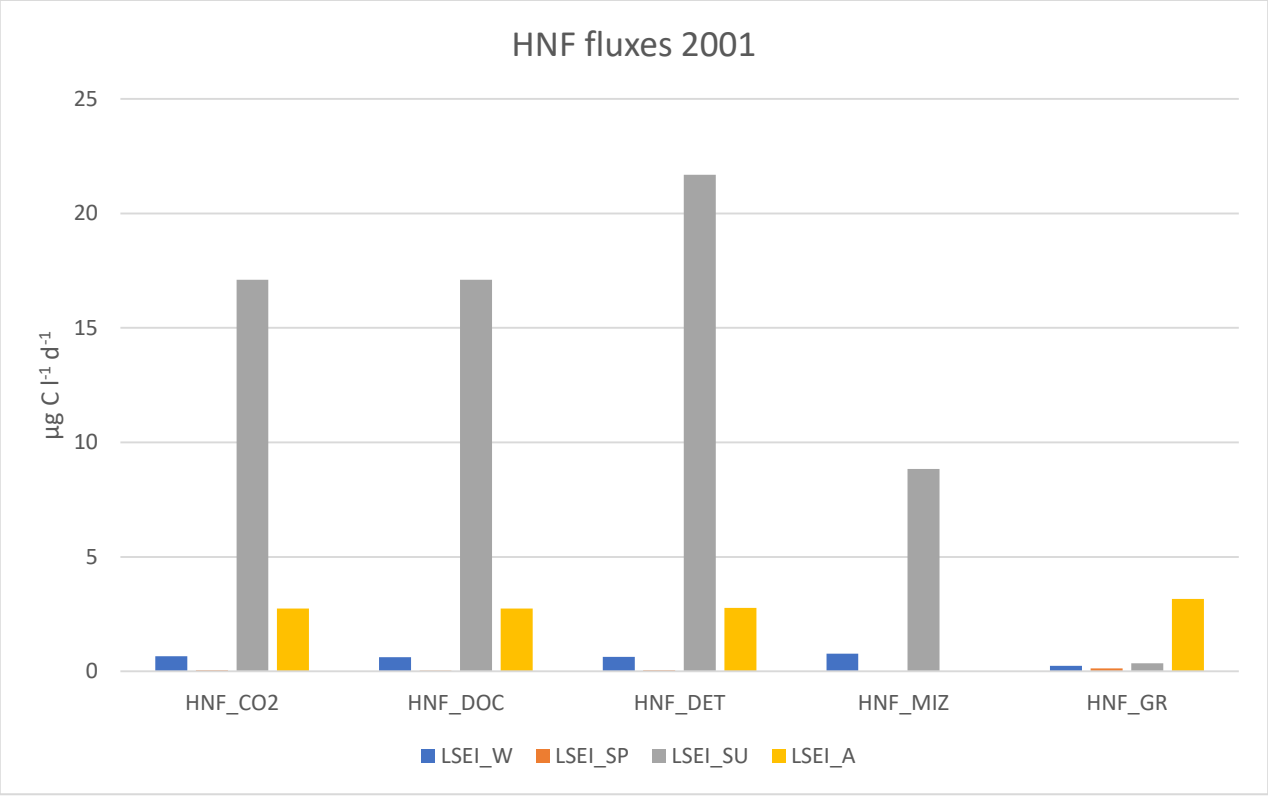

Figure 8: HNF Carbon Fluxes 2001 in µg C l^{-1} d^{-1}.

Heterotrophic nano flagellates respiration and DOC excretion fluxes have similar trends during the year (Figure 8). The maximum value is in summer, both with 19.02 µg C l^{-1} d^{-1} and the minimum values are in spring with 0.04 µg C l^{-1} d^{-1} and 0.02 µg C l^{-1} d^{-1} respectively . Similar values are in winter with 0.66 µg C l^{-1} d^{-1} and 0.62 µg C l^{-1} d^{-1}, and they have the same value with 2.73 µg C l^{-1} d^{-1}

^{1} in autumn again. Detritus fluxes vary a lot during the year: summer value is about 21.68 µg C l^{-1} d^{-1}, while winter, spring and autumn values are 0.62 µg C l^{-1} d^{-1}, 0.045 µg C l^{-1} d^{-1} and 2.76 µg C l^{-1} d^{-1} respectively. Predation by MIZ is about 8.84 µg C l^{-1} d^{-1} in summer and 0.77 µg C l^{-1} d^{-1} in winter. The fluxes to the growth compartment vary from 3.16 µg C l^{-1} d^{-1} in autumn to 0.12 µg C l^{-1} d^{-1} in spring (0.24 µg C l^{-1} d^{-1} in winter and 0.35 µg C l^{-1} d^{-1} in summer).

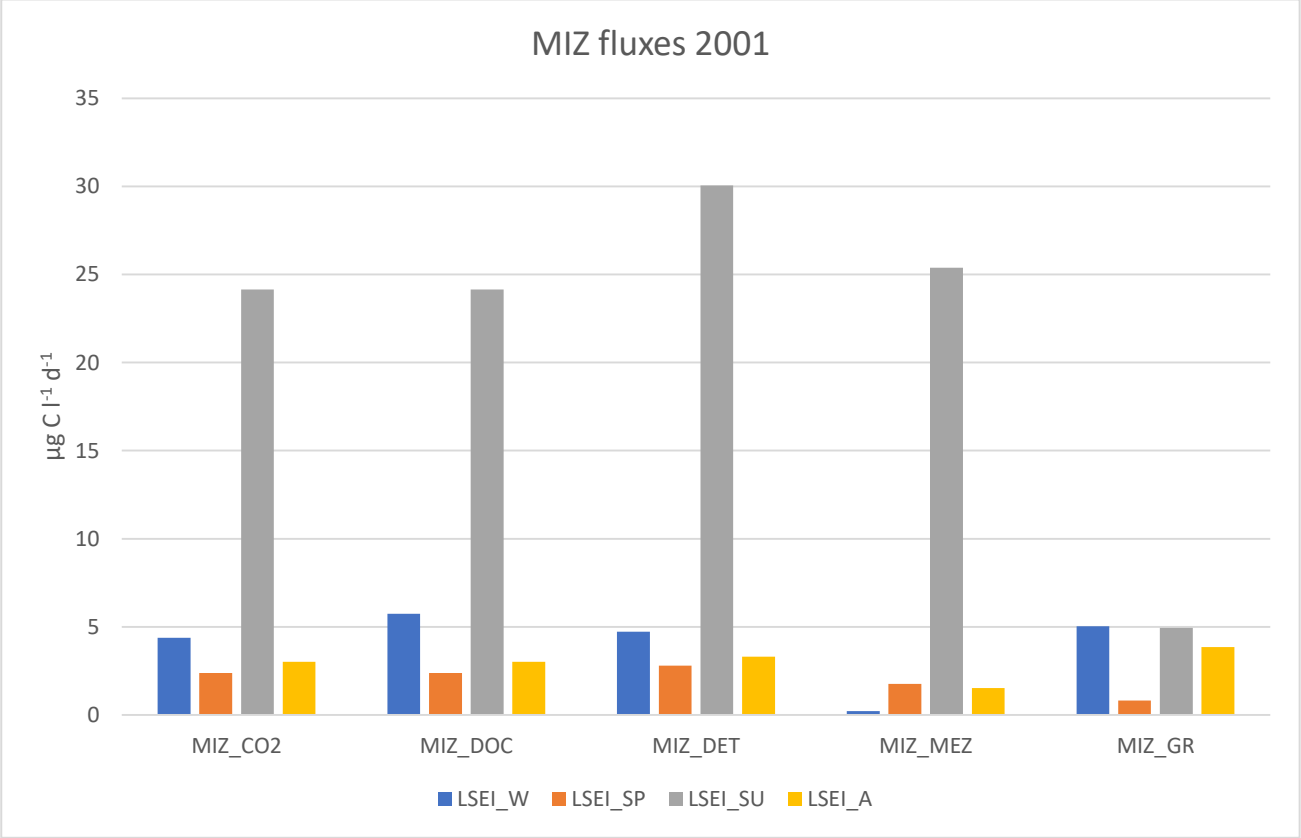

Figure 9: MIZ Carbon Fluxes 2001 in µg C l^{-1} d^{-1}.

Microzooplankton group (Figure 9) is characterized by high fluxes values in summer. Respiration values vary from 24.15 µg C l^{-1} d^{-1} in summer to 2.38 µg C l^{-1} d^{-1} in spring. Autumn value is near to the spring one (3.01 µg C l^{-1} d^{-1}), while winter respiration is a little higher (4.37 µg C l^{-1} d^{-1}). Except for the winter value (5.74 µg C l^{-1} d^{-1}), doc excretion values are the same as those of the respiration flux. Detritus flux is lower in spring (2.79 µg C l^{-1} d^{-1}) and it is maximum in summer (30.05 µg C l^{-1} d^{-1}). Predation by MEZ is active principally in summer with 25.39 µg C l^{-1} d^{-1}, while it is very low during the other seasons (0.22 µg C l^{-1} d^{-1} in winter, 1.76 µg C l^{-1} d^{-1} in spring and 1.52 µg C l^{-1} d^{-1} in

autumn). Fluxes directed to the growth compartment have a different trend: the maximum value is in winter with 5.02 µg C l^{-1} d^{-1} and the minimum one is in spring with 0.81 µg C l^{-1} d^{-1} (4.94 µg C l^{-1} d^{-1} in summer and 3.85 µg C l^{-1} d^{-1} in autumn).

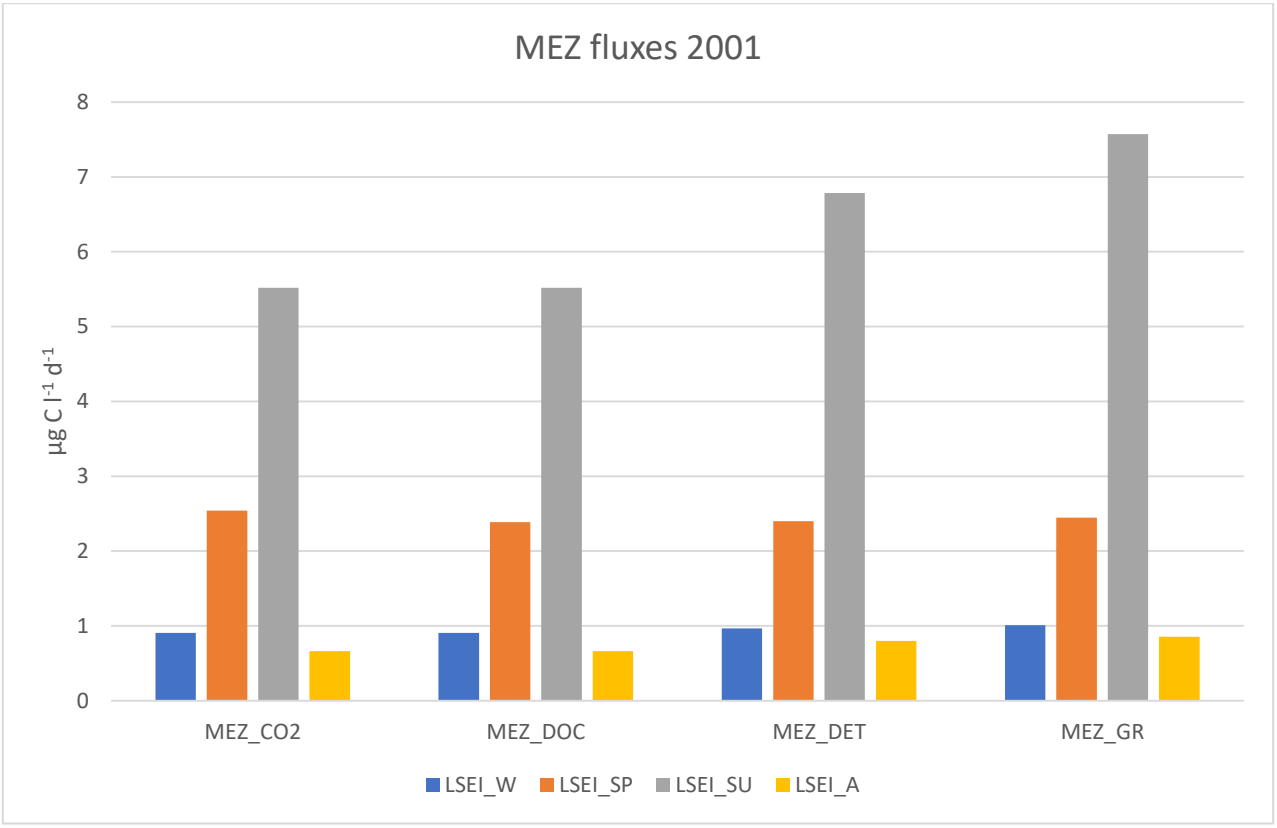

Figure 10: MEZ Carbon Fluxes 2001 in µg C l^{-1} d^{-1}.

Mesozooplankton fluxes have similar values during each season (Figure 10), except for the summer ones that vary. In spring respiration and doc excretion have the same value (0.90 µg C l^{-1} d^{-1}) while fluxes to the detritus and to growth are slightly different: 0.96 µg C l^{-1} d^{-1} and 1 µg C l^{-1} d^{-1} respectively. A similar trend is observed in summer with 5.51 µg C l^{-1} d^{-1} for respiration and doc excretion, 6.78 µg C l^{-1} d^{-1} for detritus flux and 7.57 µg C l^{-1} d^{-1} for the growth flux. In spring and autumn fluxes values are similar: 2.54 µg C l^{-1} d^{-1}, 2.38 µg C l^{-1} d^{-1}, 2.39 µg C l^{-1} d^{-1} and 2.44 µg C l^{-1} d^{-1} in spring, 0.66 µg C l^{-1} d^{-1}, 0.66 µg C l^{-1} d^{-1}, 0.79 µg C l^{-1} d^{-1} and 0.85 µg C l^{-1} d^{-1} in autumn.

As it can be seen in Figure 11, carbon fluxes values varied a lot during the year 2001.

In the autotrophic compartments, higher values are related to primary production fluxes, generally followed by predatory fluxes, respiration and dissolved organic carbon fluxes. In the heterotrophic compartments higher values are related to respiration terms and ingestion ones.

During summer the compartment with higher carbon fluxes are Bacteria compartments, both autotrophic and heterotrophic ones, followed by HNF compartment. Autumn is characterised by HB and HNF compartment carbon fluxes, while in spring MP and HB compartments are the ones with the major fluxes. Winter is characterised by AN and HB compartment in terms of carbon values.

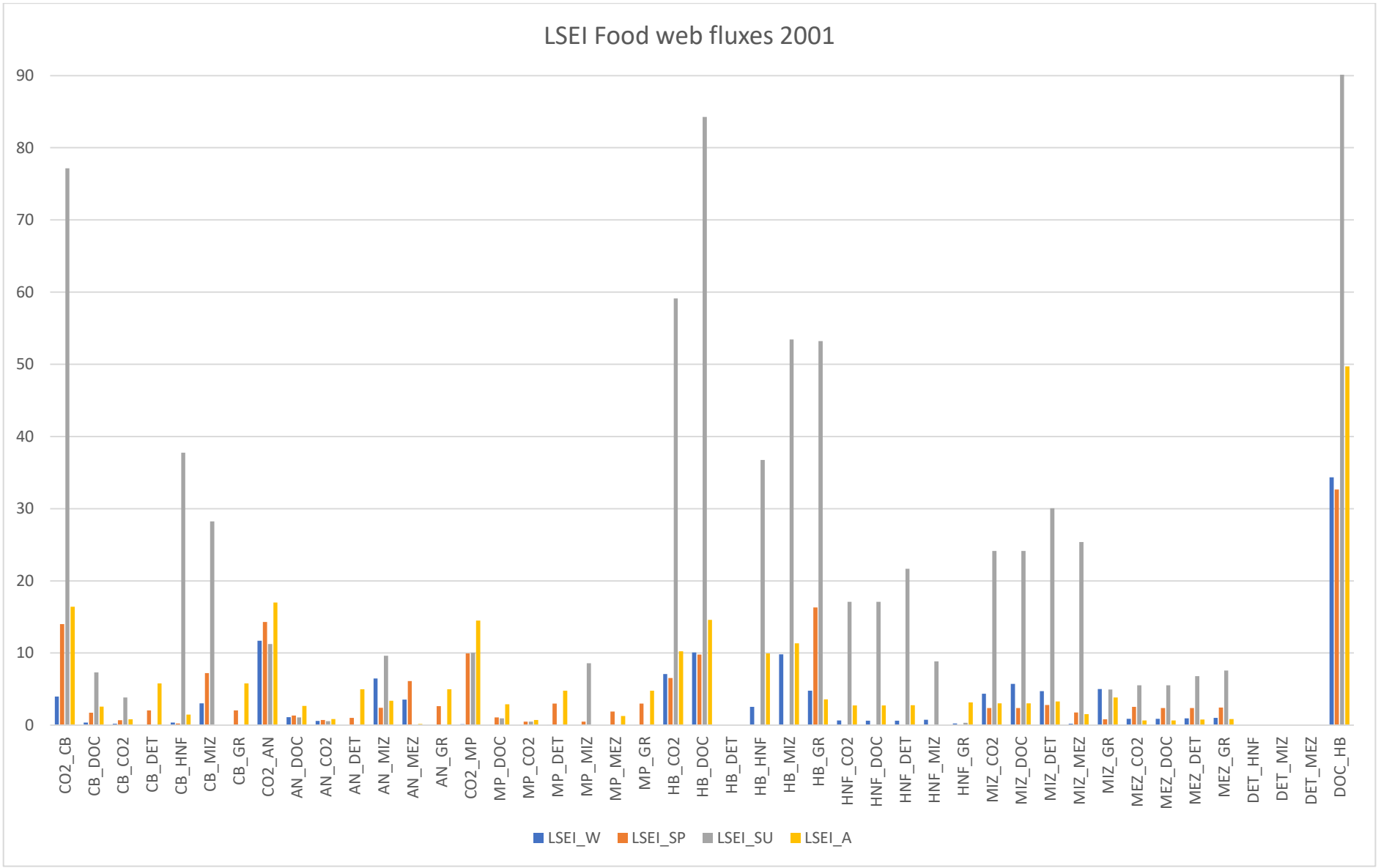

Figure 11: LSEI Food web Carbon fluxes 2001 in µg C l^{-1} d^{-1}

4.2 LIM - MCMC

In this section the solution of the LIM – MCMC technique is reported and described.

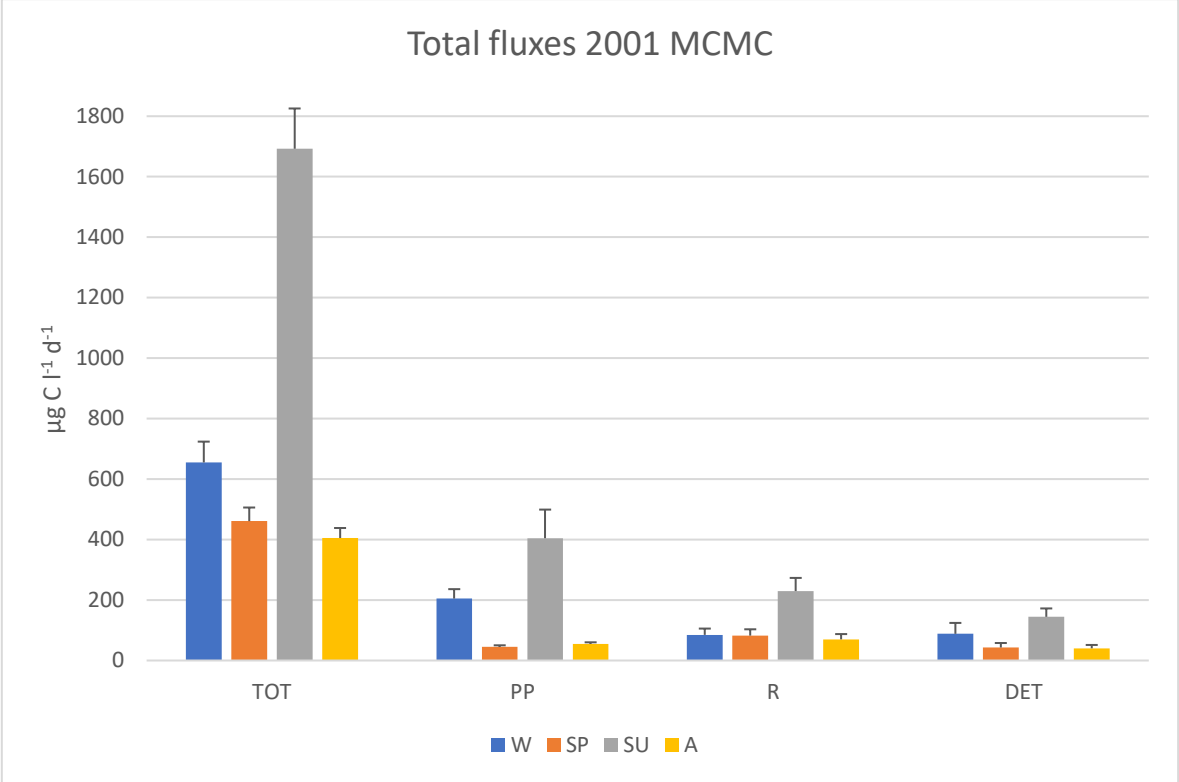

Figure 12: Total Carbon fluxes 2001 in µg C l^{-1} d^{-1}.

In figure 12 the sum of certain total fluxes relevant for the analysis of the food web is reported, which were obtained with the LIM – MCMC technique. At a first glance it is important to realize the great differences of Carbon values during the year, except for summer values that are always higher than the others. The total carbon exchanged (that is equal to the sum of the whole fluxes in the selected season), has its maximum value in summer with 1692.38 ± 133.2 µg C l^{-1} d^{-1} and the minimum one in autumn with 405.07 ± 33.14 µg C l^{-1} d^{-1}. Spring value is near the autumn one with 460.9 ± 45.05 µg C l^{-1} d^{-1} but less than the winter value that is 654.98 ± 68.85 µg C l^{-1} d^{-1}. Total gross primary production is low in spring with 44.97 ± 5.36 µg C l^{-1} d^{-1} and has a similar value in autumn with 55.01 ± 5.14 µg C l^{-1} d^{-1}. Higher values are registered in winter with 204.79 ± 31.24 µg C l^{-1} d^{-1}, and the maximum one is in summer with 404.38 ± 94 µg C l^{-1} d^{-1}. Respiration fluxes have similar values in winter and spring, with 84.83 ± 20.78 µg C l^{-1} d^{-1} and 82.30 ± 20.95 µg C l^{-1} d^{-1} respectively. The lowest value is in autumn with 69.90 ± 17.55 µg C l^{-1} d^{-1}, while the highest one is in summer with 229.56 ± 43.55 µg C l^{-1} d^{-1}. In spring and autumn, fluxes to detritus assume similar value with 42.96 ± 14.96 µg C l^{-1} d^{-1} and 40.38 ± 11.07 µg C l^{-1} d^{-1}. Higher values are registered in winter with 88.24 ± 36.12 µg C l^{-1} d^{-1}, while the maximum is in summer with 144.47 ± 27.79 µg C l^{-1} d^{-1}.

	FLUXES	MCMC_M_W	SD_W	MCMC_M_SP	SD_SP	MCMC_M_SU	SD_SU	MCMC_M_A	SD_A
1	CO2_CB	24,27	4,14	18,99	3,66	286,49	93,49	22,88	3,37
2	CB_DOC	5,97	2,87	3,27	1,64	89,02	53,56	5,16	2,45
3	CB_CO2	3,90	1,88	3,68	1,80	48,25	25,15	3,99	1,87
4	CB_DET	5,53	3,93	1,79	1,56	28,30	21,77	4,22	3,27
5	CB_HNF	0,38	0,00	1,74	1,56	37,75	0,00	1,46	0,00
6	CB_MIZ	3,02	0,00	7,21	0,00	28,23	0,00	3,86	3,03
7	CB_GR	5,57	3,89	1,79	1,57	54,95	36,00	4,36	3,26
8	CO2_AN	18,35	1,51	18,55	3,55	48,45	6,89	20,44	3,26
9	AN_DOC	3,17	1,36	3,28	1,66	11,35	5,33	4,73	2,26
10	AN_CO2	2,47	1,21	3,62	1,75	7,79	3,75	3,59	1,68
11	AN_DET	1,59	1,31	1,76	1,57	10,31	7,08	4,26	2,98
12	AN_MIZ	6,46	0,00	2,43	0,00	9,61	0,00	3,38	0,00
13	AN_MEZ	3,56	0,00	6,11	0,00	0,85	0,74	0,60	0,48
14	AN_GR	1,59	1,31	1,83	1,59	8,61	6,50	4,03	2,98
15	CO2_MP	162,18	30,93	7,43	1,69	69,44	13,63	11,69	2,12
16	MP_DOC	40,83	19,73	1,68	0,88	16,81	8,49	2,69	1,34
17	MP_CO2	27,16	13,18	1,31	0,64	11,44	5,41	1,91	0,92
18	MP_DET	51,13	34,54	1,32	1,07	15,29	10,73	2,32	1,84
19	MP_MIZ	2,69	1,95	0,49	0,00	8,58	0,00	2,20	1,77
20	MP_MEZ	2,07	1,39	1,90	0,00	0,86	0,75	0,55	0,45
21	MP_GR	38,31	32,11	1,31	1,06	16,50	11,03	2,34	1,84
22	HB_CO2	41,09	15,87	57,49	20,71	117,67	34,94	46,66	17,29
23	HB_DOC	20,85	14,33	29,92	19,29	66,71	33,90	21,94	13,52
24	HB_DET	17,98	9,47	21,59	14,18	14,53	10,51	14,52	9,41
25	HB_HNF	2,54	0,00	12,71	8,93	36,75	0,00	9,94	0,00
26	HB_MIZ	9,83	0,00	2,00	1,71	53,44	0,00	11,34	0,00
27	HB_GR	4,80	0,00	16,32	0,00	53,21	0,00	3,58	0,00
28	HNF_CO2	2,64	1,10	9,34	1,66	16,07	0,61	4,40	0,61
29	HNF_DOC	1,43	0,66	6,21	2,00	11,69	2,48	2,95	0,85
30	HNF_DET	1,75	0,94	8,67	3,85	28,30	2,64	4,01	1,67
31	HNF_MIZ	0,77	0,00	2,10	1,76	8,64	0,14	3,37	2,25
32	HNF_GR	0,24	0,00	11,41	4,66	0,35	0,00	3,51	2,30
33	MIZ_CO2	5,72	0,45	4,43	0,85	23,00	0,70	8,78	1,29
34	MIZ_DOC	2,91	1,97	2,66	0,81	17,03	3,52	5,71	1,65
35	MIZ_DET	8,01	2,05	4,73	1,28	40,51	3,76	10,36	2,89
36	MIZ_MEZ	0,22	0,00	1,76	0,00	22,20	1,04	0,65	0,51
37	MIZ_GR	8,71	2,11	0,81	0,00	4,94	0,00	11,60	3,31
38	MEZ_CO2	1,86	0,24	2,42	0,17	5,35	0,24	0,57	0,07
39	MEZ_DOC	1,22	0,34	1,66	0,39	3,76	0,83	0,38	0,10
40	MEZ_DET	2,24	0,59	3,10	0,64	7,23	1,44	0,69	0,18
41	MEZ_GR	2,66	1,14	3,65	1,19	8,49	1,76	1,19	0,77
42	DET_HNF	5,33	2,73	23,28	11,01	0,39	0,37	6,70	3,12
43	DET_MIZ	2,80	1,99	2,05	1,75	0,10	0,10	12,96	6,80
44	DET_MEZ	2,12	1,41	1,07	0,65	0,89	0,77	0,65	0,50
45	DOC_HB	97,07	18,59	140,02	26,71	342,25	22,27	107,95	18,11

Table 4: Carbon Fluxes MCMC 2001 in µg C l^{-1} d^{-1}.

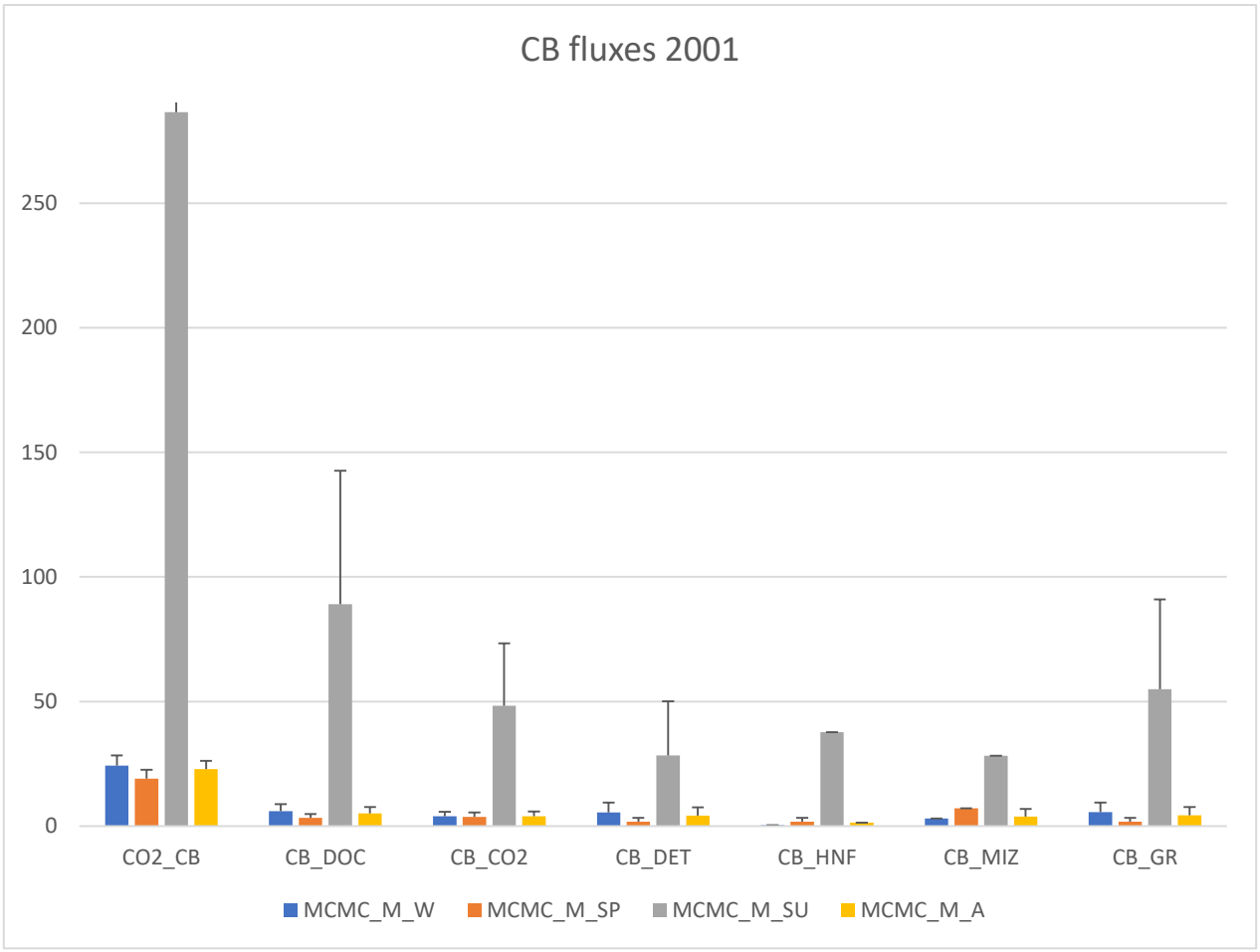

Figure 13: CB Carbon Fluxes MCMC 2001 in µg C l^{-1} d^{-1}.

Summer is the season when the maximum values of carbon for each flow of the cyanobacteria compartment (Figure 13) are registered. Gross primary production in summer is very high, about 286.49 ± 93.49 µg C l^{-1} d^{-1}, while values are similar in the other seasons: 24.26 ± 4.14 µg C l^{-1} d^{-1} in winter, 22.88 ± 3.36 µg C l^{-1} d^{-1} in autumn and 18.99 ± 3.65 µg C l^{-1} d^{-1} in spring. A similar trend is observed for the excretion of DOC, with the maximum in summer (89.01 ± 53.55 µg C l^{-1} d^{-1}) and similar values in winter (5.97 ± 2.86 µg C l^{-1} d^{-1}), autumn (5.15 ± 93.49 µg C l^{-1} d^{-1}) and lower in spring (3.27 ± 1.67 µg C l^{-1} d^{-1}). Respiration fluxes have similar values in winter, autumn and spring, with 3.90 ± 1.88 µg C l^{-1} d^{-1}, 3.68 ± 1.79 µg C l^{-1} d^{-1} and 3.98 ± 1.87 µg C l^{-1} d^{-1}, with the maximum one in summer with 48.25 ± 25.14 µg C l^{-1} d^{-1}. Detritus fluxes vary during the year: the minimum is spring with 1.79 ± 1.56 µg C l^{-1} d^{-1}, the maximum is in summer with 28.30 ± 21.76 µg C l^{-1} d^{-1}, winter value is about 5.53 ± 3.92 µg C l^{-1} d^{-1} and autumn is about 4.22 ± 3.26 µg C l^{-1} d^{-1}. Growth fluxes are like detritus ones (winter 5.56 ± 3.88 µg C l^{-1} d^{-1}, 1.78 ± 1.57 µg C l^{-1} d^{-1}, 3.26 ± 1.79 µg C l^{-1} d^{-1}) except for the one in summer, which is doubled: 54.95 ± 36 µg C l^{-1} d^{-1}. Predation fluxes estimated by the LIM – MCMC are those in spring by HNF with 1.74 ± 1.55 µg C l^{-1} d^{-1} and by MIZ in autumn with 3.85 ± 3.03 µg C l^{-1} d^{-1}.

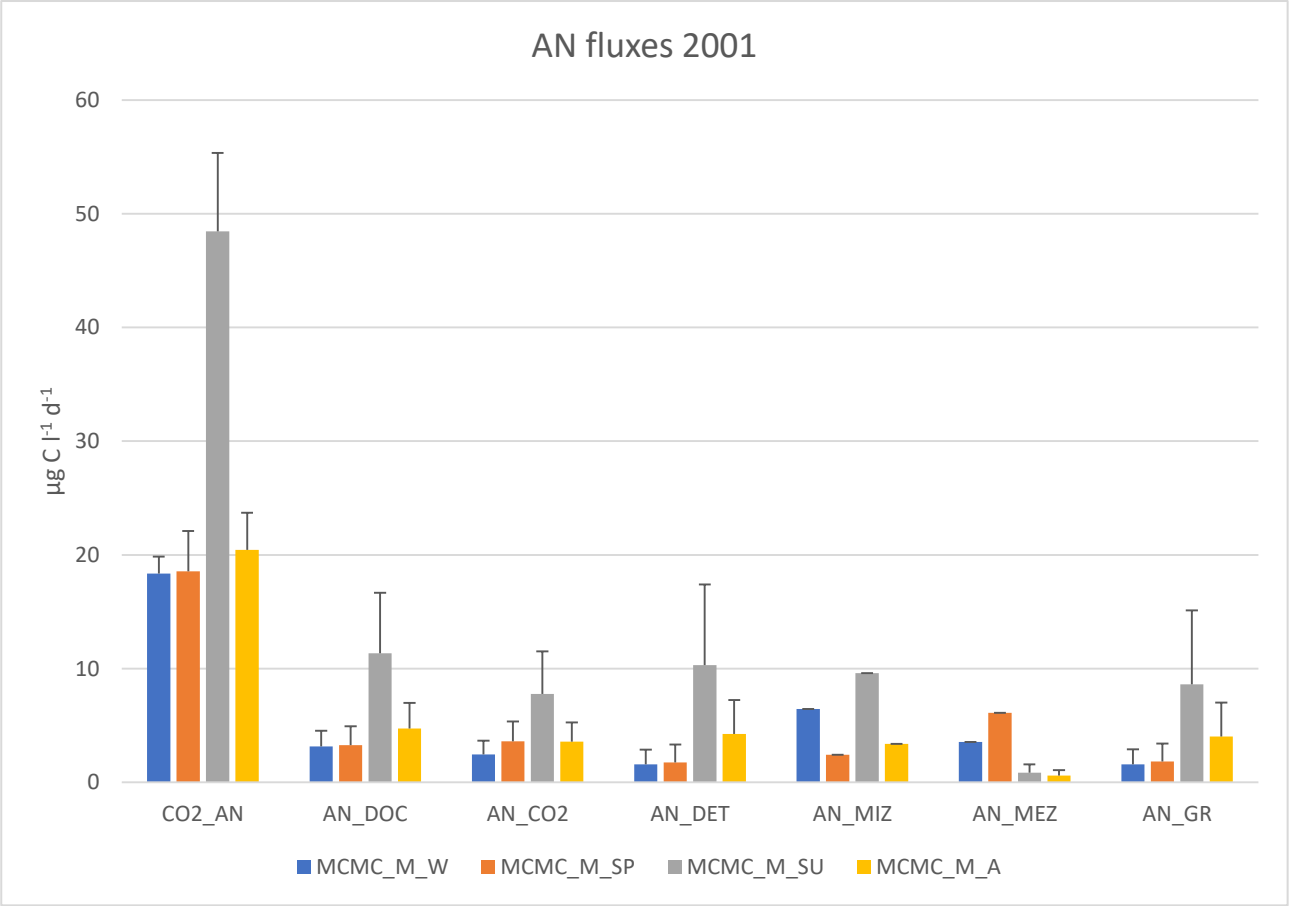

Figure 14: AN Carbon Fluxes MCMC 2001 in µg C l^{-1} d^{-1}.

AN primary production (figure 14) is characterized by a maximum of 48.44 ± 6.88 µg C l^{-1} d^{-1}in summer, similar values in winter (18.35 ± 1.51 µg C l^{-1} d^{-1}) and spring (18.54± 3.54 µg C l^{-1} d^{-1}) and higher ones in autumn (20.44 ± 3.25 µg C l^{-1} d^{-1}). The same trend is observed for DOC excretion, even if with lower values: the maximum is in summer with 11.34 ± 5.32 µg C l^{-1} d^{-1}, the minimum in winter with 3.17 ± 1.51 µg C l^{-1} d^{-1}, similar value in spring (3.27 ± 3.54 µg C l^{-1} d^{-1}) and a higher value in autumn (4.72 ± 2.25 µg C l^{-1} d^{-1}). The same can be said for the respiration flux, detritus flux and the fluxes to the growth compartment. Respiration flux and growth flux have similar values in summer, 7.78 ± 3.74 µg C l^{-1} d^{-1} and 8.6 ± 0.74 µg C l^{-1} d^{-1}, while detritus flux is higher with 10.31 ± 7.08 µg C l^{-1} d^{-1}. Winter detritus flux is equal to winter growth flux, with 1.59 ± 1.30 µg C l^{-1} d^{-1}, while in spring values are similar (1.76 ± 1.56 µg C l^{-1} d^{-1} and 1.82 ± 1.58 µg C l^{-1} d^{-1}). Similar values are shared by the respiration flux in spring (3.62 ± 1.7 µg C l^{-1} d^{-1}) and autumn (3.59 ± 1.68 µg C l^{-1} d^{-1}), detritus flux and growth flux in autumn (4.25 ± 2.98 µg C l^{-1} d^{-1} and 4.03 ± 2.97 µg C l^{-1} d^{-1}). Respiration flux is the lowest in winter with 2.46 ± 1.20 µg C l^{-1} d^{-1}. Predation fluxes obtained by the MCMC are those by MEZ in summer and autumn,0.85 ± 0.74 µg C l^{-1} d^{-1} and 0.59 ± 0.0.48 µg C l^{-1} d^{-1} respectively as the others, both by MIZ and MEZ, were defined by laboratory experiments.

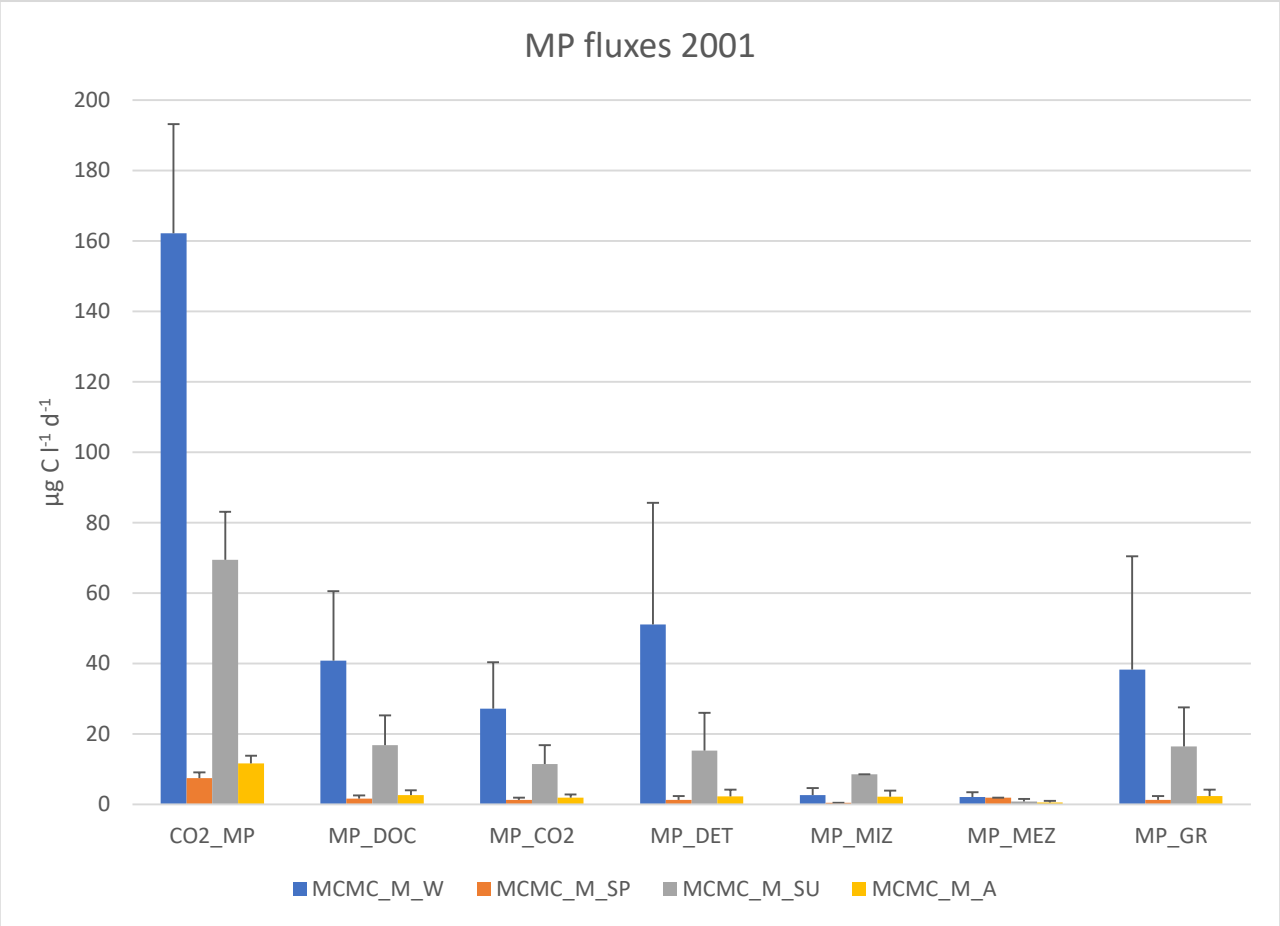

Figure 15: MP Carbon Fluxes MCMC 2001 in µg C l^{-1} d^{-1}.

MP fluxes (Figure 15) during the year are characterized by maximum values in winter followed by summer ones. MP gross primary production is defined by comparable values in spring and autumn with 7.4 ± 1.69 µg C l^{-1} d^{-1} and 11.69 ± 2.12 µg C l^{-1} d^{-1}, while the maximum value is in winter, 162.17 ± 11.69 µg C l^{-1} d^{-1}, followed by 69.44 ± 13.63 µg C l^{-1} d^{-1} in summer. Similar values are depicted in spring for the DOC excretion, respiration, detritus and growth fluxes with 1.67 ± 0.88 µg C l^{-1} d^{-1}, 1.30 ± 0.64 µg C l^{-1} d^{-1}, 1.31 ± 1.06 µg C l^{-1} d^{-1} and 1.30 ± 1.06 µg C l^{-1} d^{-1} respectively. Similar values are obtained in summer between DOC excretion flux (16.80 ± 8.48 µg C l^{-1} d^{-1}), detritus flux (15.29 ± 10.72 µg C l^{-1} d^{-1}) and growth flux (16.49 ± 11.03 µg C l^{-1} d^{-1}), while respiration flux is lower (11.44 ± 5.41 µg C l^{-1} d^{-1}). In winter, fluxes vary a lot, from 40.82 ± 19.72 µg C l^{-1} d^{-1} of DOC excretion and 38.31 ± 32.11 µg C l^{-1} d^{-1} of growth flux to 51.13 ± 34.54 µg C l^{-1} d^{-1} of detritus one and 27.16 ± 13.18 µg C l^{-1} d^{-1} of respiration. In autumn fluxes are very low and similar, with small differences between excretion flux (2.68 ± 1.33 µg C l^{-1} d^{-1}), detritus flux (2.31 ± 1.83 µg C l^{-1} d^{-1}), growth flux (2.33 ± 1.83 µg C l^{-1} d^{-1}) and respiration flux (1.91 ± 0.92 µg C l^{-1} d^{-1}). MIZ predation on MP has similar values in winter and autumn with 2.69 ± 1.94 µg C l^{-1} d^{-1} and 2.19 ± 1.77 µg C l^{-1}

d^{-1} similar to MEZ predation in winter with 2.05 ± 1.38 µg C l^{-1} d^{-1}, while it is lower in summer (0.86 ± 0.74 µg C l^{-1} d^{-1}) and autumn (0.55 ± 0.45 µg C l^{-1} d^{-1}).

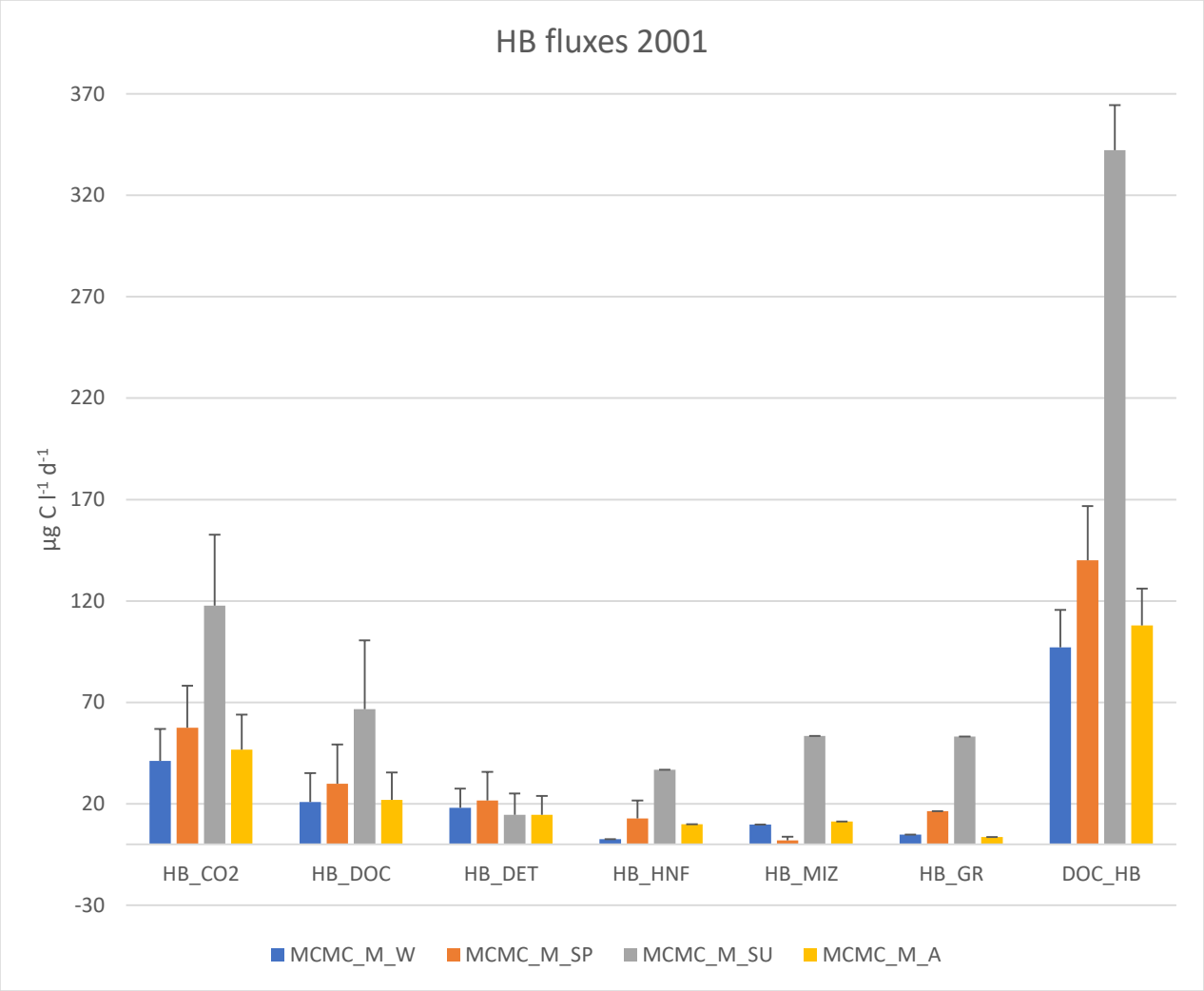

Figure 16: HB Carbon Fluxes MCMC 2001 in µg C l^{-1} d^{-1}.

HB compartment (Figure 16) is the most constrained by *in situ* and laboratory measurements, as growth fluxes and predation ones are known. DOC uptake by HB is the flux that has the highest values during the year: the maximum is in summer with 342.25 ± 22.27 µg C l^{-1} d^{-1}, decreasing to 140.01 ± 26.71 µg C l^{-1} d^{-1} and 107.94 ± 18.11 µg C l^{-1} d^{-1} in spring and autumn, and it reaches the minimum in winter with 97.06 ± 18.58 µg C l^{-1} d^{-1}. Respiration flux has similar values in autumn (46.65 ± 17.28 µg C l^{-1} d^{-1}) and winter (41.08 ± 15.87 µg C l^{-1} d^{-1}), it increases in spring with 57.49 ± 20.71 µg C l^{-1} d^{-1} reaching the maximum in summer (117.66 ± 34.93 µg C l^{-1} d^{-1}). Predation fluxes estimated through the MCMC are those detected in spring by HNF with 12.70 ± 8.9 µg C l^{-1} d^{-1} and by MIZ with 2 ± 1.71 µg C l^{-1} d^{-1}. DOC excretion is maximum in summer with 66.70 ± 33.89 µg C l^{-1} d^{-1}, it decreases in spring (29.92 ± 19.28 µg C l^{-1} d^{-1}) reaching lower values in winter (20.84 ± 14.32 µg C l^{-1} d^{-1}) and autumn (21.93 ± 13.51 µg C l^{-1} d^{-1}). Fluxes to detritus have nearly the same values

in summer and autumn with 14.53 ± 10.51 µg C l^{-1} d^{-1} and 14.51 ± 9.41 µg C l^{-1} d^{-1} respectively, they become higher in winter with 17.98 ± 9.46 µg C l^{-1} d^{-1}, reaching the maximum level in spring with 21.59 ± 14.17 µg C l^{-1} d^{-1}.

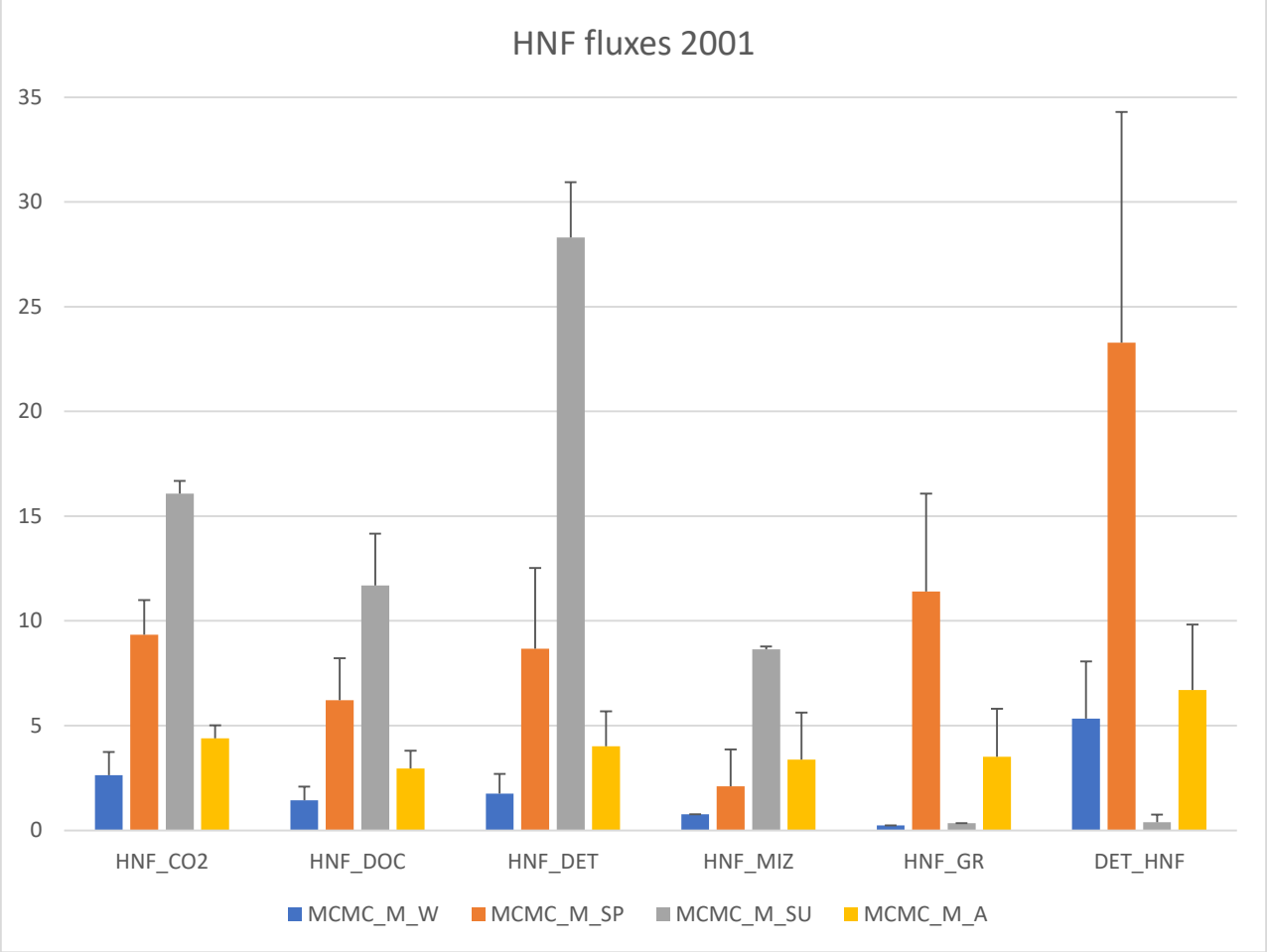

Figure 17: HNF Carbon Fluxes MCMC 2001 in µg C l^{-1} d^{-1}.

Heterotrophic nano flagellates fluxes (Figure 17) are characterized by the highest values in summer except for the growth fluxes, for which the maximum value is reached in spring with 11.40 ± 4.65 µg C l^{-1} d^{-1} and the detritus ingestion by HNF for which the highest value is in spring with 23.28 ± 11 µg C l^{-1} d^{-1}. In summer respiration flux is about 16.07 ± 0.61 µg C l^{-1} d^{-1}, decreasing to 9.34 ± 1.65 µg C l^{-1} d^{-1} in spring, 4.40 ± 0.60 µg C l^{-1} d^{-1} in autumn and 2.63 ± 1.09 µg C l^{-1} d^{-1} in winter. In winter Doc excretion and the flux to detritus have similar values, 1.42 ± 0.66 µg C l^{-1} d^{-1} and 1.75 ± 0.93 µg C l^{-1} d^{-1} respectively, while in autumn they differ a little more, with 2.94 ± 0.85 µg C l^{-1} d^{-1} and 4.01 ± 1.66 µg C l^{-1} d^{-1}. The highest level of detritus flux is in summer with 28.29 ± 2.63 µg C l^{-1} d^{-1} decreasing to 8.66 ± 3.84 µg C l^{-1} d^{-1} in spring, similar to DOC excretion flux trend: 11.69 ± 2.48 µg C l^{-1} d^{-1} in summer and 6.21 ± 2 µg C l^{-1} d^{-1} in spring. Predation by MIZ is higher in summer with 8.63 ± 0.14 µg C l^{-1} d^{-1} and it has similar lower values in spring and autumn with 2.10 ± 1.75 µg C l^{-}

^{1} d^{-1} and 3.36 ± 2.24 µg C l^{-1} d^{-1}. Detritus ingestion has similar values in winter (5.32 ± 2.72 µg C l^{-1} d^{-1}) and autumn 6.70 ± 3.11 µg C l^{-1} d^{-1}) and decreases drastically in summer with 0.38 ± 0.37 µg C l^{-1} d^{-1} only.

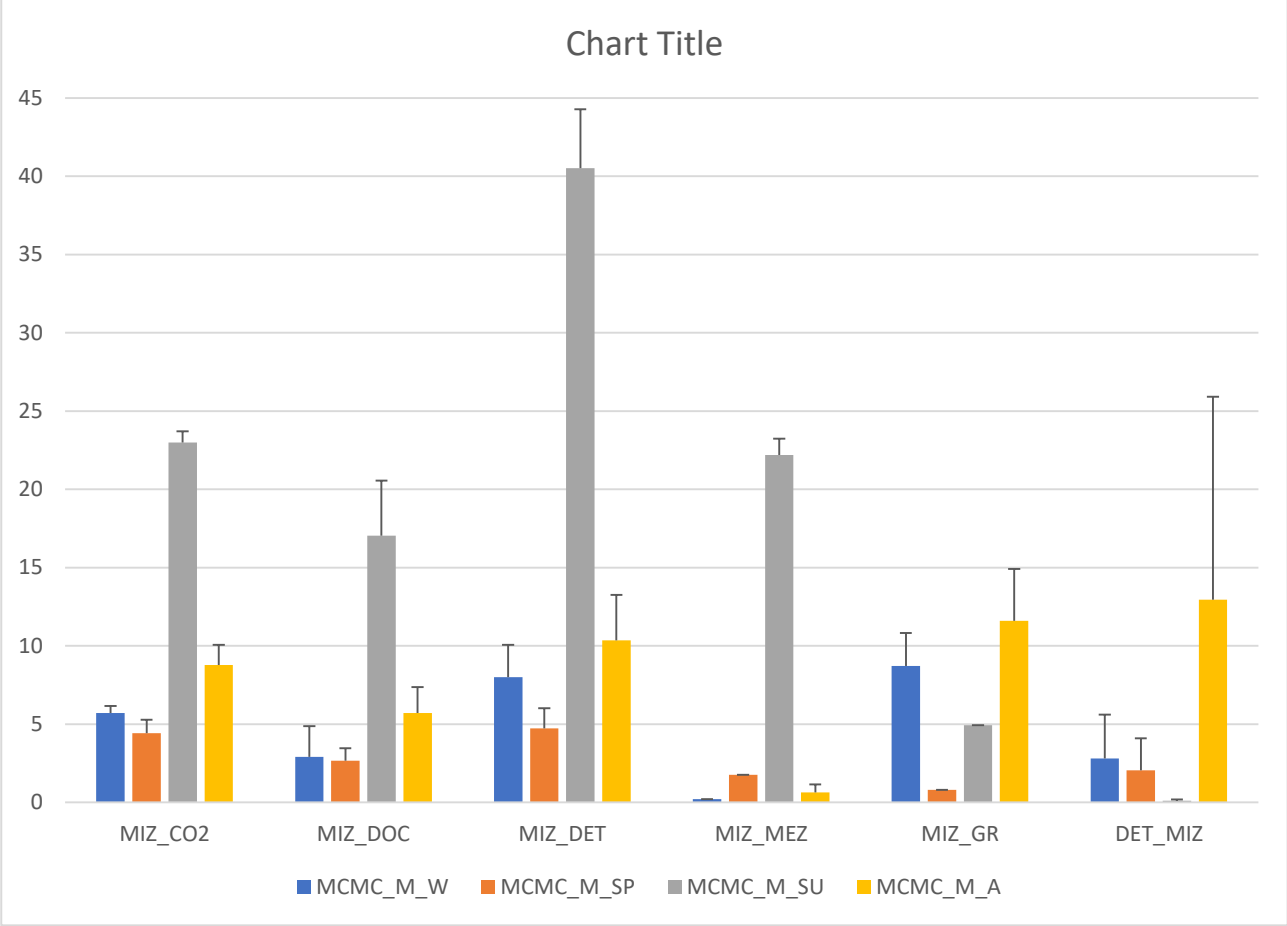

Figure 18: MIZ Carbon Fluxes MCMC 2001 in µg C l^{-1} d^{-1}.

The Microzooplankton compartment (Figure 18) is characterised by high fluxes values in summer except for detritus ingestion flux, for which the maximum value is in autumn (12.95 ± 6.79 µg C l^{-1} d^{-1}) and the minimum one in summer (0.1 ± 0.1 µg C l^{-1} d^{-1}). During winter and summer, detritus ingestion has similar values with 2.79 ± 1.98 µg C l^{-1} d^{-1} and 2.04 ± 1.74 µg C l^{-1} d^{-1} respectively. In winter fluxes to detritus and to growth are characterised by similar values (8 ± 2.05 µg C l^{-1} d^{-1} and 8.71 ± 2.11 µg C l^{-1} d^{-1}), while respiration flux doubles the doc excretion value (5.72 ± 0.44 µg C l^{-1} d^{-1} and 2.9 ± 1.9 µg C l^{-1} d^{-1}). In spring, respiration flux and detritus flux have similar values with 4.43 ± 0.85 µg C l^{-1} d^{-1} and 4.73 ± 1.28 µg C l^{-1} d^{-1} and are double than DOC excretion flux (2.66 ± 0.81 µg C l^{-1} d^{-1}). In summer the highest value is the detritus flux with 40.51 ± 6.79 µg C l^{-1} d^{-1}, higher

than 22.9 ± 0.7 µg C l^{-1} d^{-1}, 22.20 ± 1.04 µg C l^{-1} d^{-1} and 17.02 ± 3.52 µg C l^{-1} d^{-1} of respiration, MEZ predation and Doc excretion flux respectively. Autumn is characterised by a low level of predation by MEZ (0.64 ± 0.50 µg C l^{-1} d^{-1}), a similar level of detritus and growth fluxes (10.35 ± 2.89 µg C l^{-1} d^{-1} and 11.60 ± 3.31 µg C l^{-1} d^{-1}). Respiration flux is about 8.78 ± 1.29 µg C l^{-1} d^{-1} and the flux to DOC is about 5.71 ± 1.65 µg C l^{-1} d^{-1}.

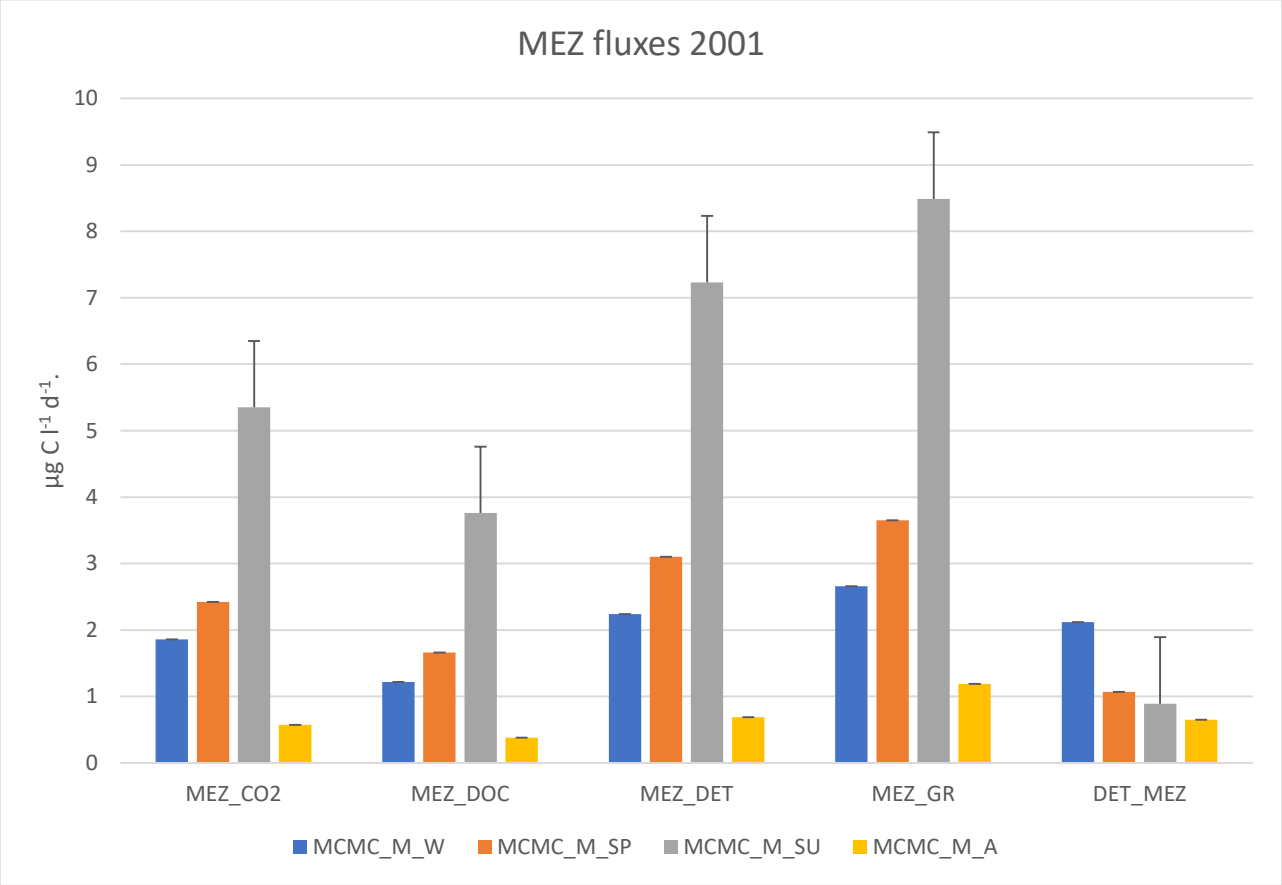

Figure 19: MEZ Carbon Fluxes MCMC 2001 in µg C l^{-1} d^{-1}

Except for detritus ingestion flux, the maximum values reached by MEZ fluxes are observed in summer (Figure 19). In winter the majority of fluxes have similar values, ranging from 2.65 ± 1.13 µg C l^{-1} d^{-1} of growth flux, to 1.22 ± 0.34 µg C l^{-1} d^{-1} of the flux to DOC compartment. Detritus flux (2.24 ± 0.59 µg C l^{-1} d^{-1}) has similar values of the detritus ingestion flux (2.11 ± 1.4 µg C l^{-1} d^{-1}), while the respiration one is lower (1.85 ± 0.24 µg C l^{-1} d^{-1}). In spring the major fluxes are the flux to detritus (3.10 ± 0.64 µg C l^{-1} d^{-1}) and the flux to growth compartment (3.65 ± 1.18 µg C l^{-1} d^{-1}), followed by respiration flux (2.42 ± 0.16 µg C l^{-1} d^{-1}), the flux to DOC (1.66 ± 0.38 µg C l^{-1} d^{-1}); the last one is the detritus ingestion flux (1.07 ± 0.65 µg C l^{-1} d^{-1}). Summer fluxes are the highest in the whole year: growth flux is 8.48 ± 1.75 µg C l^{-1} d^{-1}, detritus flux is 7.22 ± 1.43 µg C l^{-1} d^{-1} and

respiration one is 5.35 ± 0.24 µg C l^{-1} d^{-1}. The lowest value in summer is the detritus ingestion flux with 0.89 ± 0.76 µg C l^{-1} d^{-1}. Autumn is characterised by the lowest values in term of fluxes of the year. The highest value registered is 1.19 ± 0.77 µg C l^{-1} d^{-1} (Growth flux), while the lower one is 0.37 ± 0.10 µg C l^{-1} d^{-1} (Doc flux). The other fluxes range from 0.68 ± 0.18 µg C l^{-1} d^{-1} (detritus flux) to 0.56 ± 0.07 µg C l^{-1} d^{-1} (respiration flux). Growth flux is similar to the summer one, with 0.64 ± 0.5 µg C l^{-1} d^{-1}.

As it can be seen in figure 20, carbon fluxes values varied a lot during the year 2001.

In the autotrophic compartments, higher values are related to primary production fluxes, generally followed by dissolved organic carbon, detritus and predatory fluxes. In the heterotrophic compartments higher values are related to respiration, detritus and ingestion terms.

During summer the compartment with highest carbon fluxes are Bacteria compartments, autotrophic as well as heterotrophic ones, followed by MIZ compartment. Autumn and spring are characterised by HB and HNF compartment carbon fluxes. Winter is characterised by MP and HB compartments in term of carbon values.

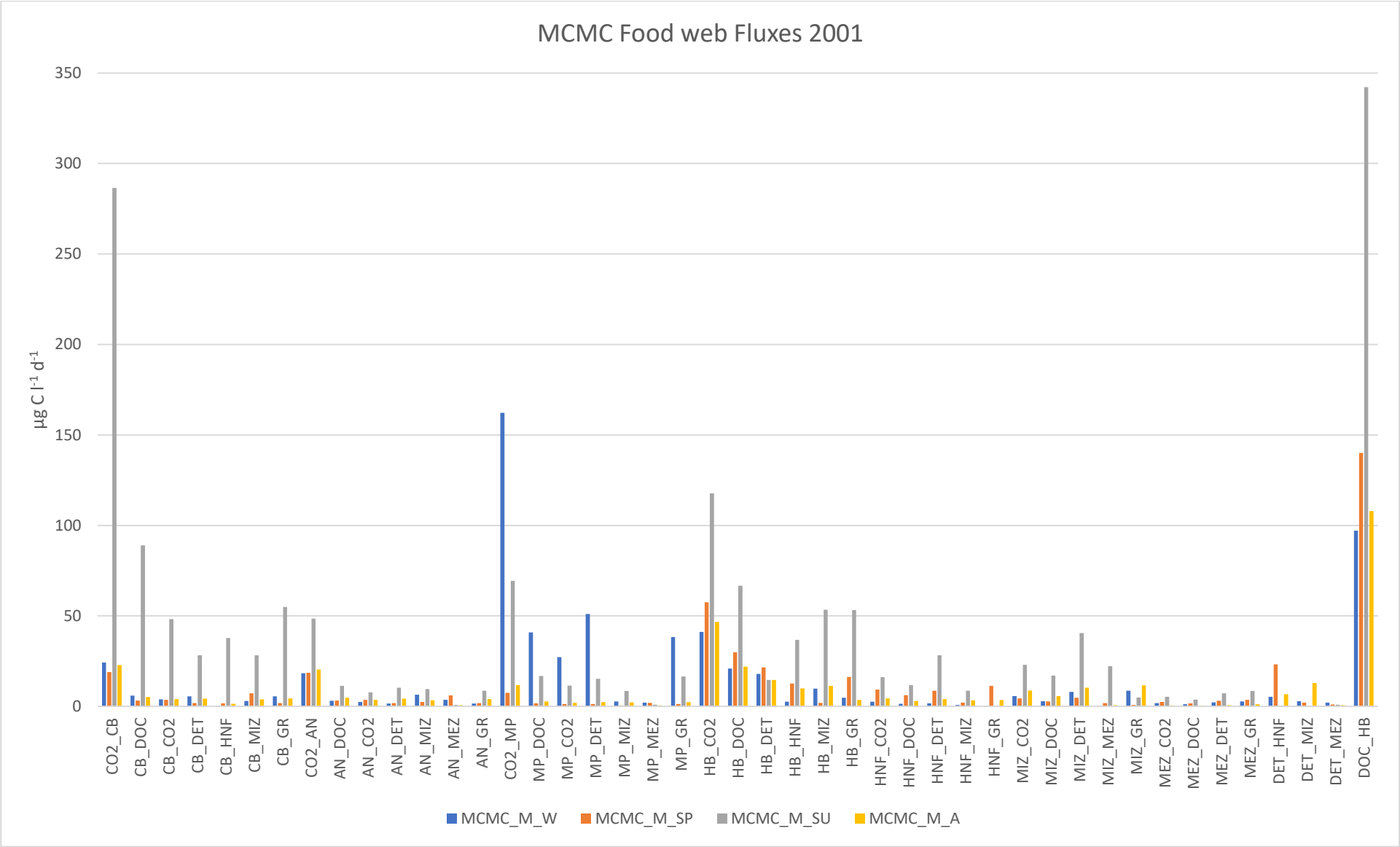

Figure 20: MCMC Food Web Carbon fluxes 2001 in µg C l^{-1} d^{-1}

5. DISCUSSION

The inverse modelling technique applied to the Gulf of Trieste gives a lot of interesting results. The LIM – MN and the LIM – MCMC produce different results starting from the same information. It happened because of the philosophy that is beyond the two different way of calculating the final solution.

The LIM – MN was created to better investigate the food web property in the late 80s, in order to help scientists in handling the insufficient and not organized information about the marine food webs. In particular, Platt (1988) applied a methodology that permits the users to directly compare different food webs in the world: searching the solution that represents the ‘‘best’’ (or most likely) set of flow values, assuming a certain food web topology and given an empirical data (Van Oevelen et al., 2010) minimising all the fluxes, as it minimizes the squared sum of all the set fluxes. It has a theoretical basis: the Ockham razor, ‘multiplicity ought not to be posited without necessity’ (Legendre & Legendre 1998; Niquil et al. 1998): based on the law of parsimony, it detects the simplest solution. This method permits to obtain solutions that could be easily compared universally, as they are based on the same mathematical principle. As reported in many papers, this way of thinking was revolutionary, as it permits to detect food web characteristics starting from poor data (obtained by *in situ* measurement) based on a rigorous mathematical construct (Van Oevelen et al., 2010). Fluxes are determined starting from other fluxes and a pre-determined model: that’s why it is called inverse modelling. This methodology permits to give reasonable values to many unknown carbon exchanges inside food webs. Brigolin et al., (2011) reported that inverse modelling has been widely used in ecosystem modelling during the last years, as they permit to consistently estimate a large number of unknown flows from a relatively small number of observations (Leguerrier et al., 2003; Vézina et al., 2004; Savenkoff et al., 2007a,b). It was also very important to understand that the method mixes *in situ* measurement with an *a priori* knowledge of the food web, giving a focus to real data and to models at the same time. It is a combination of scientific knowledge and the reality that one could touch taking experiments in that study site.

Starting from the parsimony approach, in the last decade scientists have tried to find new way of applying the LIM with new algorithm, trying to overtake some of criticism of the LIM – MN. The main critique is about the possibility that the parsimony principle could be used to represent the ecological laws in the marine food web in a proper way. Energy minimisation is one of the nature laws but can it be applied also in the sea, too? Could it be representative of the marine food web exchanges? Minimising fluxes is an arbitrary decision that simplifies the mathematical problem but

there is no evidence that it is correct. Vezina et al. (2004) reported that this MN inversion is increasingly used in comparative analyses of aquatic ecosystems (Leguerrier et al., 2003; Niquil et al., 1998; Olsen et al., 2001), even though it is recognized that this norm does not necessarily reflect how ecosystems are organized structurally (Jackson & Eldridge,1992). That's why scientists focused on a new way, which was the an LIM - MCMC that could sample the solution space in a proper manner. The main idea was to get a range of values as possible solutions represented by a mean with standard deviation. It could not be the best or the optimum solution, but among all the infinite solutions, the algorithm gives back a range that undergoes the constraints and the law imposed in the model. From an ecological point of view, we have to look at at this range as the probability that we will find the true possibility of the natural behaviour of the food web inside the solution selected.

Our first goal was to use the LIM technique to reconstruct the possible carbon exchanges in the North Adriatic Sea, using some *in situ* data coming from one of the most important ecological time series in the Mediterranean Sea.

The structure of the food web was depicted maintaining the compartments investigated in the experiments and the analysis scientists used to take in the gulf of Trieste: we maintained the *a priori* knowledge. Based also on literature, we imposed universal constrains for each compartment. We'd like to focus on this topic, the "universal" inequalities, because we decided to apply the *a priori* knowledge found in literature. We are conscious that there are equalities and inequalities that derive from worldwide experiments and studies. Some of the studies come from Mediterranean sites, and in some way, they could represent the Adriatic Sea in a proper way. Richardson et al. (2003) referred that the vast majority of constraints were based on relationships derived for temperate ecosystems (Vézina and Platt, 1988; Vézina and Pace, 1994; Vézina et al., 2000): the validity of the assumption to use the constraints for all ecosystems is not known. This means that they are universal but not specific to our case and that we don't know how deeply they could influence the solution. We are conscious that this fact may impact on the goodness of the solution, but future works coupled with *in situ* experiments could be carried out to bypass this type of problem. For this work we decided to focalize on the classical way to apply the LIM.

From a data perspective, it is important to say that they could be categorized as fluxes in term of concentrations of liter per day (µg C l^{-1} d^{-1} equivalent to mg C m^{-3} d^{-1}): they represent changes of concentrations. We didn't transform data in term of µg C m^{-2} d^{-1}, dividing them by the depth of the *in situ* measurement, because we wanted to maintain the data intrinsically the same as those in the manuscript where the data were kept to maintain a sort of continuum with the previous literature of the Gulf of Trieste.

Before starting to discuss the results, we want to focus our attention on a particular compartment: the growth compartment. It is a mathematical artefact that we implemented for the first time in literature to take into account the possibility that model compartments are growing during the study, as the food web is depicted in a static snapshot of the moment in which experimental data were collected. Taking a step back, we know that inverse modelling approach is solved in a steady state way, meaning that inflows are equal to outflows in each compartment. Daniels et al. (2006) reported that inverse solutions have tended to assume steady state due to the frequent use of snapshots of data. Furthermore Belgrano et al. (2005) referred that steady state food web models are often applied to coastal ecosystems to quantify mass and energy fluxes associated with trophic interactions between different compartments of a food web. These models generate a snapshot of the trophic network at one moment in time, which is consistent with the set of input data (Brigolin et al., 2011). Solving the system in this way does not contemplate the possibility that a compartment is gaining biomass, as the system is depicted in term of flows and not in term of biomasses. The gaining of biomass could be seen as the energy that is used to grow. From a metabolic/flux point of view it is the energy that is used for accretion, once metabolic requests are satisfied, if is not completely burned. The energy that a creature needs to live comes from primary production for autotrophs and ingestion for heterotrophs: mixotrophy is not yet implemented in this type of food webs analysed with LIM (Donali et al. 1999). As in the LIM technique we can't measure a flow that recirculate in the same compartment, we added a new compartment inside the food web that is a "ghost" compartment, that permits us to calculate the energy spent for the compartment growth. The compartment is considered as other external compartments and therefore has no mass balance equation. As it is the first time that it is implemented, we do not have any inequalities coming from literature on this type of flow, but we defined it in a strong way. It can be defined as what remains, in term of carbon, from PP/ingestion and has to be major or equal than 0, as the ≥ 0 is a request for all the fluxes. It is important to understand that all fluxes have to be major or equal to zero, as each flux has to be seen as a mathematical vector, for which the directions carried out some information. The directions explained for the flux considered, which are the source and sink compartments. A flux inferior than zero switches the source and sink compartments, leading to a nonsense from an ecological point of view (mathematically is accepted). Coming back to growth fluxes, we are conscious that we inserted new unknowns in a model that is already highly undermined, but some of these fluxes are known, as secondary HB, HNF and MIZ secondary production. As these fluxes are known, we imposed some new fix points inside the space of solution: the final total solution will be better constrained. From a mathematical point of view, with growth fluxes, we also inserted some degrees of freedom that can permit the model to have some "blank space of manoeuvre" in order to force the solution in a proper way (the tolerance needed for

the solution) similar to the detritus compartment in the Ecopath model (Christensen and Pauly, 1998). Richardson et al. (2003) allowed for the possibility of non steady state flow in his work. He used residual flows, as the possibility of non steady-state conditions was allowed. This is to remark our opinion about the use of the growth compartment: it is an artefact that can be used in studying food webs. Moreover in certain situations, which we will encounter during the discussion, i.e. diatoms blooms, it is important to identify the capability of the compartment to grow. Daniels et al. (2006) defined phytoplankton blooms as emblematic of non-steady-state plankton systems. Vezina and Pahlow's (2003) results imply that inverse solutions for phytoplankton blooms are not a priori likely to be in great error, just because they are not near a steady state (Daniels et al., 2006).

From literature we assume that the better we constrain the LIM the better the solution and the food web will be depicted. Biological constraints, such as respiration and assimilation efficiency were used to keep the unknown flows within reasonable ecological and physiological boundaries (Jackson and Eldridge, 1992; Vezina and Platt, 1988). We drew all the inequalities constrains from literature as reported in the previous chapters, except for GPP. As we didn't have GPP data, we chose to define a maximum of GPP for each compartment applying the equalities explained in the material and method chapter. We don't want to define a specific value from an *a priori* knowledge, but we want to put an upper limit for each compartment GPP to better constrain the solution. Imposing a maximum, we don't radically influence the algorithm, but we do not leave the upper part of the hyperplane solution related to GPP open: we close the solution space permitting the algorithm to work better, in the case of the MCMC. For what the LIM it concerned, the maximum permits to have an upper limit that is fundamental to constrain the solution. In literature, as far as we know, in LIM procedures authors have always declared the PP fluxes data, as it is one of the most important fluxes in the food web, from an ecology and mathematical point of view. Stukel et al. (2012) referred that they have not found a case for the inverse models of pelagic ecosystems where it is not be a measured input. From an ecology point of view it defines the inputs to our systems, while from a mathematical point of view it defines the upper part of our food web and as starting point for algorithms.

We now begin to discuss the results obtained.

Comparing the solutions obtained from the two ways of solving the LIM (Figure 21), we clearly see a difference: 0 fluxes. Zero fluxes are those fluxes that in the LIM – MN technique are settled to 0, in contrast to LIM- MCMC where no fluxes are settled to zero. Total 0 fluxes – fluxes for which the solution is always 0 during the year - are the fluxes related to detritus, to growth compartment and some predation terms. Detritus ingestion terms by heterotrophs are all settled to 0 together with HB flux to detritus.

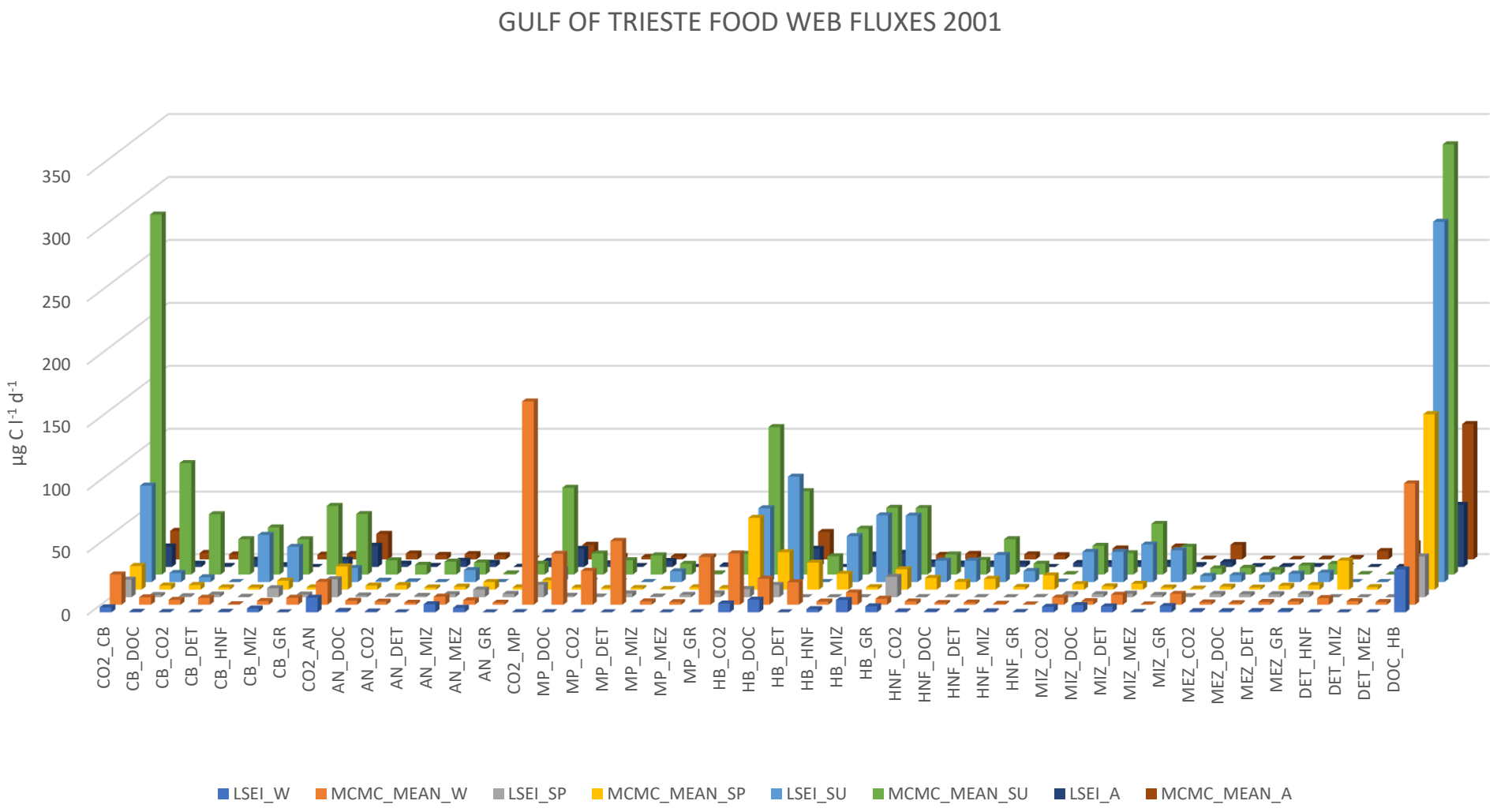

Figure 21: 2001 Gulf of Trieste food web fluxes in µg C l^{-1} d^{-1}.

For what concerned the other 0 fluxes, the percentage of the zero solution for each flux, in which 0 is the solution, varies from 25% to 50%. Growth fluxes and Detritus ingestion ones are those which are less constrained and therefore we expect that the LIM – MN chooses the easiest and lowest solution (= 0). We expected that some of the lower fluxes, in term of importance and numbers, will be settled to 0 as this is well known in literature. As reported, LIM – MN tends to zero minor flows (Vezina and pace, 2004), it sets biological constraints to maximum or minimum allowed values (Stukel and Landry, 2010). In practical terms, this means that many flows can be underestimated or overestimated (those which exit the system quickly) (Leguerrier et al., 2003), and set to zero fluxes that are not fundamental for the mass balanced (Stukel et al, 2012). Furthermore, Van Oevelen et al. (2006) underlined that some flows may be set to zero (Vezina et al., 2004; Kones et al., 2006), many flows are close to the lower bound of their ranges, which should be considered extreme values rather than likely ones (Diffendorfer and others 2001; Kones and others 2006; Steele 2009). Our results are perfectly in agreement with those reported in literature, underling that those fluxes are not very important in the whole structure of the food web according to LIM – MN. Furthermore, from an ecological point of view, setting to 0 fluxes to detritus, is equivalent to say that those compartments in such occasions are completely predated, and no carbon is channelled to the detritus compartment. Furthermore, in the LIM – MN solution, detritus is not characterized as one of the important food opportunity for the heterotrophic compartments, as its ingestion is always set to 0, in contrast to what is allowed in LIM studies: all of the grazers were allowed to consume detritus (Daniels et al., 2006).

Comparing the two methods solutions, fluxes values are comparable in most of the cases in term of values magnitude, but it is evident how LIM – MCMC values are higher than LIM – MN ones. In the next pages we will discuss the main differences season by season.

In winter, there is a great difference between the two method solutions (Figure 22). The main differences are reported in the MP compartment. According to LIM – MCMC MP fluxes are higher and more structured than those predicted by the LIM – MN. The main evidence is about MP compartment. The extreme case is represented by GPP: LIM – MCMC GPP is three magnitude order higher than LIM – MN value. It seems that LIM – MN deeply underestimates the MP compartment fluxes, creating an important gap between reality and model prediction. Furthermore, this fact highlights an important limit of the LIM – MN method: it is not linked to biomasses data. MP compartment is the biggest autotrophs group in term of biomass in winter and cannot have lower GPP values than other autotrophs. Running a quick sensitivity analysis on biomasses variation input, we find a very low flux variation (less than 3%) with a strong variation in biomasses terms (30%) that confirms our opinion.

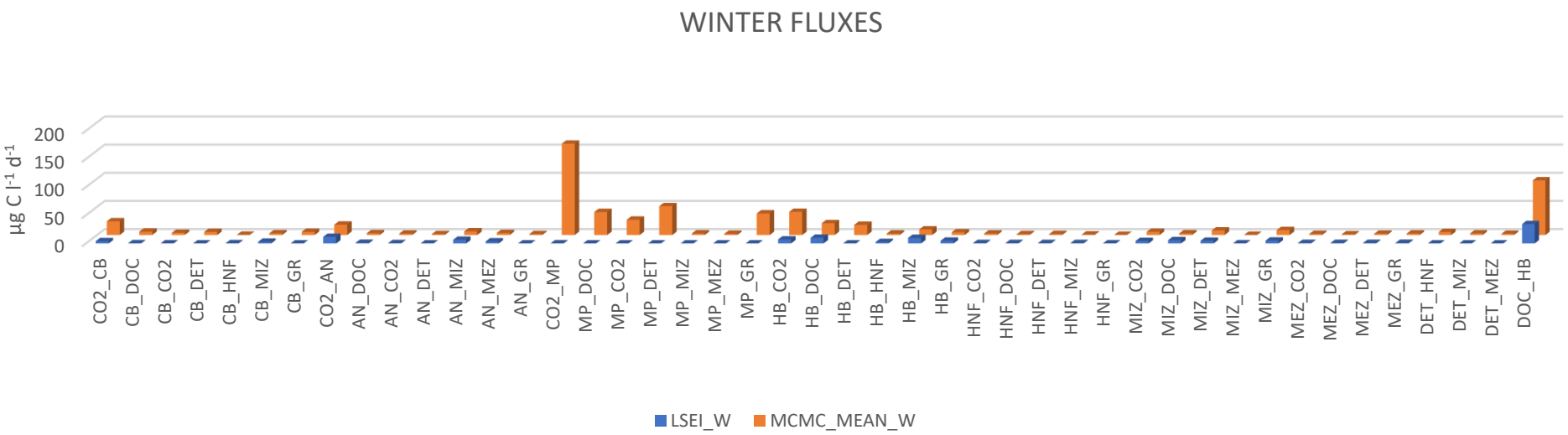

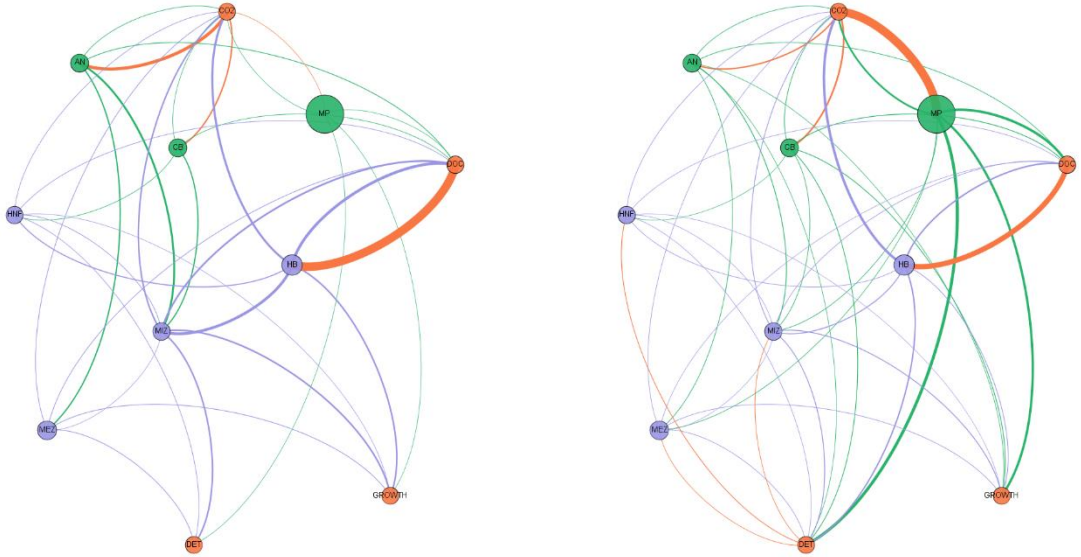

LSEI_W MCMC_MEAN_W

Figure 22: Winter fluxes in µg C l^{-1} d^{-1}.

LIM – MN underestimates GPP fluxes too, as also CB and AN GPP are very low if compared to those of LIM – MCMC. Both solutions depict HB compartment in a proper way, i.e. fluxes are relevant and structured, showing how HB group is important in channelling carbon inside the food web. This idea is confirmed by DOC uptake values that are high, if compared to those of GPP. MIZ fluxes have a similar trend in both the solution methods, maybe because they are the direct and major predators of bacteria compartments. LIM – MCMC results regarding the MP compartment are in agreement with the Gulf of Trieste knowledge: in late winter the gulf of Trieste is characterised by intense diatoms blooms (Umani et al.,2012; Mozetic et al., 1998; Harding et al., 1999), that correspond in high values in the LIM – MCMC MP group. In addition, Umani et al. (2012) reported that big diatoms that cannot be efficiently predated by MIZ and MEZ groups, mainly constituted the flux to detritus (observing sedimentation traps contents). Our results are in agreement with what was said previously: MP_DET represents the 57% of the total fluxes to detritus, followed by MIZ_DET with the 9%. MIZ (MP_MIZ) and MEZ (MP_MEZ) has similar low levels of predation, showing the scarce capacity of the two groups to feed on MP (Umani et al., 2012). Furthermore, Marquis et al. (2007) reported that the high sedimentation rate was mainly due to the downward flows of microphytoplankton material (55% and 36% of total detritus production made up by large phytoplankton) as it is usually observed after a strong bloom of diatoms in the absence of grazers (e.g. Savidge et al., 1992; Valiela, 1995). Legendre and Rassoulzadegan (1996) described this specific situation as corresponding to a rapid stabilization of the water column after a long period of mixing: it could be similar to the late winter situation of the Gulf of Trieste, where after a period of mixing (winter) the water column tends to stabilize (late winter). Our results are in agreement with those of Umani et al. (2012) for what the growth of the MIZ group is concerned too. MIZ growth is enlighted by the flux to the growth compartment in both solutions, with highest flux according to the LIM – MCMC (5.02 µg C l^{-1} d^{-1} vs 8.71 ± 2.11 µg C l^{-1} d^{-1}).

In spring the two solutions show similar trend regarding gross primary production fluxes (Figure 23). For what CB and AN compartment is concerned, MCMC values are higher than MN, but they assume the same value inside each solution. MP GPP is higher in the LIM – MN than LIM - MCMC, and corresponds to the maximum value allowed by the inequalities. Autotrophs fluxes are comparable in the values between the two solutions. The break between the two solutions appears in the HB and HNF compartment. In the LIM – MN solution three of the HB compartment fluxes (two predation fluxes and the flux to detritus) are set to zero while they are characterised by important values in the LIM – MCMC solution. It is important to say that HB secondary production (HB_GR) is an experimental measured data, suggesting that the LIM – MN deeply minimized HB flows.In the LIM – MN solution, HB mass balance is obtained by only four fluxes (DOC_HB – HB_CO2 – HB_DOC

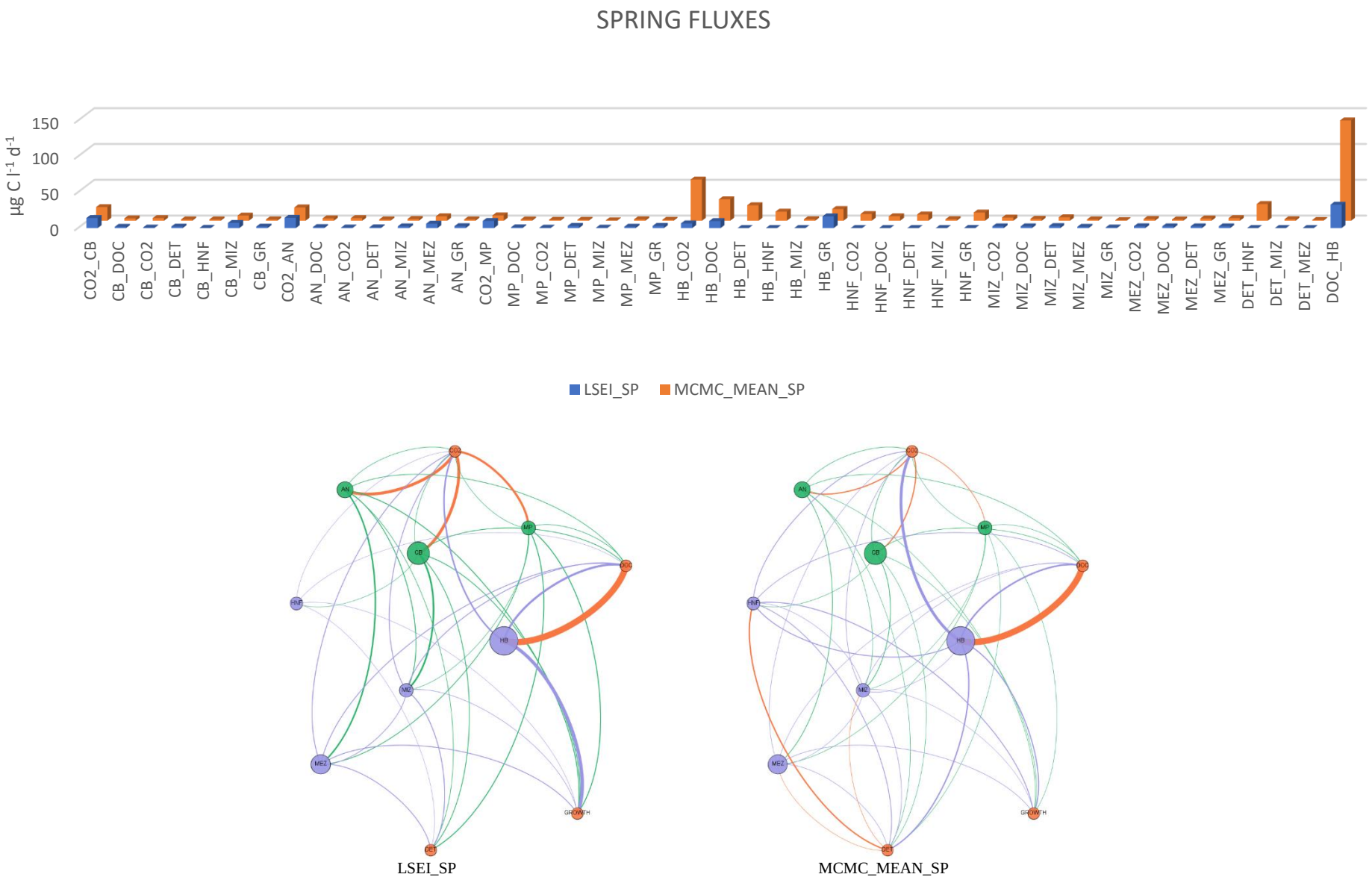

Figure 23: Spring fluxes in µg C l^{-1} d^{-1}

– HB_GR) setting the others to 0. It seems that, starting from a known data, LIM – MN tries to respect the mass balance in the easiest way, with the minor number of fluxes and preferring the smallest way carbon can leave the compartment. Our thoughts are in agreement with Niquil et al. (1998) who referred that the shortest pathway of carbon from one compartment to another is favoured when several pathways are of the same length. Furthermore when an element is not required to satisfy the constraints of the system (through the equations and inequalities), it will disappear from the system (Niquil et al., 1998). DOC uptake is the highest flux in winter in both the solutions and it is more important than GPP fluxes, suggesting that HB compartment has the leading role in channelling carbon inside the food web. Our suggestion is in agreement with Umani et al. (2012), who suggest that winter-spring DOC can sustain a high and active bacterial biomass, that becomes the most important source of energy for the whole system. Increasing of DOC uptake and therefore in bacterial carbon production is better described by the LIM – MCMC solution, in which DOC uptake goes from 97.07 ± 18.59 µg C l^{-1} d^{-1} to 140.02 ± 26.71 µg C l^{-1} d^{-1}. Umani et al. (2012) highlighted the coupling between bacterial carbon production and DOC uptake, and the same did De Laender et al. (2010) who referred that bacterial production, essentially a reflection of DOC production, because of the strong coupling, was of comparable importance as primary production to fulfil carbon requirements of protozoa. In the LIM – MN solution DOC uptake flux decreases from 34.34 µg C l^{-1} d^{-1} in winter to 32.64 µg C l^{-1} d^{-1} in spring, showing once again a worse level of prediction than LIM – MCMC. HNF compartment fluxes are underestimated by the LIM – MN too. While LIM – MN set nearly to 0 most of the HNF fluxes, near to the minimum bound, LIM – MCMC solution depicts a certain activity by the HNF group. Umani et al. (2012) reported that HNF secondary production was particularly relevant in spring: our results are in agreement with this statement as HNF_GR flux is quite high during spring (11.41 ± 4.66 µg C l^{-1} d^{-1}) in the LIM – MCMC solution, while in the LIM – MN is set to 0.12 µg C l^{-1} d^{-1}.

In summer, bacterial groups are the dominant ones inside the food web (Figure 24). In both solutions, CB are characterized by high level of GPP, representing the 78% and 71% of total GPP in the LIM – MN and LIM – MCMC respectively. GPP LIM – MCMC values are four times higher than LIM – MN for the three autotrophs compartment, showing a similar pattern in both solutions with the capability by the LIM – MCMC to explore the solution space better. Autotrophs fluxes, different from GPP ones, are deeply underestimated by the LIM – MN solution: this fact is evident in the CB compartment more than others are. It is important to say that predation fluxes on CB group are known by laboratory experiments, proving again how LIM – MN algorithm is not capable to determine a comprehensive solution of all fluxes, as starting from fix values try to find the easiest solution with the fastest pathway to exit the compartment.

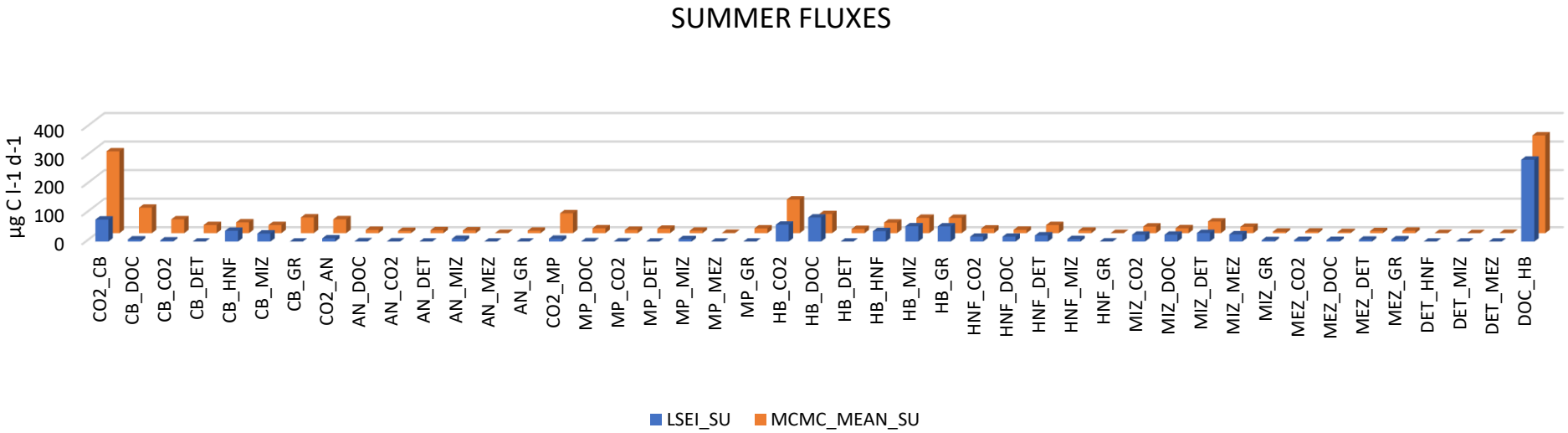

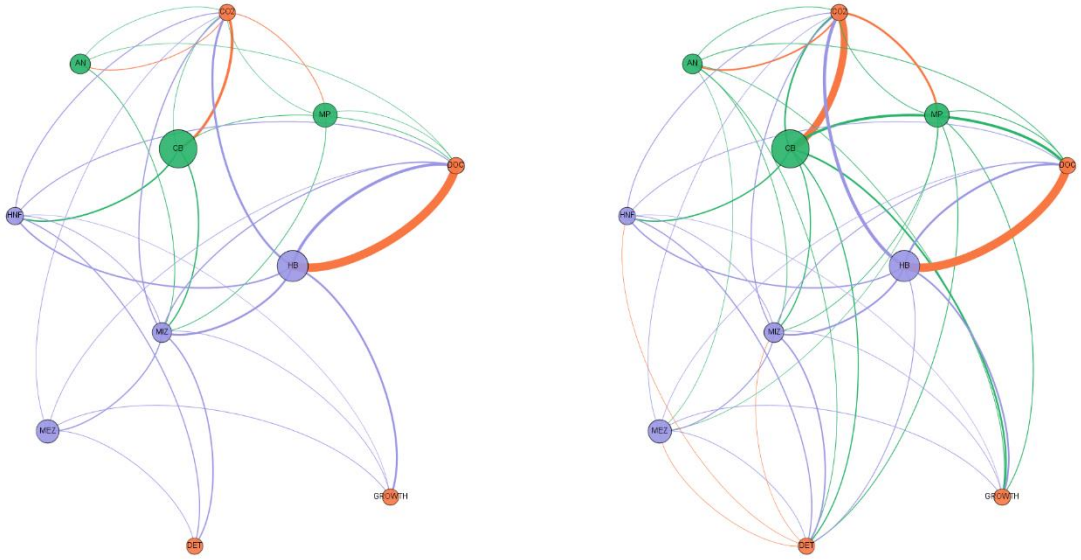

Figure 24: Summer fluxes in µg C l^{-1} d^{-1}.

HB compartment is characterized by a high level of DOC uptake in both solutions. HB respiration flux is higher in the LIM – MCMC while flux to DOC is higher in the LIM – MN (predatory fluxes are known by laboratory experiments). HB growth flux (whose value derived from in situ experiments), which represents the bacterial carbon production, permits us to explain the high level of DOC uptake registered by the two solutions. High level of secondary production can be explained by the coupling with high values of DOC uptake. Our results are in agreement with Umani et al. (2012) who referred how the system was mostly supported by picoplankton biomasses, which fuelled and were respired within the microbial part of the food web. Highest DOC concentrations permitted highest DOC uptake values in the whole year. Moreover, DOC produced by all processes was consumed by bacteria because it is the only sink of DOC: such a tight control of the DOC stock by bacteria is realistic in marine ecosystems (Vargas et al. 2007). MIZ compartment has discrete fluxes values, showing high predation activity. In agreement with Umani et al. (2012), MIZ predation fluxes on lower classes are higher than MEZ predation activity, showing that MIZ predates more efficiently than MEZ. Watching MEZ predation activity, we see that this group preferably feed on MIZ with similar values in both the solution, in agreement with Umani et al. (2012): bacterial biomass fuels microzooplankton and HNF and the former were actively predated by mesozooplankton in summer. Detritus ingestion by heterotrophs groups are settled to zero by the LIM - MN and are nearly zero with high standard deviation in the LIM – MCMC solution. Heterotroph groups do not need detritus support in their diet as they feed efficiently on lower classes, in agreement with the solution values that are similarly low.

Autumn is characterised by low levels of activity by all groups if compared to summer (Figure 25). GPP is splitted nearly equally between the three autotrophs group according to LIM – MN solution, while in LIM – MCMC solution MP_GPP was lower than the other groups. Figuring out which could be the motivation of this differences, we looked at the possible ranges of our solution, and we realize that LIM – MN puts MP_GPP on the maximum bound allowed by the inequalities, while in the LIM – MCMC GPP was lower than the maximum value allowed by inequalities. Autotrophs fluxes were generally low and lower than summer in both solutions: biomasses values are low too. HB compartment is the only one with a certain activity coupled with MIZ. Umani et al. (2012) described the importance of this compartment in the autumn period, although bacterial carbon production is lower than in the summer period. Our results are in agreement with what concerns HB DOC uptake values: uptake value is similar to the one in winter and it seems that HB are not capable to uptake more due to the refractory characteristics of autumn DOC itself (Umani et al., 2012). In agreement with Umani et al. (2012), data describe lower levels in all the secondary productions. Between MIZ and MEZ compartment, MIZ is the compartment which is more active in term of predation.

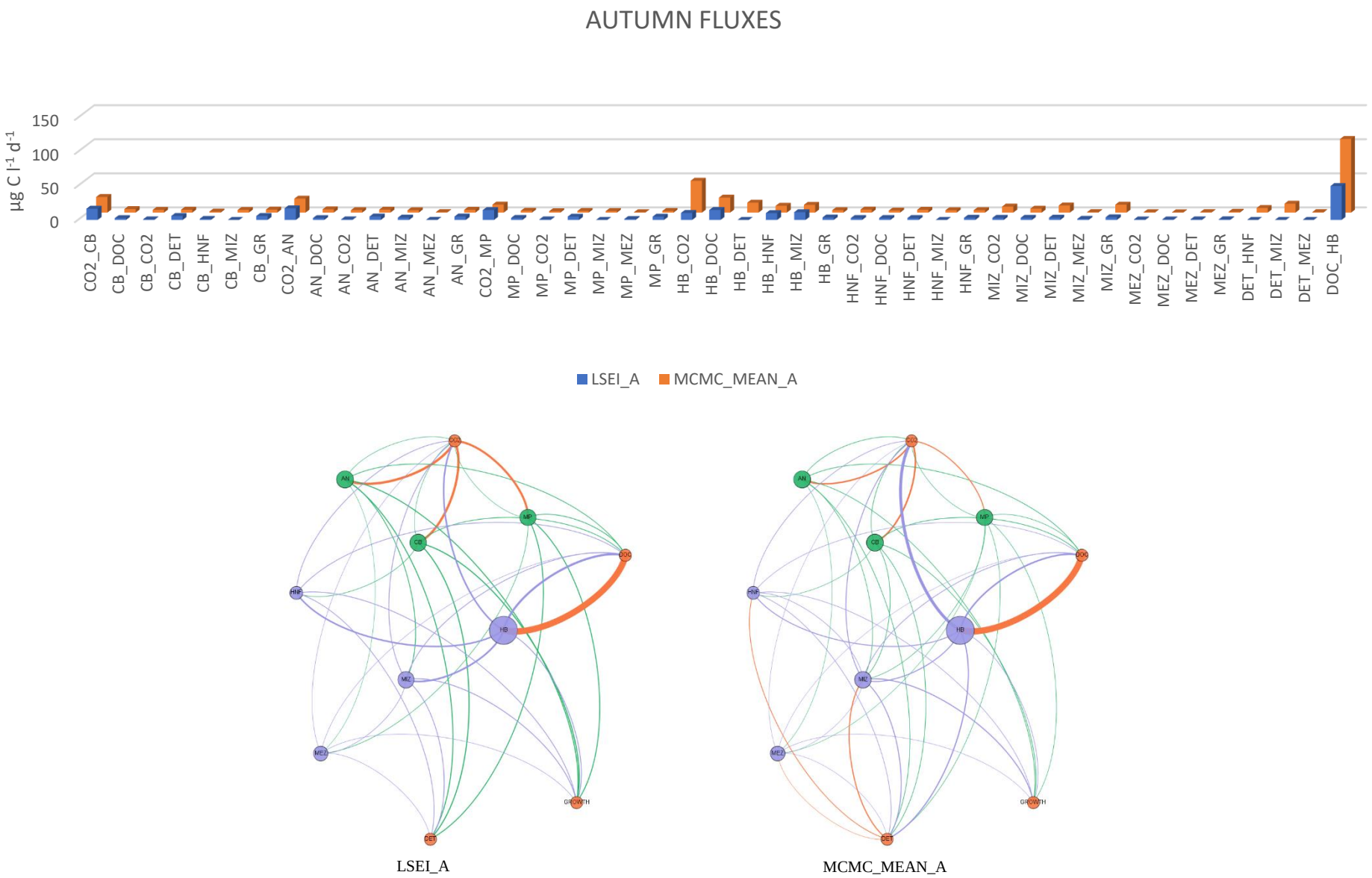

LSEI_A MCMC_MEAN_A

Figure 25: Autumn fluxes in µg C l^{-1} d^{-1}

In agreement with Umani et al. (2012) we found MIZ high preference on HB, feeding also not efficiently on MP and CB according to the LIM – MCMC solution. In the LIM – MN one, MIZ seems to feed nearly exclusively on HB (that is the only flux value known by laboratory experiments), less on AN and doesn't feed on MP. Again, the MCMC seems to predict better real fluxes than LIM – MN.

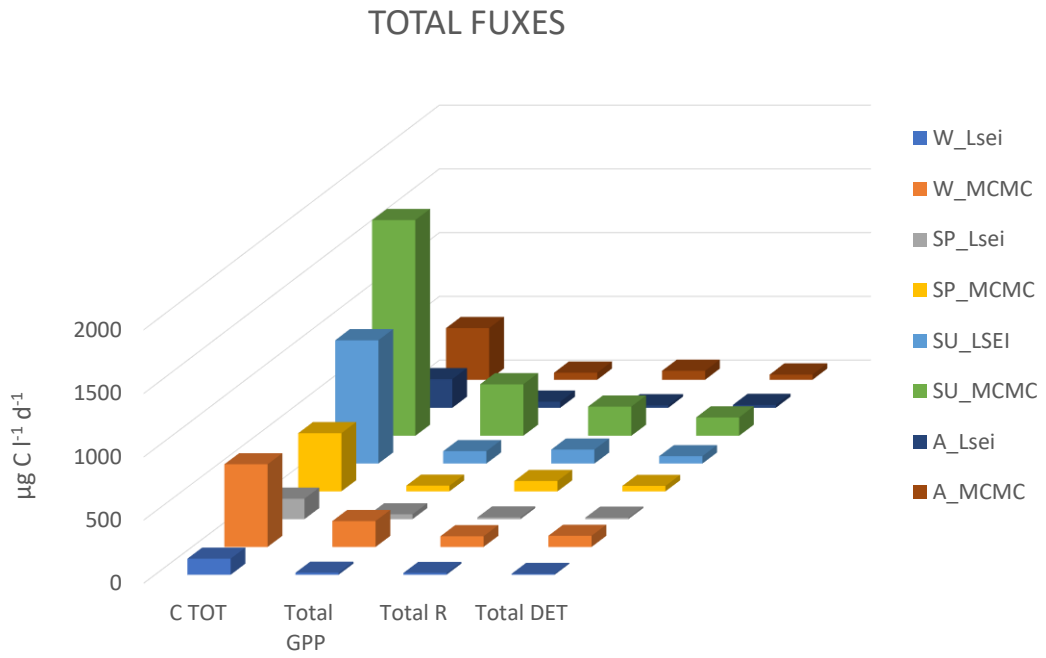

Figure 26: Total GPP, R, detritus and carbon total fluxes in µg C l^{-1} d^{-1}.

Total fluxes values (Figure 26) reflect what we discussed in the previous pages. LIM – MCMC fluxes are generally higher than those of the LIM – MN. The total carbon flux we present here is the total systems throughput (TST) of the food web, which is the sum of all flows in the model (Heymans et al., 2014) and is considered an overall measure of the ''ecological size'' of the system (Fins, 1976) and total activity of the system (Ulanowicz, 1986). From the figure it is possible to see that LIM – MCMC TST are nearly double than LIM – MN ones, in particular in the winter and spring cases. TST values vary from 2161.19 mg C m^{-2} d^{-1} in winter to 16484 mg C m^{-2} d^{-1} in summer according to LIM – MN, while in the LIM – MCMC solutions values range from 6886.33 mg C m^{-2} d^{-1} in autumn to 28770 mg C m^{-2} d^{-1} in summer. TST values reflect high values in term of total carbon flows: they are comparable to Grami et al. (2008) TST values which vary from 2900 mg C m^{-2} d^{-1} to 8398 mg C m^{-2} d^{-1}, to Bondavalli et al. (2006) with 3510 mg C m^{-2} d^{-1}. Summer values are very high according to both solutions, but they are comparable to TST value found by Baird and Ulanowicz (1993) at the Swartkops estuary, where TST reached 17,541 mg C m^{-2} d^{-1}. TST values in our case study are high

due to GPP rates, which are less constrained on the top boundary, and HB DOC uptakes fluxes, that remark the important part of heterotrophic bacteria in the food web.

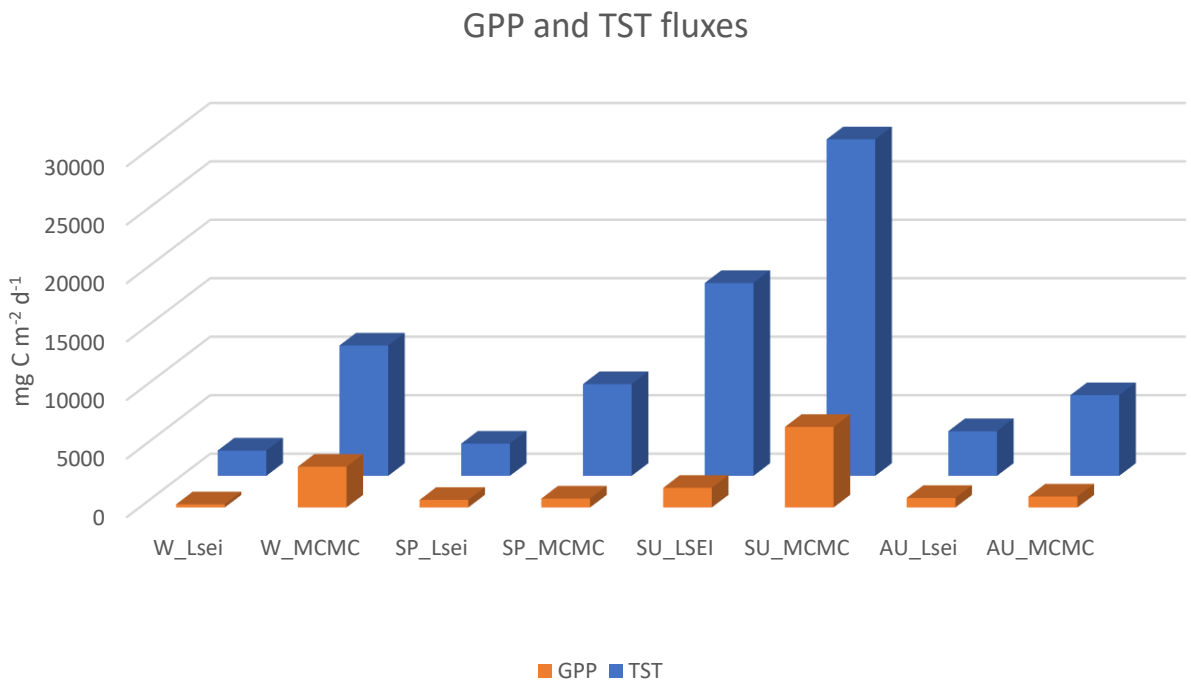

Figure 27: Total GPP and TST fluxes in mg C m^{-2} d^{-1}.

GPP production fluxes vary from 269.18 mg C m^{-2} d^{-1} in winter to 814.56 mg C m^{-2} d^{-1} in summer according to LIM – MN solution, while in the LIM – MCMC one GPP ranges from 764.49 mg C m^{-2} d^{-1} (0.76 g C m^{-2} d^{-1}) to 6874.53 mg C m^{-2} d^{-1} (6.8 g C m^{-2} d^{-1}) in summer (Figure 27). GPP values are in agreement with those reported by Umani et al. (2007): they considered net primary production saying that values were generally under 1 g C m^{-2} d^{-1}. Furthermore, LIM - MCMC values are comparable to gross primary production values reported by Gramy et al. (2008) with 1.87 g C m^{-2} d^{-1}, by Berman et al. (2004) in Lake Kinneret with 1.53 g C m^{-2} d^{-1}, by Niquil et al. (2001) in the Takapoto Lagoon with 1.60 g C m^{-2} d^{-1} and by Niquil et al. (2006) in Lake Biwa with 1.57 g C m^{-2} d^{-1}. GPP fluxes denote large gross primary production (Gramy et al. 2008), maybe overestimated by the LIM – MCMC. Stukel et al. (2012) referred that LIM – MN was far better than MCMC method in predicting primary production when it is not known. He suggested that PP prediction might be significantly improved by placing a more stringent upper bound on phytoplankton growth rate, as they allowed an unrealistic high growth rate for that environment. Our opinion is that it would be useful to put a more stringent upper bound on GPP fluxes. Our upper bound is far larger, as we don't consider nutrient limitation in the equation that determines GPP upper level, which is used as a constraint. Our idea was to have a maximum range not too low but realistic at the same time, so we

didn't impose nutrient limitation and we used mean day light hours. Initially, we started working with a realistic value of GPP found in literature, that gives an upper bound to GPP. We had to change this settlement because in most of the runs we found out that this solution was problematic, as GPP had to be divided into three compartments, thus allowing too much freedom to algorithms in order to find a proper solution (the algorithm doesn't know how to divide total GPP value in the three different groups). We saw GPP uncertainty from MCMC algorithm: the algorithm did not converge to a fix range, never reaching the plateau. We then changed the way of constraining GPP fluxes. We searched into the world of biogeochemical model for a Mediterranean biogeochemical model that was similar to ours. We chose the biogeochemical flux model, BFM (Vichi et al. 2013). We used the parameters found in the manual to adjust the GPP equation to our interests. In particular, it permitted us to give a maximum GPP bound to each of the autotrophic compartments. This allowed us to defeat the algorithm instability due to a great solution space.

The study of the stability of the solution was different for the two methods. In the LIM – MN, we controlled the stability of the solution by repeating the solution calculation of a lot of times, being sure that the solution didn't change: solution changes were eliminated thanks to the upper bounds in the GPP fluxes. In the MCMC facts were different.

MCMC is a much newer technique (Stukel et al., 2012) and there is not a sort of good guide to use it. The method relies on some parameters that can be controlled by the user. First of all the jump length. Van de Meerche et al. (2009) suggested that a suitable jump length is often in the same order of magnitude as the ranges of the unknowns when sampling the feasible region uniformly. Starting from the suggestion of Van de Meerche et al. (2009), we decided to look for the best jump: we tested jump parameters for different values, from 0.001, 0.01, 0.1, 1, 10 to 100. We ran the MCMC for each season, for each jump. Jump parameter is very important as it determines the "jump" in the hyperplane of solution from one point to the next one. These jump lengths have a significant influence on the efficiency of the mirror algorithm, as they define the distance covered within the solution space in one iteration, but also the number of reflections in the solution boundaries (Van de Meerche et al., 2009). A small jump can collapse the algorithm in a local minimum, while a bigger one could not represent the solution space in a proper manner and can block the algorithm if it continually falls out of boundary constraints (that are the wall of the hyperplanes solution space): both happened. We noticed that jump under 0.1 were too small to permit the MCMC solution to reach a convergence value in a reasonable time, while jump over 0.1 created some problems during the runs, beacaue we have fluxes that have different value ranges. Fluxes have dimensional ranges which are very different between each other, reaching in certain cases two order of dimension diversity. Dimension number of fluxes was also referred by Van Ovelen et al. (2010), reporting that in the recent years food web

ecologists have realized that the values of food web flows can differ over order of magnitudes. That was a problem, as we have to find a jump that works efficiently in all cases. After lots of algorithm test runs, we choose the jump = 0.1. Once selected the jump length, we had choose the number of iterations. In literature, iterations numbers vary a lot: Raftery and Lewis (1996) suggested a minimum of 3000 iterations to reach the extremes, Van de Meerche et al. (2009) used 3000 iterations, Luonget et al. (2014) used 5000 iterations, Kones et al. (2009) used 25000 and 100000 iterations in two different cases and Stukel et al. (2012) used 10000 iterations. We decided to test the number of iterations season by season incrementally varying the number of iterations. We started from 5*10^2, 5*10^3, 5*10^4, 5*10^5, 5*10^6, 15*10^6, 25*10^6 and finally 50*10^6. All these tests were made season by season and, to be certain of results, with 0.1 and 1 as a length jump, doubling the cases. We check the convergence of the solution plotting each MCMC run, sample by sample, with iterative mean, iterative standard deviation and model error. As proposed by Kones et al. (2009), we visually verified the convergence of the MCMC sampling from the graphs. When convergence is reached, the sample-by-sample graph reached a plateau, the iterative mean and iterative standard deviation stabilized on low ranges values. After all these runs, we decided to take 15*10^6 iterations as fix parameters for our LIM – MCMC. We noted that certain fluxes stabilized very soon and others stabilised later. The most problematic ones were the GPP fluxes (especially in summer) and HB DOC uptake ones, as those fluxes were the ones with the bigger ranges and therefore uncertainty. Other fluxes which were problematic to stabilise were the detritus fluxes and growth fluxes due to the absence of an upper limit/boundary. We suggested to use this way of identifying critical fluxes as a sort of sensitivity analysis: it does not give the range of changes but denotes key fluxes and their uncertainties. The final representation, at jump = 0.1 and 15*10^6 number of iterations is reported from figure 28 to figure 31. In order to handle such a great number of iterations, we worked on clusters, using R from remote with 1 cpu and 120 gb of ram. Managing graphs with high numbers of data was difficult, so we decided to sample solutions every 100 samples in order to get a good representation.

From figures 28 to figure 31 we represented the sampling iterative process solution of each flux by the MCMC (solid grey line), the iterative mean (dashed line), the iterative standard deviation (dotted line), the iterative model error (dark line) and the single value of the Lsei solution (red dot). In the graphs, we can see all the fluxes, starting from the first one in the higher left corner corresponding to the first flux in the calculation (CO2_CB). Flux correspondence is going from left to right incrementally: the second flux in the first row is the second flux in the calculation (CB_DOC) and so on. From these graphs it is possible to denote fluxes which are more stable and less problematic in the samples routine.

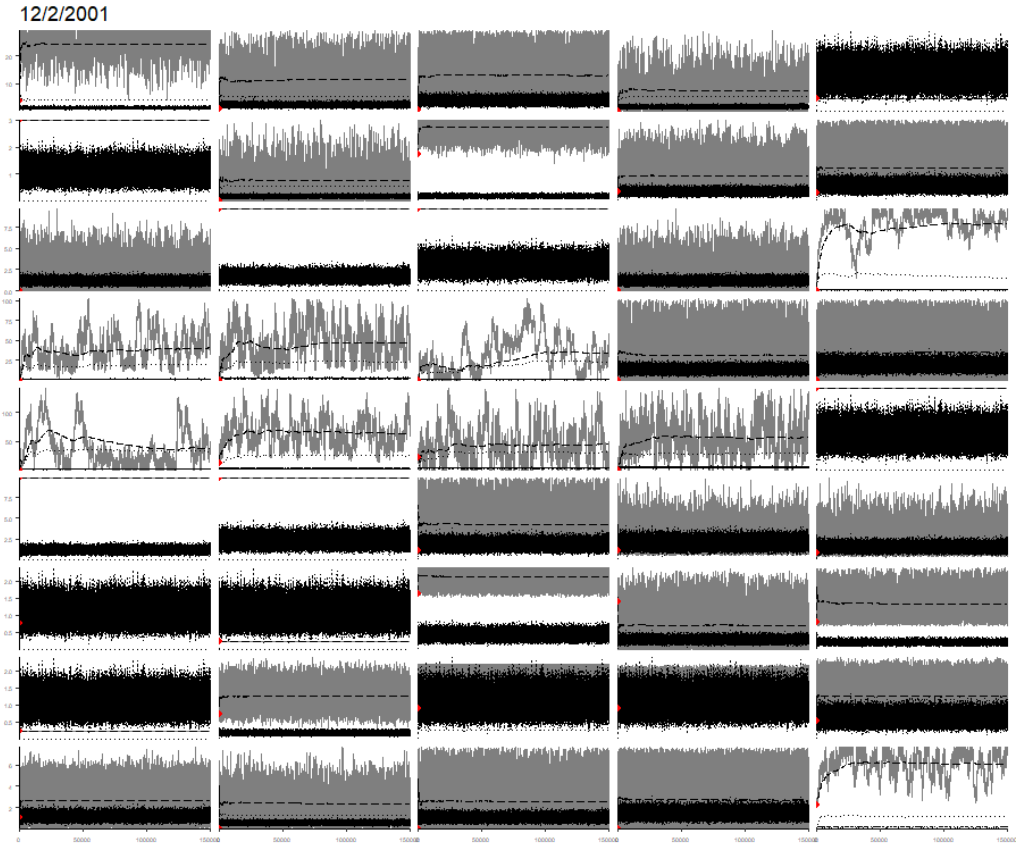

Figure 28: Winter case study fluxes in µg C l^{-1} d^{-1} (y axis) and number of iterations (x axis).

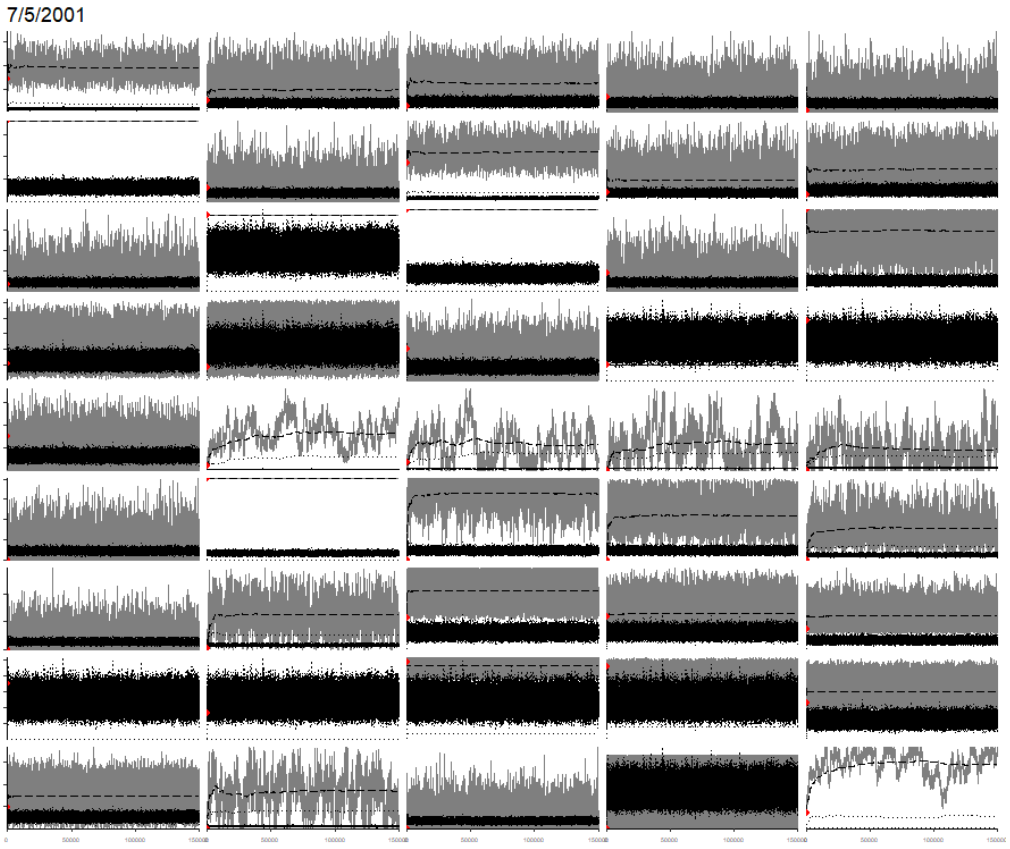

Figure 29: Spring case study fluxes in µg C l^{-1} d^{-1} (y axis) and number of iterations (x axis).

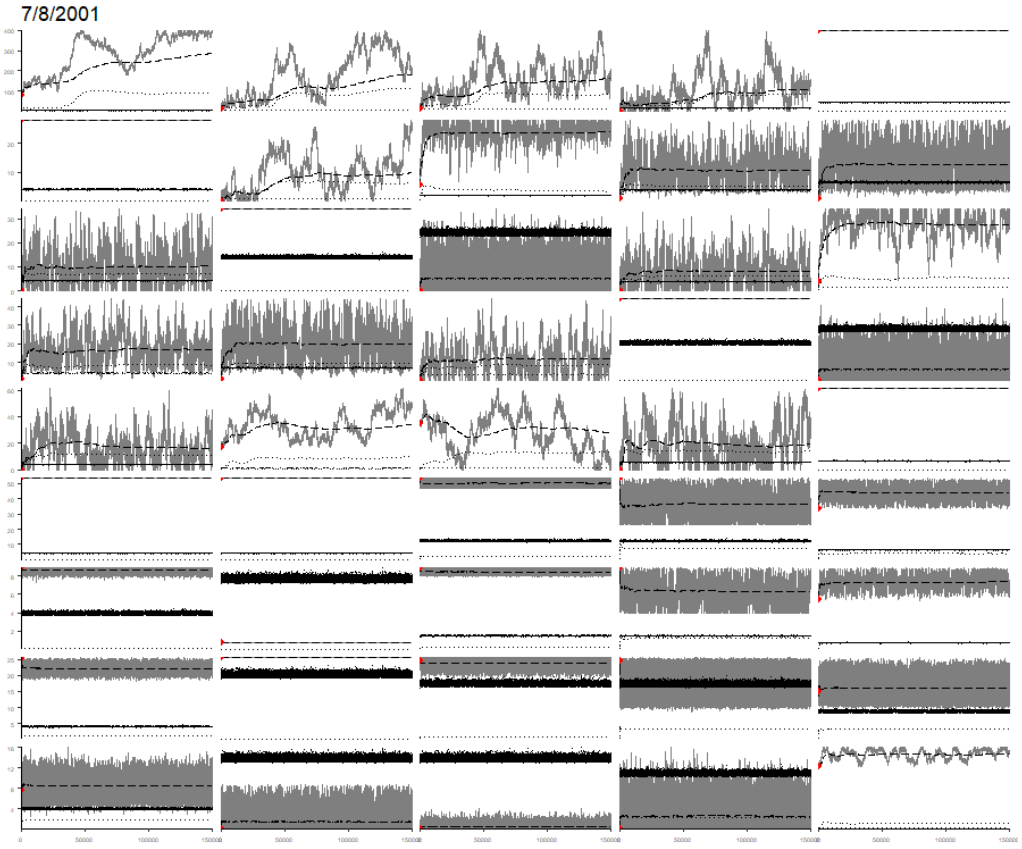

Figure 30: Summer case study fluxes in µg C l^{-1} d^{-1} (y axis) and number of iterations (x axis).

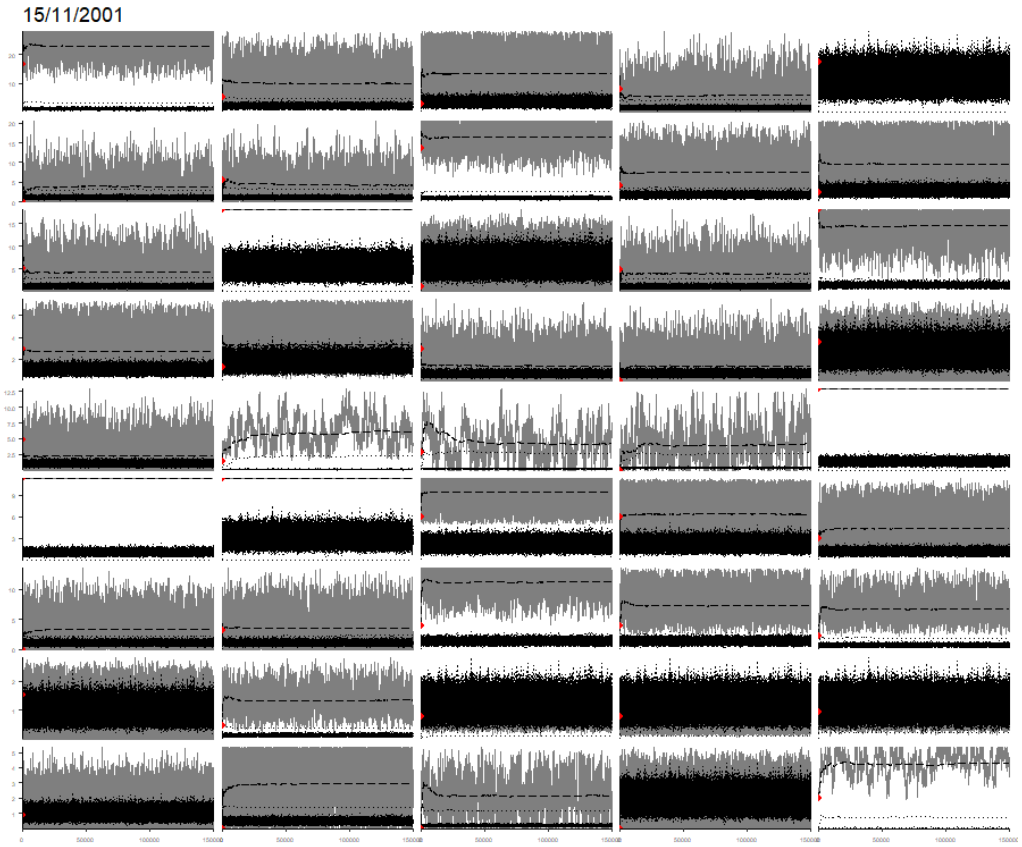

Figure 31: Winter case study fluxes in µg C l^{-1} d^{-1} (y axis) and number of iterations (x axis).

It is clear how the iterative solution converges to a stable value reaching the plateau, underlined by the stabilization of the iterative mean and standard deviation values. In the first part of each sub graph we clearly see how the iterative solution grows to reach the plateau in the initial part of the sample routine. In some graphs, the graph seems to be cut: obviously, it is not cut but it shows the evidence that the iterative solution is blocked in the upper values by the inequality constraints.

The last important part to define for the MCMC is the initialisation of the MCMC itself. Van de Meerche et al. (2009), in defining the initialisation points for the MCMC, suggested two solutions: the Lsei solution and the 0 solution (trivial). The 0 solution is the base one, as all the fluxes have 0 as lower bound and therefore it is the lowest solution possibility. The Lsei solution was suggested to favour the algorithm in reaching the plateau: it is the minimum solution valid for the MCMC. In literature, Soetart et al. 2009 used the Lsei solution when other particular ones are not provided. We tested both the 0 and the Lsei solution as initial MCMC points, season by season, with the jump and number of iteration chosen before. We decided to use the Lsei solution to initialise the MCMC as the convergence to the plateau is more rapid.

MCMC gives a wide number of solutions as a result: those that fall inside the constraint ranges. The last decision is how to establish the way to represent all the possible solutions. Van Ovelen et al. (2010) demonstrate that the calculation of the mean involves a linear operation on the solution set, which in turn gives a valid solution, and that the mean flow values always closely approximate the medians, and therefore, the mean flow vector seems to provide a good central estimate that is consistent with the LIM. He also showed how the mean of each set of solutions, e.g. the mean of each probability density function - being a linear operation - could be used to generate a mass balanced solution that fits all the constraints (Van Oevelen et al.,2010). Stukel and Laundry (2010) reported that the mean solution set by averaging each flow from a random compilation of all vectors that solve both the equality and the inequality constraints, may consequently provide a simpler and perhaps more ecologically relevant answer to the under constrained ecosystem model. Furthermore, we compared the median and the mean of MCMC samples: we chose the mean of the fluxes samples as the final solution for the MCMC.

Finally, we compared the two different solutions, the LIM – MN vs the LIM – MCMC. Following the idea of Kones et al. (2006), the comparison on the differences between the mean and parsimonious solutions was based on the non-parametric Wilcoxon signed ranks test. We used non-parametric Wilcoxon test because solutions are not normal, dependent and therefore paired. In contrast with Kones et al. (2006) we found out that the two solutions are very different between each other. The solutions that differ the most are winter ones with a p-value = $1.1e^{-06}$ and the spring ones that have a

p-value = $4.07e^{-05}$. Summer and autumn solutions are more similar but significantly different at the same time, with a p-value = 0.0004203 and a p-value = 0.0007598 respectively. We expected such results, especially for winter and spring solutions that are completely different in term of values and compartment size. Furthermore, to compare the two solutions we plotted the LIM – MCMC and the LIM – MN fluxes, first in a boxplot graph (Figure 32) and then in frequency histograms season by season (Figure 33 to Figure 36).

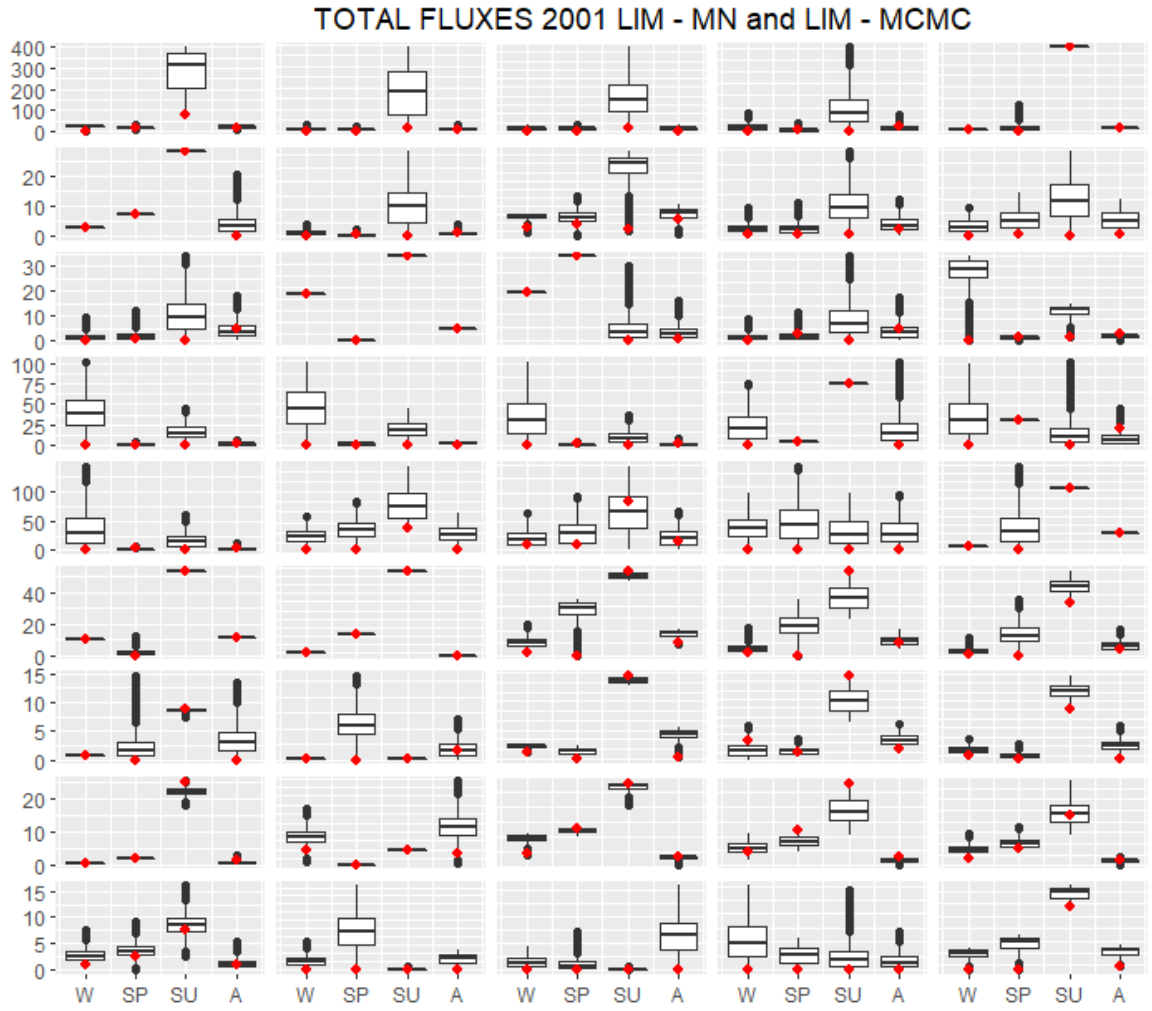

Figure 32: Box plot graphs of 2001 fluxes in µg C l^{-1} d^{-1}.

In figure 32, dark box plots are the representation of the LIM – MCMC solution, while red spots are the LIM – MN solution. In the graphs we can see all the fluxes, starting from the first one in the higher left corner corresponding to the first flux in the calculation (CO2_CB). Flux correspondence is going from left to right incrementally: the second flux in the first row is the second flux in the calculation (CB_DOC) and so on. From the boxplots graphs, we can clearly see how the LIM – MN solution is settled in the lower part of the LIM – MCMC solution, except for some rare cases.

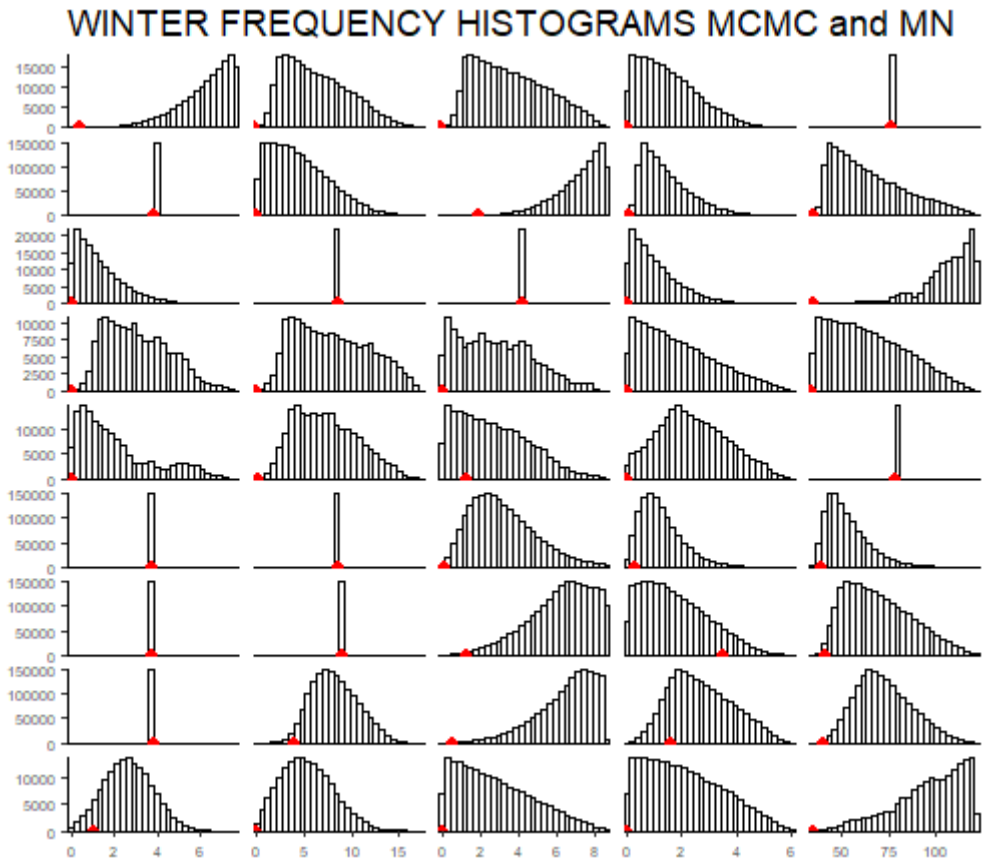

Figure 33: Winter frequency histograms of LIM – MCMC and LIM – MN solution in µg C l^{-1} d^{-1} (x axis).

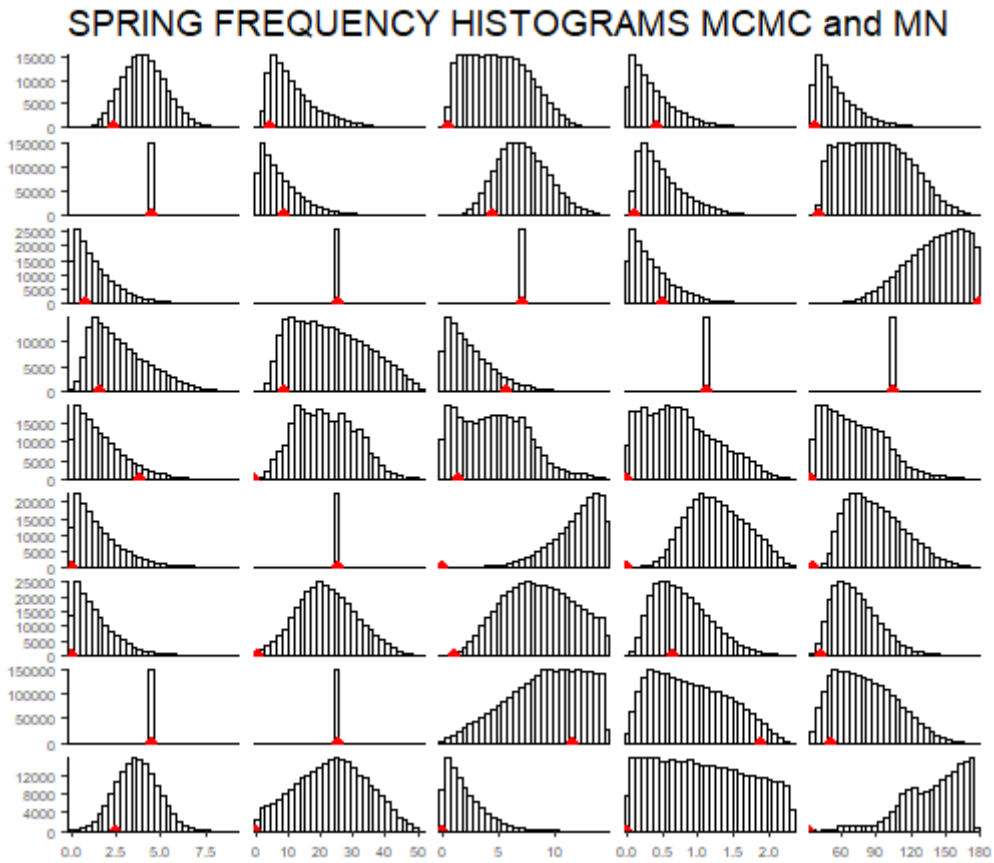

Figure 34: Spring frequency histograms of LIM – MCMC and LIM – MN solution in µg C l-1 d-1 (x axis).

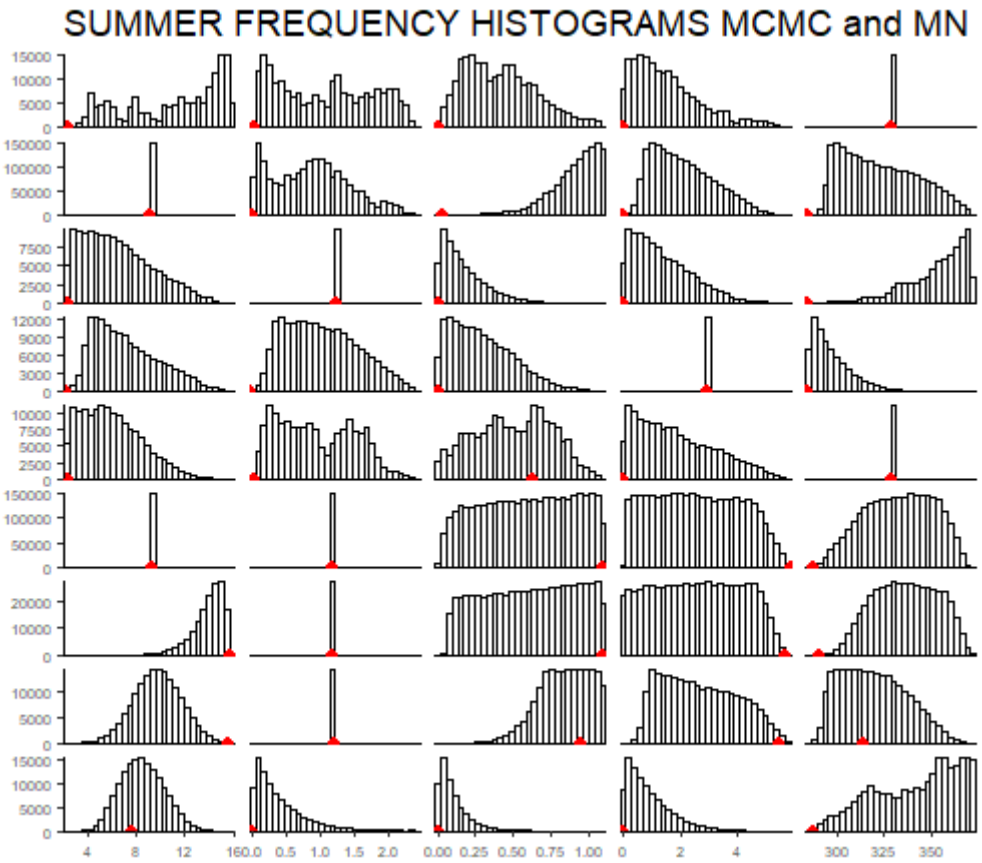

Figure 35: Summer frequency histograms of LIM – MCMC and LIM – MN solution in µg C l^{-1} d^{-1} (x axis).

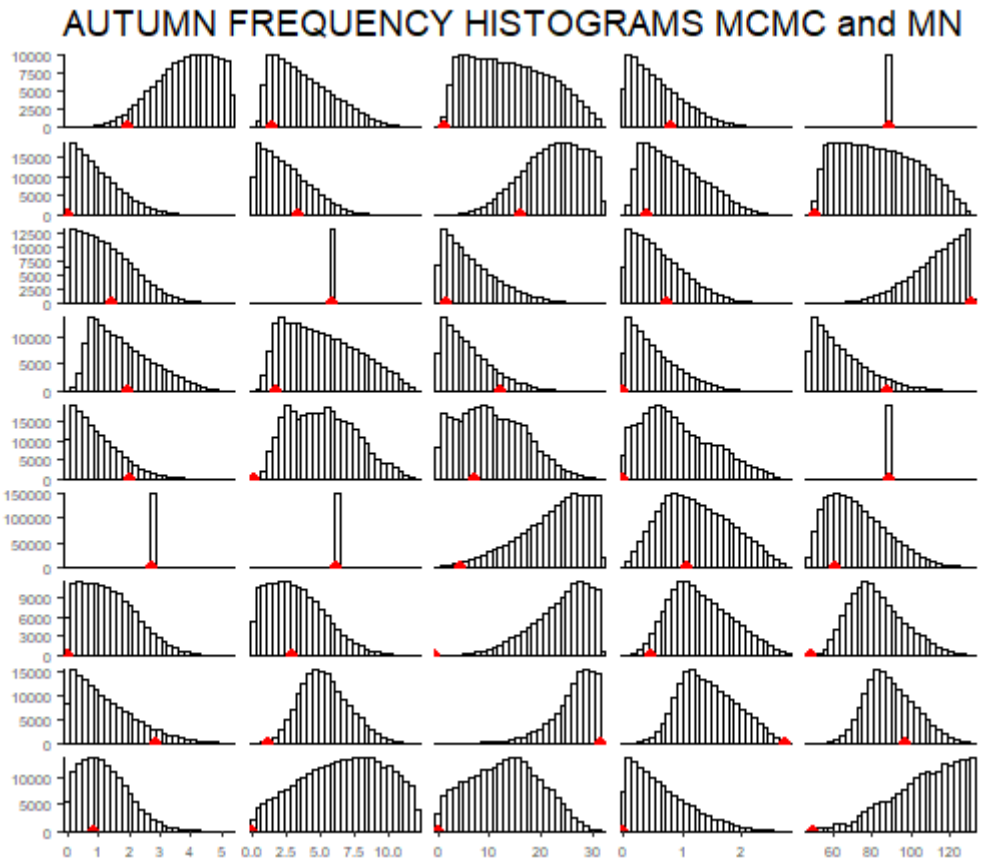

Figure 36: Autumn frequency histograms of LIM – MCMC and LIM – MN solution in µg C l^{-1} d^{-1} (x axis).

In particular LIM – MN values are settled in the boxplot part corresponding to outliers and minimum values of LIM – MCMC: it gives an idea of how the LIM – MN technique underestimates fluxes value. From the graph, we can also see the possible ranges of the MCMC solutions, which are very large sometimes.

From figure 33 to figure 36, we represented all the histogram frequency of the LIM – MCMC solutions season by season, compared with the single value of the LIM – MN solution (red dot). In the graphs, we can see all the fluxes, starting from the first one in the higher left corner corresponding to the first flux in the calculation (CO2_CB). Flux correspondence is going from left to right incrementally: the second flux in the first row is the second flux in the calculation (CB_DOC) and so on.

From the graphs, it is clear that most of the times the Lsei solution corresponds to the frequency histogram less represented in the MCMC solution. It is also possible to see how the solutions are not normal and how most of the solutions distributions correspond to a skewed truncated Gaussian curve. Sometimes the graphs seem to be cut in a different way. This is the effect of constraint planes of inequalities as reported by Niquil et al. (2010): probability density function could be not normal, sometimes truncated by the inequality constraints and sometimes uniform if the model and data are not sufficient to constrain the value of a flow.

In order to better evaluate the algorithm, we calculated the algorithm error (ε) on the solutions. The error was obtained through the following procedure. We multiplied each vector solution for the matrix A ($A\,x - b = \varepsilon$), obtaining an error vector with seven rows, each of them corresponding to its equation. Subsequently, we squared each row and summed up all the values. Then we divided for seven, and finally we square rooted the value, obtaining the mean model error. LIM – MCMC error values are higher than the LIM – MN ones. Values are reported in table 5.

	E LIM - MN	E LIM - MCMC
W	6.8 e-15	0.56
SP	9.25 e-15	0.78
SU	3.56	3.73
AU	2.31 e-14	0.2

Table 5: LIM –MN and LIM – MCMC mean square root error.

Error values are near to zero for the LIM – MN solution and low for the LIM – MCMC one. Both solutions are not constrained well in summer, when the fluxes registered higher values. Our opinion is that the LIM – MN is the lowest biased solution as it minimises all the fluxes minimising the squared error - $||A\,x - b||^2$, e.g. $\sum \varepsilon^2$. Therefore error values should be lower than the LIM – MCMC. Error values in the LIM – MCMC are very low if compared to fluxes values and so they are

satisfactory. It is the first time, as far as we know, that model errors are compared between the two solutions.

6. CONCLUSIONS

A complete measurement of all food web flows is generally not possible in natural complex food webs. Therefore, we studied the planktonic food web of the Gulf of Trieste using linear inverse modelling. We mixed the *a priori* knowledge (the food web design), some *in situ* data and literature knowledge, using a modellistic approach. The methodology we used permitted us to depict all the fluxes inside the planktonic food web. We obtained two solutions that were compared and analyzed.

Both LIM methods give back reasonable solutions, which are obtained by different arbitrary choices. The LIM – MN selects the best solution minimizing the sum of squared flows, while the LIM – MCMC selects the solution through an exhaustive sampling of the solution space. Both solutions respect the inequalities and all the ecological requests and therefore are valid. The LIM- MN usually underestimates all the fluxes, while the LIM – MCMC gives a good representation of the flows ranges, rarely overestimating not very well bounded fluxes. Growth fluxes behave well, especially the LIM – MCMC ones, and give a good response as they are in agreement with the scientific knowledge of the Gulf of Trieste. Implementing this type of compartment could be a good compromise in using a steady state condition.

It is our opinion that LIM – MCMC solution is the best way to depict all the planktonic food web fluxes of the Gulf of Trieste. Values of fluxes are the best representation of what is the *a priori* ecological knowledge found in the literature. In particular, the solution explains the important role of bacterial compartments that are fundamental for the Gulf of Trieste marine life, as they channelled most of the carbon inside the food web. The so-called microbial loop is very strong, and sets the microzooplankton as the main actor in channelling carbon from lower ecotrophic levels to higher ones, including fishes. Moreover, thanks to the values found in this study, the Gulf of Trieste planktonic ecosystem could be compared with more productive ecosystems on a world scale.

Future works may focus on identifying more stringent and *in situ* dedicated equalities and inequalities, coupling the modellistic approach with some experimental studies. Moreover, the depicted ecosystem could be expanded including higher ecotrophic levels, trying to determine the carry capacity of the ecosystem in order to prevent exploitations by human activity. Moreover, the linear inverse modelling could be applied to all the Adriatic Long Term Ecological Research (LTER) data, studying the changes that are happening in the ecosystem in a more focused way. Scientific research could then be coupled with future actions by stake holders, in order to prepare a good planning for the coastal ecosystem management.

7. REFERENCES

Baird, D., & Ulanowicz, R. E. (1993). Comparative study on the trophic structure, cycling and ecosystem properties of four tidal estuaries. Marine Ecology Progress Series, 221-237.

Bastian, M., Heymann, S., & Jacomy, M. (2009). Gephi: an open source software for exploring and manipulating networks. International AAAI Conference on Weblogs and Social Media.

Belgrano, A. (Ed.). (2005). Aquatic food webs: an ecosystem approach. Oxford University Press.

Berman, T., Parparov, A., & Yacobi, Y. Z. (2004). Planktonic community production and respiration and the impact of bacteria on carbon cycling in the photic zone of Lake Kinneret. Aquatic microbial ecology, 34(1), 43-55.

Bondavalli, C., Bodini, A., Rossetti, G., & Allesina, S. (2006). Detecting stress at the whole-ecosystem level: the case of a mountain lake (Lake Santo, Italy). Ecosystems, 9(5), 768-787.

Brigolin, D., Savenkoff, C., Zucchetta, M., Pranovi, F., Franzoi, P., Torricelli, P., & Pastres, R. (2011). An inverse model for the analysis of the Venice lagoon food web. Ecological modelling, 222(14), 2404-2413.

Cataletto, B., Feoli, E., Umani, S. F., & Cheng-Yong, S. (1995). Eleven years of time-series analysis on the net-zooplankton community in the Gulf of Trieste. ICES Journal of Marine Science, 52(3-4), 669-678.

Christensen, V., & Pauly, D. (1992). ECOPATH II—a software for balancing steady-state ecosystem models and calculating network characteristics. Ecological modelling, 61(3-4), 169-185.

Cossarini, G., & Solidoro, C. (2008). Global sensitivity analysis of a trophodynamic model of the Gulf of Trieste. Ecological Modelling, 212(1), 16-27.

Daniels, R. M., Richardson, T. L., & Ducklow, H. W. (2006). Food web structure and biogeochemical processes during oceanic phytoplankton blooms: an inverse model analysis. Deep Sea Research Part II: Topical Studies in Oceanography, 53(5), 532-554.

De Laender, F., Van Oevelen, D., Soetaert, K., & Middelburg, J. J. (2010). Carbon transfer in herbivore-and microbial loop-dominated pelagic food webs in the southern Barents Sea during spring and summer. Marine Ecology Progress Series, 398, 93-107.

Diffendorfer, J. E., Richards, P. M., Dalrymple, G. H., & DeAngelis, D. L. (2001). Applying Linear Programming to estimate fluxes in ecosystems or food webs: an example from the herpetological assemblage of the freshwater Everglades. Ecological Modelling, 144(2), 99-120.

Donali, E., Olli, K., Heiskanen, A. S., & Andersen, T. (1999). Carbon flow patterns in the planktonic food web of the Gulf of Riga, the Baltic Sea: a reconstruction by the inverse method. Journal of Marine Systems, 23(1), 251-268.

Eldridge, P. M., & Jackson, G. A. (1992). Benthic food web flows in the Santa Monica Basin estimated using inverse methodology. In Deep-Sea Food Chains and the Global Carbon Cycle (pp. 255-276). Springer Netherlands.

Falkowski, P. G., Barber, R. T., & Smetacek, V. (1998). Biogeochemical controls and feedbacks on ocean primary production. Science, 281(5374), 200-206.

Fasham, M.J.R. (Editor), 1984. Flows of Energy and Materials in Marine Ecosystems. Plenum Publishing Corporation, New York

Finn, J. T. (1976). Measures of ecosystem structure and function derived from analysis of flows. Journal of theoretical Biology, 56(2), 363-380.

Grami, B., Niquil, N., Hlaili, A. S., Gosselin, M., Hamel, D., & Mabrouk, H. H. (2008). The plankton food web of the Bizerte Lagoon (South-western Mediterranean): II. Carbon steady-state modelling using inverse analysis. Estuarine, Coastal and Shelf Science, 79(1), 101-113.

Harding, L. W., Degobbis, D., & Precali, R. (1999). Production and fate of phytoplankton: annual cycles and interannual variability. Ecosystems at the Land-Sea Margin: Drainage Basin to Coastal Sea, 131-172.

Haskell, K. H., & Hanson, R. J. (1981). An algorithm for linear least squares problems with equality and nonnegativity constraints. Mathematical Programming, 21(1), 98-118.

Heymans, J. J., Coll, M., Libralato, S., Morissette, L., & Christensen, V. (2014). Global patterns in ecological indicators of marine food webs: a modelling approach. PloS one, 9(4), e95845.

Jassby, A. D., & Platt, T. (1976). Mathematical formulation of the relationship between photosynthesis and light for phytoplankton. Limnology and oceanography, 21(4), 540-547.

Kones, J. K., Soetaert, K., van Oevelen, D., Owino, J. O., & Mavuti, K. (2006). Gaining insight into food webs reconstructed by the inverse method. Journal of Marine Systems, 60(1), 153-166.

Kones, J. K., Soetaert, K., van Oevelen, D., & Owino, J. O. (2009). Are network indices robust indicators of food web functioning? a monte carlo approach. Ecological Modelling, 220(3), 370-382.

Lazzari, P., Solidoro, C., Ibello, V., Salon, S., Teruzzi, A., Béranger, K., & Crise, A. (2012). Seasonal and inter-annual variability of plankton chlorophyll and primary production in the Mediterranean Sea: a modelling approach. Biogeosciences, 9(1), 217.

Legendre, L., & Rassoulzadegan, F. (1996). Food-web mediated export of biogenic carbon in oceans: hydrodynamic control. Marine Ecology Progress Series, 179-193.

Legendre, P., & Legendre, L. (1998). Numerical ecology: second English edition. Developments in environmental modelling, 20.

Leguerrier, D., Niquil, N., Boileau, N., Rzeznik, J., Sauriau, P. G., Le Moine, O., & Bacher, C. (2003). Numerical analysis of the food web of an intertidal mudflat ecosystem on the Atlantic coast of France. Marine ecology progress series, 246, 17-37.

Luong, A. D., De Laender, F., Olsen, Y., Vadstein, O., Dewulf, J., & Janssen, C. R. (2014). Inferring time-variable effects of nutrient enrichment on marine ecosystems using inverse modelling and ecological network analysis. Science of the Total Environment, 493, 708-718.

Malej, A., Mozetič, P., Malačič, V., Terzić, S., & Ahel, M. (1995). Phytoplankton responses to freshwater inputs in a small semi-enclosed gulf (Gulf of Trieste, Adriatic Sea). Marine Ecology Progress Series, 111-121.

Marquis, E., Niquil, N., Delmas, D., Hartmann, H. J., Bonnet, D., Carlotti, F., Vézina, A. (2007). Inverse analysis of the planktonic food web dynamics related to phytoplankton bloom development on the continental shelf of the Bay of Biscay, French coast. Estuarine, Coastal and Shelf Science, 73(1), 223-235.

Marquis, E., Niquil, N., Vézina, A. F., Petitgas, P., & Dupuy, C. (2011). Influence of planktonic foodweb structure on a system's capacity to support pelagic production: an inverse analysis approach. ICES Journal of Marine Science, 68(5), 803-812.

Moloney, C. L., & Field, J. G. (1989). General allometric equations for rates of nutrient uptake, ingestion, and respiration in plankton organisms. Limnology and Oceanography, 34(7), 1290-1299.

Mozetiĉ, P., Umani, S. F., Cataletto, B., & Malej, A. (1998). Seasonal and inter-annual plankton variability in the Gulf of Trieste (northern Adriatic). ICES Journal of Marine Science, 55(4), 711-722.

Niquil, N., Jackson, G. A., Legendre, L., & Delesalle, B. (1998). Inverse model analysis of the planktonic food web of Takapoto Atoll (French Polynesia). Marine Ecology Progress Series, 17-29.

Niquil, N., Arias-González, J. E., Delesalle, B., & Ulanowicz, R. E. (1999). Characterization of the planktonic food web of Takapoto Atoll lagoon, using network analysis. Oecologia, 118(2), 232-241.

Niquil, N., Pouvreau, S., Sakka, A., Legendre, L., Addessi, L., Le Borgne, R., & Delesalle, B. (2001). Trophic web and carrying capacity in a pearl oyster farming lagoon (Takapoto, French Polynesia). *Aquatic Living Resources*, *14*(3), 165-174.

Niquil, N., Bartoli, G., Urabe, J., Jackson, G. A., Legendre, L., Dupuy, C., & Kumagai, M. (2006). Carbon steady-state model of the planktonic food web of Lake Biwa, Japan. Freshwater Biology, 51(8), 1570-1585.

Niquil, N., Kagami, M., Urabe, J., Christaki, U., Viscogliosi, E., & Sime-Ngando, T. (2011). Potential role of fungi in plankton food web functioning and stability: a simulation analysis based on Lake Biwa inverse model. Hydrobiologia, 659(1), 65-79.

Niquil, N., Soetaert, K. E. R., Johnson, G. A., Van Oevelen, D., Bacher, C., Saint-Béat, B., & Vézina, A. F. (2011). Inverse modelling in modern ecology and application to coastal ecosystems. In E. Wolanski, & D. Mclusky (Eds.), Estuarine and Coastal Ecosystem Modelling (Vol. 9.07, pp. 115-133). (Treatise on Estuarine and Coastal Science). Elsevier

Olsen, Y., Reinertsena, H., Vadsteina, O., Andersen, T., Gismervik, I., Duarte, C., Agusti, S., Stibord, H., Sommer, U., Lignell, R., Tamminen, T., Lancelot, C., Rousseau, V., Hoell, E., & Sanderud, K. A. (2001). Comparative analysis of food webs based on flow networks: effects of nutrient supply on structure and function of coastal plankton communities. Continental Shelf Research, 21(18–19), 2043–2053.

Parker, R. L. (1977). Understanding inverse theory. Annual Review of Earth and Planetary Sciences, 5(1), 35-64.

Patrıcio, J., Ulanowicz, R., Pardal, M. A., & Marques, J. C. (2004). Ascendency as an ecological indicator: a case study of estuarine pulse eutrophication. *Estuarine, Coastal and Shelf Science*, *60*(1), 23-35.

Pimm, S. L. (1982). Food webs. In Food webs (pp. 1-11). Springer Netherlands.

Querin, S., Crise, A., Deponte, D., & Solidoro, C. (2006). Numerical study of the role of wind forcing and freshwater buoyancy input on the circulation in a shallow embayment (Gulf of Trieste, Northern Adriatic Sea). Journal of Geophysical Research: Oceans, 111(C3).

Raftery, A. E., & Lewis, S. M. (1996). Implementing mcmc. Markov chain Monte Carlo in practice, 115-130.

Richardson, T. L., Jackson, G. A., & Burd, A. B. (2003). Planktonic food web dynamics in two contrasting regions of Florida Bay, US. Bulletin of Marine Science, 73(3), 569-591.

Richardson, T. L., Jackson, G. A., Ducklow, H. W., & Roman, M. R. (2006). Spatial and seasonal patterns of carbon cycling through planktonic food webs of the Arabian Sea determined by inverse analysis. Deep Sea Research Part II: Topical Studies in Oceanography, 53(5), 555-575.

Roberts, G. O. (1996). Markov chain concepts related to sampling algorithms. Markov chain Monte Carlo in practice, 57.

Robinson, N. A. (1992). Agenda 21 & the UNCED proceedings (No. 333.715 A265). The Commission on Environmental Law of the World Conservation Union, Gland (Suiza) IUCN, Gland (Suiza).

Rockström, J., Steffen, W., Noone, K., Persson, Å., Chapin III, F. S., Lambin, E., ... & Nykvist, B. (2009). Planetary boundaries: exploring the safe operating space for humanity. Ecology and society, 14(2).

Sarmiento, J. L., & Gruber, N. (2006). Ocean biogeochemical cycles. Princeton University.

Savenkoff, C., Castonguay, M., Chabot, D., Hammill, M. O., Bourdages, H., & Morissette, L. (2007a). Changes in the northern Gulf of St. Lawrence ecosystem estimated by inverse modelling: Evidence of a fishery-induced regime shift?. Estuarine, Coastal and Shelf Science, 73(3), 711-724.

Savenkoff, C., Swain, D. P., Hanson, J. M., Castonguay, M., Hammill, M. O., Bourdages, H., Chabot, D. (2007b). Effects of fishing and predation in a heavily exploited ecosystem: comparing periods before and after the collapse of groundfish in the southern Gulf of St. Lawrence (Canada). Ecological modelling, 204(1), 115-128.

Savidge, G., Turner, D. R., Burkill, P. H., Watson, A. J., Angel, M. V., Pingree, R. D., Richards, K. J. (1992). The BOFS 1990 spring bloom experiment: temporal evolution and spatial variability of the hydrographic field. Progress in Oceanography, 29(3), 235-281.

Sigman, D. M., & Boyle, E. A. (2000). Glacial/interglacial variations in atmospheric carbon dioxide. Nature, 407(6806), 859-869.

Soetaert, K., & van Oevelen, D. (2008). LIM: Linear Inverse Modelling. R package version, 1.

Soetaert, K., & Van Oevelen, D. (2009). LIM: Linear Inverse Model examples and solution methods.

Soetaert, K., Van den Meersche, K., & Van Oevelen, D. (2009). Package limSolve, solving linear inverse models in R. See http://cran. r-project. org/web/packages/limSolve.

Soetart, K., & van Oevelen, D. (2009). Modeling food web interactions in benthic deep-sea ecosystems: a practical guide. Oceanography, 22(1), 128-143.

Steele, J. H. (2009). Assessment of some linear food web methods. Journal of Marine systems, 76(1), 186-194.

Steffen, W., Richardson, K., Rockström, J., Cornell, S. E., Fetzer, I., Bennett, E. M., … & Folke, C. (2015). Planetary boundaries: Guiding human development on a changing planet. Science, 347(6223), 1259855.

Stukel, M. R., & Landry, M. R. (2010). Contribution of picophytoplankton to carbon export in the equatorial Pacific: A reassessment of food web flux inferences from inverse models. Limnology and Oceanography, 55(6), 2669-2685.

Stukel, M. R., Landry, M. R., Ohman, M. D., Goericke, R., Samo, T., & Benitez-Nelson, C. R. (2012). Do inverse ecosystem models accurately reconstruct plankton trophic flows? Comparing two solution methods using field data from the California Current. Journal of Marine Systems, 91(1), 20-33.

Szyrmer, J., & Ulanowicz, R. E. (1987). Total flows in ecosystems. Ecological Modelling, 35(1-2), 123-136.

Terzić, S., Ahel, M., Cauwet, G., & Malej, A. (1998). Group-specific phytoplankton biomass/dissolved carbohydrate relationships in the Gulf of Trieste (Northern Adriatic). In Eutrophication in Planktonic Ecosystems: Food Web Dynamics and Elemental Cycling (pp. 191-205). Springer Netherlands.

Ulanowicz, R. E. (1980). An hypothesis on the development of natural communities. Journal of theoretical Biology, 85(2), 223-245.

Ulanowicz, R. E. (1986). NETWRK3: A package of Computer Algorithms to analyze ecological flow networks. Chesapeake Biological Laboratory.

Ulanowicz, R. E., & Wolff, W. F. (1991). Ecosystem flow networks: loaded dice?. Mathematical Biosciences, 103(1), 45-68.

Ulanowicz, R. E. (1997). Ecology, the ascendent perspective: Robert E. Ulanowicz. Columbia University Press.

Umani, S. F., Franco, P., Ghirardelli, E., & Malej, A. (1992). Outline of oceanography and the plankton of the Adriatic Sea. Marine eutrophication and population dynamics, 347-365.

Umani, S. F. (1996). Pelagic production and biomass in the Adriatic Sea. Sci. Mar, 60(2), 65-77.

Umani, S. F., & Beran, A. (2003). Seasonal variations in the dynamics of microbial plankton communities: first estimates from experiments in the Gulf of Trieste, Northern Adriatic Sea. Marine Ecology Progress Series, 247, 1-16.

Umani, S. F., Del Negro, P., Larato, C., De Vittor, C., Cabrini, M., Celio, M., Flaconi, C., Tamberlich, F., Azam, F. (2007). Major inter-annual variations in microbial dynamics in the Gulf of Trieste (northern Adriatic Sea) and their ecosystem implications. Aquatic Microbial Ecology, 46(2), 163-175.

Umani, S. F., Malfatti, F., & Del Negro, P. (2012). Carbon fluxes in the pelagic ecosystem of the Gulf of Trieste (Northern Adriatic Sea). Estuarine, Coastal and Shelf Science, 115, 170-185.

Valiela, I., 1995. Marine Ecological Processes. Springer-Verlag, New York, 686 pp.

Van den Meersche, K., Soetaert, K., & Van Oevelen, D. (2009). xsample (): an R function for sampling linear inverse problems. Journal of Statistical Software, 30(Code Snippet 1).

Van Oevelen, D., Soetaert, K., Middelburg, J. J., Herman, P. M., Moodley, L., Hamels, I., ... & Heip, C. H. (2006). Carbon flows through a benthic food web: Integrating biomass, isotope and tracer data. Journal of Marine Research, 64(3), 453-482.

Van Oevelen, D., Van den Meersche, K., Meysman, F. J., Soetaert, K., Middelburg, J. J., & Vézina, A. F. (2010). Quantifying food web flows using linear inverse models. Ecosystems, 13(1), 32-45.

Vargas, C. A., Cuevas, L. A., González, H. E., & Daneri, G. (2007). Bacterial growth response to copepod grazing in aquatic ecosystems. Journal of the Marine Biological Association of the United Kingdom, 87(3), 667-674.

Vézina, A. F., & Platt, T. (1988). Food web dynamics in the ocean. I. Best-estimates of flow networks using inverse methods. Marine Ecology Progress Series, 269-287.

Vézina, A. F., & Pace, M. L. (1994). An inverse model analysis of planktonic food webs in experimental lakes. Canadian Journal of Fisheries and Aquatic Sciences, 51(9), 2034-2044.

Vézina, A. F., & Savenkoff, C. (1999). Inverse modeling of carbon and nitrogen flows in the pelagic food web of the northeast subarctic Pacific. Deep Sea Research Part II: Topical Studies in Oceanography, 46(11), 2909-2939.

Vézina, A. F., Savenkoff, C., Roy, S., Klein, B., Rivkin, R., Therriault, J. C., & Legendre, L. (2000). Export of biogenic carbon and structure and dynamics of the pelagic food web in the Gulf of St. Lawrence Part 2. Inverse analysis. Deep Sea Research Part II: Topical Studies in Oceanography, 47(3), 609-635.

Vézina, A. F., & Pahlow, M. (2003). Reconstruction of ecosystem flows using inverse methods: how well do they work?. Journal of Marine Systems, 40, 55-77.

Vézina, A. F., Berreville, F., & Loza, S. (2004). Inverse reconstructions of ecosystem flows in investigating regime shifts: impact of the choice of objective function. Progress in Oceanography, 60(2), 321-341.

Vichi, M., Cossarini, G., Gutierrez Mlot, E., Lazzari, P., Lovato, T., Mattia, G.,Zavatarelli, M. (2013). The Biogeochemical Flux Model (BFM): equation description and user manual. BFM version, 5, 87.

Vichi, M., Lovato, T., Lazzari, P., Cossarini, G., Mlot, E. G., Mattia, G., Tedesco, L. (2015). The biogeochemical flux model (BFM): Equation description and user manual, BFM version 5.1. BFM Rep. Ser, 1, 104.

Williams, R. G., & Follows, M. J. (2011). Ocean dynamics and the carbon cycle: Principles and mechanisms. Cambridge University Press.

Wunsch, C. (1978). The North Atlantic general circulation west of 50 W determined by inverse methods. Reviews of Geophysics, 16(4), 583-620.

R CODE

In this section, we report an example of the code to implement the LIM.

12/2/2001 case study:

```
## COMPARTMENTS

#AUTOTROPHS

CB = CB_biomass # Cyanobacteria # Autotrophic Picoplankton
AN = AN_biomass # Nanoplankton  # Autotrophic Nanoplankton
MP = MP_biomass # Microphytoplankton

#HETEROTROPHS

HB = HB_biomass  # Bacteria # Hetererotrophic-Pikoplankton
HNF = HNF_biomass # Heterotrophic_Nanoplankton
MIZ = MIZ_biomass # Microzooplankton
MEZ = MEZ_biomass # Mesozooplankton

## END COMPARTEMENTS

##EXTERNALS

CO2 #= Respiration + GPP
DOC #= DOC_stock # Dissolved #organic carbon
DET #= DET_stock # DETRITUS #
GROWTH #= C to growth

##END EXTERNALS

##PARAMETERS

#Biomasses

CB_biomass = 8.24
AN_biomass = 6.61
MP_biomass = 151

HB_biomass = 25
HNF_biomass = 1.33
MIZ_biomass = 4.40
MEZ_biomass = 13.52

# Constrained parameters

#T = 10.27
#T_eff = exp(0.0693*(T-20))  #T effect
T_eff = 0.5095186

#W of each compartment in pg C cell-1

W_CB = 0.200 # Umani et al. 2012
W_HB = 0.020 # Umani et al. 2012
```

```
W_HNF = 5.63 # Vezina et al. 2000
W_MIZ = 582.96 # Vezina et al. 2000
W_MEZ = 3800000 # Richardson et al., 2006

# Respiration

min_CB_CO2 = 0.05 # 5% of gpp
max_CB_CO2 = 0.3 # 30% of gpp
min_AN_CO2 = 0.05 # 5% of gpp
max_AN_CO2 = 0.3 # 30% of gpp

min_MP_CO2 = 0.05 # 5% of gpp
max_MP_CO2 = 0.3 # 30% of gpp

min_HB_CO2 = 0.2 # # 20% of DOC uptake or total ingestion
#max_HB_CO2 = 3.6*(W_HB^-0.25)*T_eff  # maximum specific ingestion term*biomass
max_HB_CO2 = 4.877587

min_HNF_CO2 = 0.2 # 20% of total ingestion
#max_HNF_CO2 = 14*(W_HNF^-0.25)*T_eff  # maximum specific ingestion term*biomass
max_HNF_CO2 = 4.630852

min_MIZ_CO2 = 0.2 # 20% of total ingestion
#max_MIZ_CO2 = 14*(W_MIZ^-0.25)*T_eff  # maximum specific ingestion term*biomass
max_MIZ_CO2 = 1.451705

min_MEZ_CO2 = 0.2 # 20% of total ingestion
#max_MEZ_CO2 = 14*(W_MEZ^-0.25)*T_eff  # maximum specific ingestion term*biomass
max_MEZ_CO2 = 0.1615631 #

# Exudation (Excretion) of DOC

min_CB_DOC = 0.1  # 10 % of NPP (Net primary production)
max_CB_DOC = 0.55 # 55 % of NPP

min_AN_DOC = 0.1  # 10 % of NPP (Net primary production)
max_AN_DOC = 0.55 # 55 % of NPP

min_MP_DOC = 0.1  # 10 % of NPP (Net primary production)
max_MP_DOC = 0.55 # 55 % of NPP

min_HNF_DOC = 0.1 # 10 % of total ingestion
max_HNF_DOC = 1   # >equal to their respiration

min_MIZ_DOC = 0.1 # 10 % of total ingestion
max_MIZ_DOC = 1   # >equal to their respiration

min_MEZ_DOC = 0.1 # 10 % of their ingestion
max_MEZ_DOC = 1   # >equal to their respiration

#HB uptake of DOC or total ingestion

#max_HB_UPT = 3.6*(W_HB^-0.25)*T_eff # max uptake of DOC term*biomass
max_HB_UPT = 4.877587 # max uptake of DOC term*biomass

# Net Production efficiency
```

```
min_HB_NPEF = 0.50 # 50% of DOC uptake
max_HB_NPEF = 0.75 # 75% of DOC uptake

# Gross Production efficiency

min_HNF_GPEF = 0.50 # 50% of Total Ingestion
max_HNF_GPEF = 0.75 # 75% of Total Ingestion

min_MIZ_GPEF = 0.50 # 50% of Total Ingestion
max_MIZ_GPEF = 0.75 # 75% of Total Ingestion

min_MEZ_GPEF = 0.50 # 50% of Total Ingestion
max_MEZ_GPEF = 0.75 # 75% of Total Ingestion

#Ingestion

#max_HNF_ING = 63*(W_HNF^-0.25)*T_eff # max Ingestion term*biomass
max_HNF_ING = 20.83884 #

#max_MIZ_ING = 63*(W_MIZ^-0.25)*T_eff # max Ingestion term*biomass
max_MIZ_ING = 6.532672 #

#max_MEZ_ING = 63*(W_MEZ^-0.25)*T_eff # max Ingestion term*biomass
max_MEZ_ING = 0.7270339 #

#Assimilation efficiency

min_HNF_ASSEFF = 0.1 #of total ingestion
max_HNF_ASSEFF = 0.5 #of total ingestion

min_MIZ_ASSEFF = 0.2 #of total ingestion
max_MIZ_ASSEFF = 0.5 #of total ingestion

min_MEZ_ASSEFF = 0.2 #of total ingestion
max_MEZ_ASSEFF = 0.5 #of total ingestion

##END PARAMETERS

##VARIABLES

#R

CO2_micro = Flowto(CO2) - MEZ_CO2

#PP and NPP

NPP_CB = CO2_CB - CB_CO2
NPP_AN = CO2_AN - AN_CO2
NPP_MP = CO2_MP - MP_CO2

GPP = CO2_CB + CO2_AN + CO2_MP
NPP = NPP_CB + NPP_AN + NPP_MP

#Total ingestion terms
```

```
TOT_ing_HNF = CB_HNF + HB_HNF + DET_HNF # Total Ingestion of Heterotrophic nanoplankton
TOT_ing_MIZ = CB_MIZ + AN_MIZ + MP_MIZ + HB_MIZ + HNF_MIZ + DET_MIZ   # Total #ingestion of Microzooplankton
TOT_ing_MEZ = AN_MEZ + MP_MEZ + MIZ_MEZ + DET_MEZ                     # Total #ingestion of Mesozooplankton

#GROWTH

CB_GR = CO2_CB - CB_DOC - CB_CO2 - CB_DET - CB_HNF - CB_MIZ
AN_GR = CO2_AN - AN_DOC - AN_CO2 - AN_DET - AN_MIZ - AN_MEZ
MP_GR = CO2_MP - MP_DOC - MP_CO2 - MP_DET - MP_MIZ - MP_MEZ
HB_GR = DOC_HB - HB_CO2 - HB_DOC - HB_DET - HB_HNF - HB_MIZ
HNF_GR = TOT_ing_HNF - HNF_CO2 - HNF_DOC - HNF_DET - HNF_MIZ
MIZ_GR = TOT_ing_MIZ - MIZ_CO2 - MIZ_DOC - MIZ_DET - MIZ_MEZ
MEZ_GR = TOT_ing_MEZ - MEZ_CO2 - MEZ_DOC - MEZ_DET

##END VARIABLES

##FLOWS

##CB # Cyanobacteria # Autotrophic Picoplankton

CO2_CB : Flow(CO2,CB)   ## GPP
CB_DOC : Flow(CB,DOC)   ## Exudation
CB_CO2 : Flow(CB,CO2)   ## Respiration
CB_DET : Flow(CB,DET)   ## To POC
CB_HNF : Flow(CB,HNF)   ## Predation by HNF
CB_MIZ : Flow(CB,MIZ)   ## Predation by MIZ
CB_GR  : Flow(CB,GROWTH)  # NET primary production

##AN # Nanoplankton  # Autotrophic nanoplankton

CO2_AN : Flow(CO2,AN)   ## GPP
AN_DOC : Flow(AN,DOC)   ## Exudation
AN_CO2 : Flow(AN,CO2)   ## Respiration
AN_DET : Flow(AN,DET)   ## To POC
AN_MIZ : Flow(AN,MIZ)   ## Predation by MIZ
AN_MEZ : Flow(AN,MEZ)   ## Predation by MEZ
AN_GR  : Flow(AN,GROWTH)    # NET primary production

##MP # Microphytoplankton

CO2_MP : Flow(CO2,MP)   ## GPP
MP_DOC : Flow(MP,DOC)   ## Exudation
MP_CO2 : Flow(MP,CO2)   ## Respiration
MP_DET : Flow(MP,DET)   ## To POC
MP_MIZ : Flow(MP,MIZ)   ## Predation by MIZ
MP_MEZ : Flow(MP,MEZ)   ## Predation by MEZ
MP_GR  : Flow(MP,GROWTH)    # NET primary production

##HB  # Bacteria # Hetererotrophic pikoplankton

HB_CO2  : Flow(HB,CO2)   ## Respiration
HB_DOC  : Flow(HB,DOC)   ## Exudation
HB_DET  : Flow(HB,DET)   ## To POC
HB_HNF  : Flow(HB,HNF)   ## Predation by HNF
```

HB_MIZ : Flow(HB,MIZ) ## Predation by MIZ
HB_GR : Flow(HB,GROWTH) #Secondary production

##HNF # Heterotrophic nanoplankton

HNF_CO2 : Flow(HNF,CO2) ## Respiration
HNF_DOC : Flow(HNF,DOC) ## Exudation
HNF_DET : Flow(HNF,DET) ## To POC
HNF_MIZ : Flow(HNF,MIZ) ## Predation by MIZ
HNF_GR : Flow(HNF,GROWTH) #Secondary production

MIZ # Microzooplankton

MIZ_CO2 : Flow(MIZ,CO2) ## Respiration
MIZ_DOC : Flow(MIZ,DOC) ## Exudation and sloppy feeedings
MIZ_DET : Flow(MIZ,DET) ## To POC (sloppy feeding, fecal pellets)
MIZ_MEZ : Flow(MIZ,MEZ) ## Predation by MEZ
MIZ_GR : Flow(MIZ,GROWTH) #Secondary production

MEZ # Mesozooplankton

MEZ_CO2 : Flow(MEZ,CO2) ## Respiration
MEZ_DOC : Flow(MEZ,DOC) ## Exudation and sloppy feedings
MEZ_DET : Flow(MEZ,DET) ## To POC (sloppy feeding, fecal pellets)
MEZ_GR : Flow(MEZ,GROWTH) #Secondary production

DET # Detritus

DET_HNF : Flow(DET,HNF) ## Ingestion by HNF
DET_MIZ : Flow(DET,MIZ) ## Ingestion by MIZ
DET_MEZ : Flow(DET,MEZ) ## Ingestion by MEZ

DOC

DOC_HB : Flow(DOC,HB) ## DOC uptake

##END FLOWS

##EQUATIONS

AN_MIZ = 6.46
HNF_MIZ = 0.77
HB_MIZ = 9.83
CB_MIZ = 3.02
AN_MEZ = 3.56
MP_MEZ = 47.08
MIZ_MEZ = 0.22
HB_HNF = 2.54
CB_HNF = 0.38

HNF_GR = 0.24
HB_GR = 4.80

##END EQUATIONS

INEQUALITIES

Respiration

#min_CB_CO2*CO2_CB < CB_CO2
#CB_CO2 < max_CB_CO2*CO2_CB

CB_CO2 = [min_CB_CO2,max_CB_CO2]*CO2_CB

min_AN_CO2*CO2_AN < AN_CO2
AN_CO2 < max_AN_CO2*CO2_AN

min_MP_CO2*CO2_MP < MP_CO2
MP_CO2 < max_MP_CO2*CO2_MP

min_HB_CO2*DOC_HB < HB_CO2
HB_CO2 < max_HB_CO2*HB_biomass

min_HNF_CO2*TOT_ing_HNF < HNF_CO2
HNF_CO2 < max_HNF_CO2*HNF_biomass

min_MIZ_CO2*TOT_ing_MIZ < MIZ_CO2
MIZ_CO2 < max_MIZ_CO2*MIZ_biomass

min_MEZ_CO2*TOT_ing_MEZ < MEZ_CO2
MEZ_CO2 < max_MEZ_CO2*MEZ_biomass

Exudation/Excretion of DOC

min_CB_DOC*NPP_CB < CB_DOC
CB_DOC < max_CB_DOC*NPP_CB

min_AN_DOC*NPP_AN < AN_DOC
AN_DOC < max_AN_DOC*NPP_AN

min_MP_DOC*NPP_MP < MP_DOC
MP_DOC < max_MP_DOC*NPP_MP

min_HNF_DOC*TOT_ing_HNF < HNF_DOC
HNF_DOC < max_HNF_DOC*HNF_CO2

min_MIZ_DOC*TOT_ing_MIZ < MIZ_DOC
MIZ_DOC < max_MIZ_DOC*MIZ_CO2

min_MEZ_DOC*TOT_ing_MEZ < MEZ_DOC
MEZ_DOC < max_MEZ_DOC*MEZ_CO2

max uptake DOC by HB

DOC_HB < max_HB_UPT*HB_biomass

#Net production efficiency

min_HB_NPEF*DOC_HB < HB_CO2 + HB_DOC
HB_CO2 + Hb_DOC < max_HB_NPEF*DOC_HB

#Gross production efficiency

min_HNF_GPEF*TOT_ing_HNF < HNF_CO2 + HNF_DOC + HNF_DET
HNF_CO2 + HNF_DOC + HNF_DET < max_HNF_GPEF*TOT_ing_HNF

min_MIZ_GPEF*TOT_ing_MIZ < MIZ_CO2 + MIZ_DOC + MIZ_DET
MIZ_CO2 + MIZ_DOC + MIZ_DET < max_MIZ_GPEF*TOT_ing_MIZ

min_MEZ_GPEF*TOT_ing_MEZ < MEZ_CO2 + MEZ_DOC + MEZ_DET
MEZ_CO2 + MEZ_DOC + MEZ_DET < max_MEZ_GPEF*TOT_ing_MEZ

#Ingestion

TOT_ing_HNF < max_HNF_ING*HNF_biomass

TOT_ing_MIZ < max_MIZ_ING*MIZ_biomass

TOT_ing_MEZ < max_MEZ_ING*MEZ_biomass

#Assimilation efficiency

min_HNF_ASSEFF*TOT_ing_HNF < HNF_DET
HNF_DET < max_HNF_ASSEFF*TOT_ing_HNF

min_MIZ_ASSEFF*TOT_ing_MIZ < MIZ_DET
MIZ_DET < max_MIZ_ASSEFF*TOT_ing_MIZ

min_MEZ_ASSEFF*TOT_ing_MEZ < MEZ_DET
MEZ_DET < max_MEZ_ASSEFF*TOT_ing_MEZ

#GPP

CO2_CB < 29.38482
CO2_AN < 20.18485
CO2_MP < 197.1707

##END INEQUALITIES

GPP CALCULATION

Example with 12/2/2001 data
CB-autotrophic picoplankton - P3 group in BFM

```
r0p<-3.5 # growth parameter
pc<- 8.24   # CB autotroph biomass
q10<-2.00
T<-10.27
fpt<-q10^((T-10)/10)
Epar<- 1756.24 * 37800 ##winter: February 10.5*3600 = 37800,
                ##spring: May 15*3600 = 54000
                ##summer: August 14*3600 = 50400
                ##autumn: November 9*3600 = 32400
pl<- 0.45
alpha<- 1.52*(10^-5)
fpe<- (1 - exp(- ((alpha*Epar*pl)/(r0p*pc))))
```

```
fpp<-1 # No nutrient limitation as we use GPP as a maximum value
CO2_CB<- fpt*fpe*fpp*pc*r0p

AN-auototrophic nanoplankton - P2 group in BFM

r0p<-3.0 ## growth parameter
pc<- 6.61   ##AN autotroph biomass
q10<-2.00
T<-10.27
fpt<-q10^((T-10)/10)
Epar<- 1756.24 * 37800 ##winter: february 10.5*3600 = 37800,
##spring: May 15*3600 = 54000
##summer: August 14*3600 = 50400
##autumn: November 9*3600 = 32400
pl<- 0.45
alpha<- 0.46*(10^-5)
fpe<- (1 - exp(- ((alpha*Epar*pl)/(r0p*pc))))
fpp<-1 # No nutrient limitation as we use GPP as a maximum value
CO2_AN<- fpt*fpe*fpp*pc*r0p

MP-Microphytoplankton - P1&P4 group in BFM (we use average values)

r0p<-2.0 ## growth parameter - mean between P1 2.5 and P4 1.5
pc<- 151    ## MP autotroph biomass
q10<-2.00
T<-10.27
fpt<-q10^((T-10)/10)
Epar<- 1756.24 * 37800 ##winter: february 10.5*3600 = 37800,
##spring: May 15*3600 = 54000
##summer: August 14*3600 = 50400
##autumn: November 9*3600 = 32400
pl<- 0.45
alpha<- 1.035*(10^-5) ## mean between 1.38 P1 and 0.68 P4
fpe<- (1 - exp(- ((alpha*Epar*pl)/(r0p*pc))))
fpp<-1 # No nutrient limitation as we use GPP as a maximum value
CO2_MP<- fpt*fpe*fpp*pc*r0p
```